Fall 2021

Insights Into Rational Catalysts Synthesis

Abolfazl Shakouri

INSIGHTS INTO RATIONAL CATALYSTS SYNTHESIS

by

Abolfazl Shakouri

Bachelor of Science
Isfahan University of Technology, 2007

Master of Science
Isfahan University of Technology, 2009

Doctor of Philosophy
Ferdowsi University of Mashhad, 2015

Submitted in Partial Fulfillment of the Requirements

For the Degree of Doctor of Philosophy in

Chemical Engineering

College of Engineering and Computing

University of South Carolina

2021

Accepted by:

Christopher T. Williams, Major Professor

John R. Regalbuto, Major Professor

John R. Monnier, Committee Member

Aaron K. Vannucci, Committee Member

Melissa A. Moss, Committee Member

Tracy L. Weldon, Vice Provost and Dean of the Graduate School

DEDICATION

To my better half, Horie Adabi for asking critical questions that led to this success story.

ACKNOWLEDGEMENTS

Thank you to my supervisors, Dr. Williams and Dr. Regalbuto, for your patience, guidance, and support. I have benefited greatly from your wealth of knowledge. I am extremely grateful that you took me on as a student and continued to have faith in me over the years.

Thank you to my committee members, Dr. Vannucci and Dr. Monnier. Your encouraging words and thoughtful, detailed feedback have been very important to me.

My success would not have been possible without the support and nurturing of my lovely spouse, Horie Adabi, for constantly listening to me rant and talk things out, for cracking jokes when things became too serious, and for the sacrifices you have made in order for me to pursue my passions.

My dear sister, Neda Shakouri, you were always there, wherever and whenever that was. I am grateful and deeply indebted to you and your awesome spouse, Farid Gholami, for your unconditional, unequivocal, and loving support.

Special thanks to my mother, Hamideh Azimian, for your endless support.

I would like to express my deepest gratitude to my friends, Dr. Marjorie Nicholson, and Dr. Ralph White, for their unconditional support.

My warm and heartfelt thanks go to Hanna Soucie, for being an awesome friend.

Many thanks to all of my friends, teachers, and the members of staff in the University of South Carolina for their kind support during my PhD study.

ABSTRACT

Atomically distributed metal centers with maximized atom utilization efficiency called single-atom catalysts (SACs) have attracted significant attention in catalysis. SACs with the advantages of both homogeneous and heterogeneous catalysts have been rising as a new frontier in the field of catalysis. New catalytic technologies are ever-growing, considering 90% of all chemical processes employ catalysts, securing modern society's sustainable future. A classical field in catalysis has been dedicated to catalysis by supported metals. Recently, a vast effort has been devoted to smaller catalyst particles where size is restricted to a single atom on a surface. Single atoms supported or embedded on the surface of solid support involving covalent, coordination, or ionic bonds help rationalize the structure and the reactivity.

Heterogeneous single-atom catalysts have tremendous potential, but a facile synthesis at high metal loadings remains a challenge. Herein, we present two simple, scalable methods for doing so, applicable to a wide variety of metals and carbon and oxide supports. The methods of "switched solvent synthesis" (SwiSS) and "chelate fixation" (CheFi) prevent precursor agglomeration during drying and reduction caused by the presence of water. A non-soluble chelating agent dissolved in a polar solvent with a higher dipole moment of water can replace water and fixate the precursor ions during activation of the catalyst. These methods can yield relatively high loadings of single atoms, up to at least 1 atom per nm^2. In this manner, CheFi applied to carbon support with a surface area of 1200 m^2/g has

yielded 30wt% Pt as single isolated atoms. This density is achievable over other carbons, including those with no functional groups (diamond powder) as well as on oxide supports.

TABLE OF CONTENTS

LIST OF TABLES

LIST OF FIGURES

CHAPTER 1

INTRODUCTION

Overview of Single-Atom Catalyst

Atomically distributed metal centers with maximized atom utilization efficiency called single-atom catalysts (SACs) have attracted significant attention in catalysis. SACs with the advantages of both homogeneous and heterogeneous catalysts have been rising as a new frontier in the field of catalysis. New catalytic technologies are ever-growing, considering 90% of all chemical processes employ catalysts, securing modern society's sustainable future. A classical field in catalysis has been dedicated to catalysis by supported metals. Recently, a vast effort has been devoted to smaller catalyst particles up to where size is restricted to a single atom on a surface. Single atoms supported or embedded on the surface of solid support involving covalent, coordination, or ionic bonds help rationalize the structure and the reactivity. Earlier than SACs, surface organometallic catalysis (SOMCat) emerged, including single metal atoms covalently or ionically bound to a solid substrate (**figure 1.1**).

Isolated atoms in SACs feature unique reactivity. Considering the host materials having similar functions to ligands in homogeneous catalysis, the robust nature and recovery of the heterogeneous catalysts make them very attractive. A scalable and facile synthesis method for SACs is of great importance to fully exploit their potential for commercial applications. A large number of synthesis method resulting in a varied population of atomic species have been developed but a facile targeted synthesis of isolated

metal atoms remained a challenge. The previous methods are not readily scalable for larger scale (X. Sun et al. 2020; Kaiser et al. 2020; K. Qi, Chhowalla, and Voiry 2020).

Zhang et al. first established the term heterogeneous single-atom catalyst referring to cases in which the active sites consisted of metal atoms (Qiao et al. 2011). The definition of a single-atom catalyst can be expanded to an ensemble that consists of an atom of any element (metal, metalloid, non-metal, halogen) that is spatially isolated from atoms of the same chemical identity directly bound to a solid carrier. The electronic structure of the minority element can be significantly hybridized with the host because of the degree of orbital overlap (e.g., heteroatom-doped carbons). Diversity of anchoring sites in the host results in various structural and electronical coordination environment so the active centers are not necessarily uniform. Either organic or inorganic ligands may be present due to synthesis procedure or reaction condition comprising surface organometallic catalysts. A distinguished fundamental characteristic of SACs is that the single atom must be directly involved in the catalytic cycle keeping SACs apart from single atom dopants/promoters and catalytically active agglomerates (i.e., dimers, trimers, clusters, or nanoparticles) during reaction (Samantaray et al. 2020; Hulva et al. 2021).

Figure 1.2 represents the geometrical and electronical structures of nanoparticles, cluster, and single atom in gas phase. The electronic structure of a metal nanoparticle with a size about 5 nm is a continuous metal energy band while the electronic structure of metal cluster of 1 nm looks like discrete molecular orbitals. In theory, the electronic structure of a metal single atom in gas phase is expected to represent atomic orbitals that may be promising for uniformity of active sites. However, heterogeneous catalysis is only possible for supported catalyst on the surface of a support substrate. The microenvironment of the

single atom greatly contributes to the electronic structure of the catalyst. For example, DFT speciation analysis of Pt single atom on nitrogen doped carbon (Kaiser et al. 2020) showed that there are a number of anchoring sites on the surface of the support (**figure 1.2**). Each site on the surface of the support contributes differently to the electronic structure of the single atom catalyst resulting in different reactivity and stability for each given anchoring site.

As utilized herein, the term "single-atom catalyst" can refer to an ensemble that includes an atom of any element (metal, metalloid, non-metal, halogen) that is spatially isolated from atoms of the same chemical identity and directly adhered (e.g., physically and/or chemically bonded) to a solid support. The electronic structure of a minority element can be significantly hybridized with a host due to the degree of orbital overlap (e.g., heteroatom-doped carbons). Diversity of anchoring sites in a host support can result in various structural and electronical coordination environments so the active centers are not necessarily uniform. Either organic or inorganic ligands may be present in a catalyst/ support composite due to synthesis procedure or reaction condition comprising surface supported organometallic catalysts. Extremely high surface area and single atom catalysts are highly desirable as they can provide the highest possible utilization efficiency of the catalyst materials with high activity levels and selectivity as well as providing unique reactivity in some embodiments. Unfortunately, formation of such catalysts remains difficult and elusive, particularly for large scale production.

Thermo-catalytic, electrocatalysis, and photocatalysis applications have expanded to major areas of interest for single atom catalysis in the last years holding high promises for the fields. The choice of host materials expanded with the growing in the scope of

applications. A wide range of technology is ever growing to produce well defined SACs (Chang et al. 2021; Huiyu Zhang et al. 2021; Fan et al. 2021; Weon et al. 2021; Shen et al. 2021; Hu et al. 2020; Singh et al. 2021; Ahn et al. 2021; Babucci, Guntida, and Gates 2020; Q. Xu et al. 2021; R. Liu et al. 2021; Zhao et al. 2021; Maurer et al. 2020; Tieu et al. 2021; Jing Zhang et al. 2021; H Sykes and Christopher 2020; J. Qi et al. 2020; Zhou et al. 2020; Tang et al. 2019; Thang et al. 2018; DeRita et al. 2017; Malta et al. 2020; Serp 2021; Bulushev and Bulusheva 2021; Owen and Jenkins 2021; J. Wang et al. 2021; D. Gao et al. 2021; J. Wu, Li, and Yu 2021; Z. Li et al. 2021). Here, we review the most widely used approaches and concisely review their current limitations. The major approaches to produce SACs are divided into two categories, direct (bottom-up) synthesis method in which the minority element is isolated during the preparation of the host and the post (top-down) synthesis approach where the minority element hosted to an existing substrate with desired characteristics (Kaiser et al. 2020; X. Sun et al. 2020).

The second approach, post (top-down) synthesis; the introduction of minority precursors into the pre-prepared substrate materials included wet chemistry, electrochemical, and gas phase approaches. The majority of the literature reported these methods depend on existence of appropriate coordination sites on the support substrates mostly stable with very low areal density of minority element. The attractive features of the top-down approach are benefiting the surface location of the catalytically active sites and in case of wet chemistry, its low cost, easy steps, and amenability to scalable procedures. There are some draw backs because of no control over capillary forces during drying. The wet chemistry approach usually is consisting of two steps, deposition of precursor ions and activation of the catalyst (**Figure**). The effecting parameters on

generation of single atom sites are including choice of solvent, pH, temperature, chelating agents, and stabilizers/linkers (X. Sun et al. 2020; Kaiser et al. 2020).

It is known that capillary forces cause inhomogeneity in the resulting catalysts using wet chemistry approaches. Sun et al. (X. Sun et al. 2020) used an effective approach to produce single atom catalysts from exotic acetylacetonates precursors soluble in acetone (almost insoluble in water) and used low-boiling-point, low-polarity solvent such as acetone to impregnate 1 wt.% Pd/C, Pt/C, Ru/C and Au/C materials through wet impregnation. They systematically investigated the synthesis of Au/C by wet impregnation of $HAuCl_4$ in aqueous solution, different mixtures of acetone/water, and pure acetone. The aqueous solution and mixtures resulted in Au nanoparticles and pure acetone resulted in single atom catalysts(X. Sun et al. 2020).

Atomically dispersed metal precursors form ultrasmall nanoparticles upon drying and pretreatment; in the presence of excess water (sample placed into reduction furnace before completely dried) the NPs were larger (**Figure 1.4**). This hints that the remaining water in the sample exerts a major influence on metal precursor movement during pretreatment. Hutchings recently demonstrated the isolation of Au, Ru, Pd, and Pt atoms using acetone as a solvent, together with acetylacetonate and other metal precursors soluble in acetone. They concluded that atom isolation is accomplished by combining a low polarity solvent which increases support wettability with mild drying conditions.

Typical catalyst formation methods include defect engineering, metal-support interaction, heteroatom tethering, spatial confinement, and atomic alloying, among others. While aspects of the various formation approaches can vary greatly, many catalyst formation techniques include wet chemistry approaches in which a salt solution of the

catalyst precursor is deposited on a support. Following deposition, the solution is dried to provide precursor ions on the support. Subsequent activation of the precursor ions forms the catalyst. Unfortunately, such formation techniques do not adequately prevent migration and agglomeration of the precursor ions and thus relatively large precursor crystallites and subsequent catalyst nanoparticles are formed rather than the preferred smaller and single atom catalysts.

Disclosed methods have been developed through insight to the root causes of precursor ion migration and agglomeration common in previously known wet chemistry approaches. In particular, disclosed methods have been developed through understanding of the affinity of precursor ions toward the high dielectric constant solvents used in traditional wet chemistry formation techniques (generally water) combined with the surface tension of the high dielectric constant solvents on the supports of interest and the effect of interactions between precursor ions and support materials on the solvent surface tension. The combined result of such interactions leads to migration and agglomeration of the precursor ions, with eventual formation of relatively large nano-sized particles of the catalysts.

To resolve these issues, the presently disclosed methods utilize a two-solvent approach in which an initial solvent that exhibits desirably high dielectric constants and dipole moments so as to be useful for initial formation of a precursor solution can be displaced with a second solvent following application of the initially-formed solution to a support. The second solvent can be one that exhibits a lower surface tension on the support and prevents agglomeration of the precursor ions prior to and during activation. In some embodiments, a method need not include drying of the support and removal of the solvent

prior to activation. In other embodiments, however, the solvent(s) of a solution can be removed prior to activation by drying in an atmosphere that is free of water. Beneficial, through displacement of a first solvent with a second solvent, disjoining pressure between precursor ions in the second solvent can be retained during activation and as such there is no need in disclosed methods to include anchoring functional sites on a support surface as is often required in other previously known catalyst formation techniques.

The presently disclosed methods are based upon the identification of problems such as those mentioned above due to the use of highly polar solvents such as water in wet chemistry-based catalyst formations. Water is the most common solvent for ionic compounds because of its high polarity, i.e., the negative (oxygen) side of a dipolar water molecule attracts and is attracted by any positive ion in solution and similarly, the positive (hydrogen) ends of water molecules are attracted to negative ions, providing excellent solvating characteristics. Unfortunately, however, the use of such solvents also leads to the formation of nanoparticles during drying and activation of the catalyst.

Disclosed methods answer these issues by utilizing two different solvents during a catalyst formation process. A first solvent can be one that is useful for initial formation of a precursor solution, e.g., water or another highly polar solvent. A second solvent can be selected that can exhibit suitable polarity so as to maintain the precursor in solution, but also exhibits a lower surface tension on the support as compared to the first solvent so as to prevent the formation of droplets and consequently agglomeration of the precursor ions prior to and during activation.

According to disclosed methods, a first solvent of a precursor solution can be displaced, or switched, with a second solvent prior to activation. The second solvent can

be a wetting solvent that exhibits a lower surface tension on the support than the first solvent and that can form a uniform thin film of a precursor solution during activation of the catalyst.

Depending upon the parameters of a formation approach, disclosed methods can be utilized to produce single atom catalysts or small nanoparticle catalysts. For instance, relative dielectric constant, surface tension, viscosity, boiling point, hydrogen bonding and other physical properties of the two solvents can affect the characteristics of a formed catalyst. The ratio of the solvents, heating ramp, and activation process of the catalyst can also be utilized to control the final form of the catalyst.

By way of example, and without limitation, **Table 1.1** and **Table 1.2**, below, provide examples and physical characteristics of typical polar protic (**Table 1.1**) and aprotic (**Table 1.2**) solvents as may be utilized in disclosed methods. Following formation, a precursor solution including the first solvent can be applied to a support. There is no particular limitation on supports that can be utilized in the formation process, and generally, any support known or unknown suitable for supporting the catalyst in the desired application can be utilized. For instance, and depending upon the desired application of the catalyst, a support can be highly stable in harsh environments for chemical applications and/or can exhibit good electrical conductivity for electrochemical applications.

A second solvent can be added to a system following application of the initial precursor solution to the support. Upon this addition, the second solvent can displace and replace the initial solvent at the support surface. The addition can be carried out according to any suitable methodology, with a preferred approach generally depending upon the nature of the catalytic system. For instance, in those embodiments in which the

support is a particulate and the first precursor solution system is in the form of a suspension or dispersion, the addition of the second solvent can be carried out simply by adding an amount of the second solvent to the suspension/dispersion. In those embodiments in which the support is of a larger form, e.g., a film, fibers, or the like and the support is immersed in the first precursor solution, an amount of the second solvent can be added to the system.

In general, the amount of the second solvent to be added to the system can be greater than the amount of the first solvent in the system. For instance, the molar ratio of the second solvent to the first solvent can be greater than 1, greater than 2, or greater than 3, in some embodiments. For instance, the molar ratio of the second solvent to the first solvent can be from 1:1 to 10:1, or from about 2:1 to about 8:1 in some embodiments.

In order to successfully replace the initial solvent, the second solvent can have a lower surface tension on the support as compared to that of the first solvent. Without wishing to be bound by any particular theory, it is understood that the Marangoni effect provides the driving force for replacement of the first solvent and the resulting desirable distribution of precursors on the support during activation.

The Marangoni effect (also known as the Gibbs-Marangoni effect) describes mass transfer along an interface between two fluids due to a gradient of the surface tension at the interface. As surface tension can depend on temperature, this phenomenon is also referred to thermo-capillary convection. Briefly, a permanent nonuniformity of temperature or concentration (for a multicomponent system) at an interface between two fluids can cause a surface tension gradient. The interfacial area with lower surface tension

expands at the expense of an area with greater surface tension, which in turn establishes a steady flow pattern in the liquid.

The lower surface tension of the second solvent can prevent droplet formation as the solvent dries prior to or during the initial stages of activation and as such can prevent agglomeration of the precursor ions at this stage of the catalyst formation. In addition, the second solvent can improve formation of single atom or ultra-small nanoparticle catalysts due to improved disjoining pressure as compared to a higher surface tension solvent. When a liquid film on a support becomes very thin, the intermolecular attractive forces between the molecules in the liquid and those in the solid tend to pull the liquid to the liquid film. For a flat liquid file, absent capillary pressure, the total pressure in the liquid film can thus be changed by an amount referred to as the disjoining pressure, causing the liquid pressure to be less than the vapor pressure and generating a pressure gradient within the thin liquid film. The disjoining pressure can be considerably effective as long-range intermolecular forces in the range of 0.2 to 10 nm spacing regardless of the medium between the species originating in van der Waals forces including London dispersion and electrostatic interactions (Faghri and Zhang 2006b, 2006a).

The disjoining pressure becomes more significant in case of ultra-thin liquid films as will form on a support surface as the surface dries and the precursor is activated. This increased significance is due to the fact that the liquid-vapor interface of an ultra-thin film is closer to the solid surface which can be explained by

$$P_d(\delta) = -\frac{2A_H}{\pi(n-2)(n-3)}\delta^{3-n}$$

in which Pd is the disjoining pressure on a liquid film of thickness δ. AH is the Hamaker constant that relates the interactive van der Waals energy to the distant of separation

between two molecules where the interactive forces are independent of intervening media. The interactions between particles are relative to the refractive index n and the dielectric constant ε. The Hamaker constant takes account for both temperature dependent forces like Keesom and Debye polar molecular forces and temperature independent forces like London dispersion forces resulting from the orbiting electron frequency and the refractive index, n. The Hamaker constant may be related to the interfacial tension between the two surfaces separated by intermolecular distance, δ (Donaldson and Alam 2008; Faghri and Zhang 2006c).

The fluid properties such as density, volatility, viscosity, van der Waals forces, and molecular electrical interacting forces control the spreading characteristics of a fluid. The disjoining pressure (i.e., the pressure required to lift the liquid from solid) is a product of attractive van der Waals forces, electrostatic forces, and hydration forces which suggests that in an equilibrium thin film containing precursor ions in the second solvent, which is a relatively low surface tension solvent, the liquid molecules will better adhere to the solid support and maintain the precursor ions dispersed on the solid support as the solvent dries and leaves the support surface.

Following displacement of the first solvent with the second solvent, the support can carry a solution of the second solvent and the precursor ions at a surface of the support. The precursor can then be activated to form the catalyst according to standard methods as are known in the art.

In order to avoid formation of large catalyst nanoparticles, the support including the second solvent solution at the surface should not be contacted with water, as the precursor may be capable of adsorbing moisture from the surrounding atmosphere, which

can lead to the formation of precursor crystallites and subsequent catalyst in relatively large nanoparticle form. Accordingly, the support and second solvent solution can be immediately transferred to a reducing atmosphere or other activation atmosphere without drying. In other embodiments, the precursor composition can be dried to remove the second solvent (and any remaining first solvent in the system) prior to activation, but in this embodiment, the drying step can be carried out in a water-free environment, e.g., under an inert atmosphere, or in a reducing atmosphere.

Characterization Methods

Scanning Transmission Electron Microscopy (STEM)

Advancement in the resolution of the STEM instruments made it possible to distinguish between a single atom catalyst active center and the background of a support substrate. However, STEM imaging comes with some limitations in terms of the structural information arising from 2D projection of 3D structures, induced structural changes from the electron beam, suitable Z-contrast between metal and the support substrate, and stability.

X-ray Photoelectron Spectroscopy (XPS)

The most widely used tool to probe the electronic structure of the surface species is XPS which allows the identification of multiple oxidation states of an element within the catalyst. In situ XPS studies reveal the treatment conditions and what to expect from various activation strategies together with some information about the stability of the catalyst in different atmosphere types.

The XPS measurement does not guarantee the homogeneity of each species in term of having a certain oxidation state. For example, Pt^0 in a catalyst containing nanoparticles of Pt may include different speciation such as multiple facets, edge sites, teras sites, bulk sites, and defect sites.

X-ray Absorbance Spectroscopy (XAS)

Multiple scattering paths of an ejected photoelectron causes fluctuations in absorption observed by XAS resulting in the local coordination data. All species present in the system coordination numbers and local structures (average interatomic distances) can be interpreted by fitting the spectra.

In Situ CO Adsorption DRIFTS/FTIR

This technique provides structural and chemical information related to the species on the surface of the catalysts through measurements of CO stretching vibrations as a probe. The specific characteristics of the measurements on SACs is the peak position and narrow peaks. The full width half maximum of the peak (FWHM) is a measure of uniformity of SACs in addition to the peak position for linearly adsorbed CO on single atoms. Although some broadening effects may be show up in the spectra from neighboring species or other site vibrations in the wider vibrational frequency for the peaks.

CO Temperature Programmed Desorption (CO-TPD)

Temperature programmed desorption of CO is a characterization tool to distinguish between SACs and catalysts containing nanoparticles. Because of different electronic structures of single atom catalyst and nanoparticles, the CO adsorption energy and the

temperature required for CO desorption are different. There are several literature reporting this effect to distinguish between SACs and nanoparticles (Jeong et al. 2020; Hulva et al. 2021).

Table 1.1. Properties of common protic solvents.

Solvent	Dielectric Constant	Dipole Moment	Boiling Point (°C)	Surface Tension (mN/m)
Water	80.1	1.85	100	72.80 @20˚C
Methanol	33.0	1.69	64.5	22.70 @20˚C
Ammonia	31.6	1.42	-33.34	
Ethanol	25.3	1.69	78.3	22.10 @20˚C
n-propanol	20.1	1.68	97	24.00 @25˚C
Isopropyl alcohol	19.92	1.66	82.5	23.00 @20˚C
t-butanol	10.9	1.70	83	20.00 @25˚C
Acetic acid	6.20	1.74	118	27.00 @25˚C

Table 1.2. Properties of common aprotic solvents.

Solvent	Dielectric Constant	Dipole Moment	Boiling Point (°C)	Surface Tension (mN/m)
Dimethylsulfoxide (DMSO)	46.68	3.96	189	42.27 @30˚C
Dimethylformamide (DMF)	36.71	3.86	153	37.10 @20˚C
Acetonitrile (MeCN)	38.8	3.92	81.6	29.10 @20˚C
Hexamethylphosphoric acid (HMPA)	30.0	5.54	233	
Acetone	20.7	2.88	56	25.20 @20˚C
Dichloromethane	8.93	1.60	39.6	26.50 @20˚C
Tetrahydrofuran	7.58	1.75	66	26.40 @20˚C
Methyl acetate	6.7	1.69	57	24.50 @25˚C
Ethylacetate	6.02	1.78	77.1	23.2 @25˚C

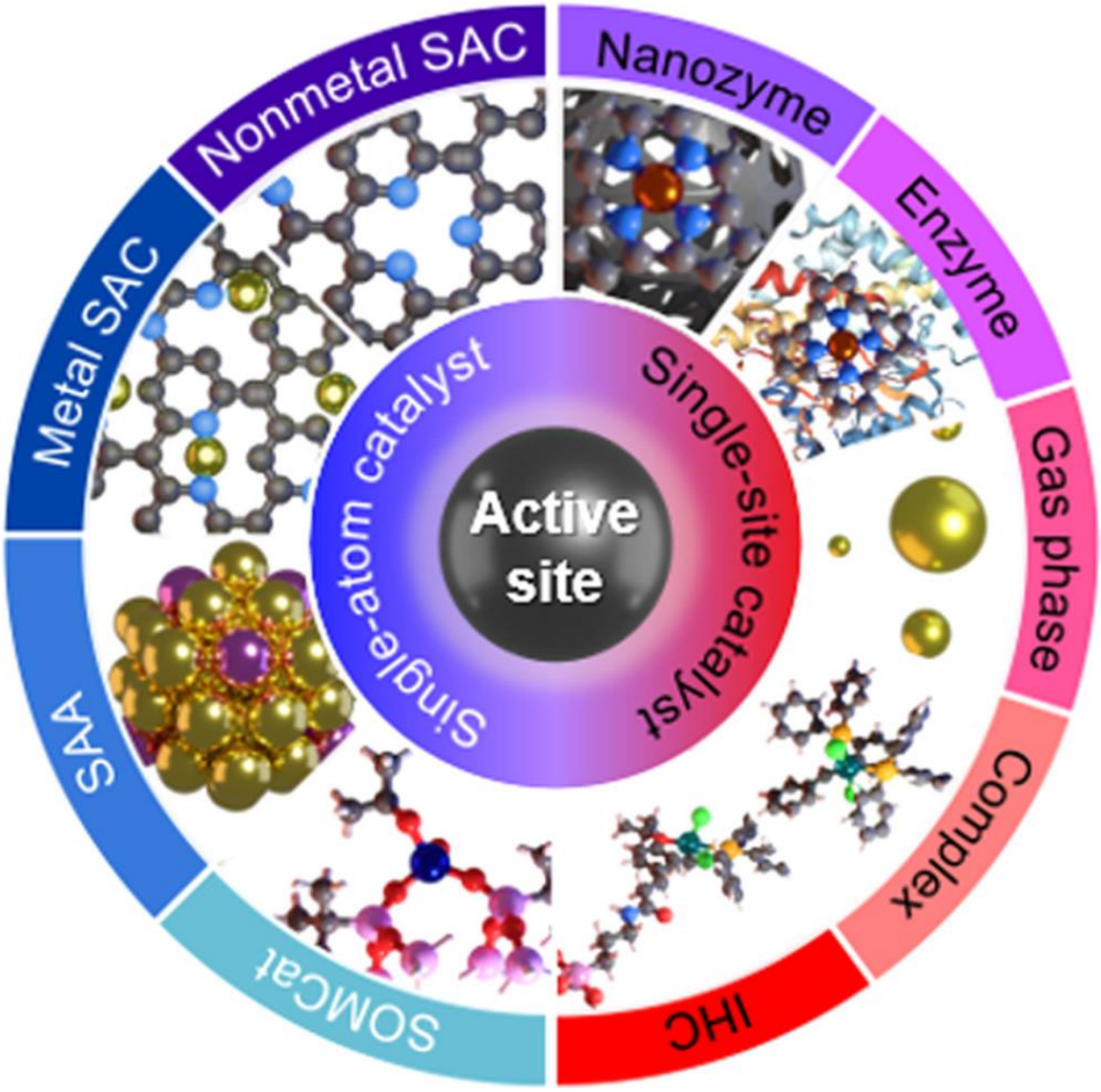

Figure 4.1. Overview of subclasses of catalysts consists of isolated atoms, including single-atom catalysts (SACs), single-atom alloys (SAAs), surface organometallic catalysts (SOMCats), and metal complexes (including immobilized homogeneous catalysts).

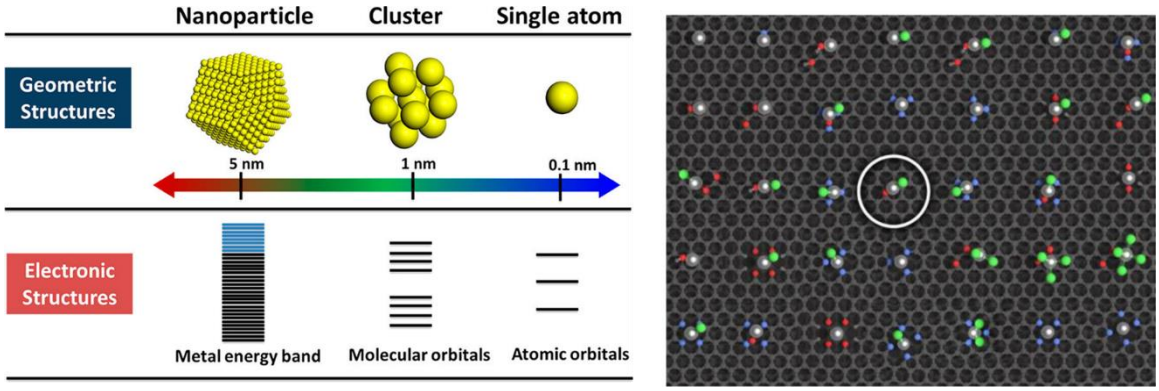

Figure 1.2. Geometric and electronic structures of nanoparticle, cluster and single atom; and speciation analysis of Pt single atoms hosted on N-doped carbon for acetylene hydrochlorination. Partially reprinted with permission from (M. Sun, Wu, and Huang 2020; Kaiser et al. 2020). Copyright (2020) American Chemical Society.

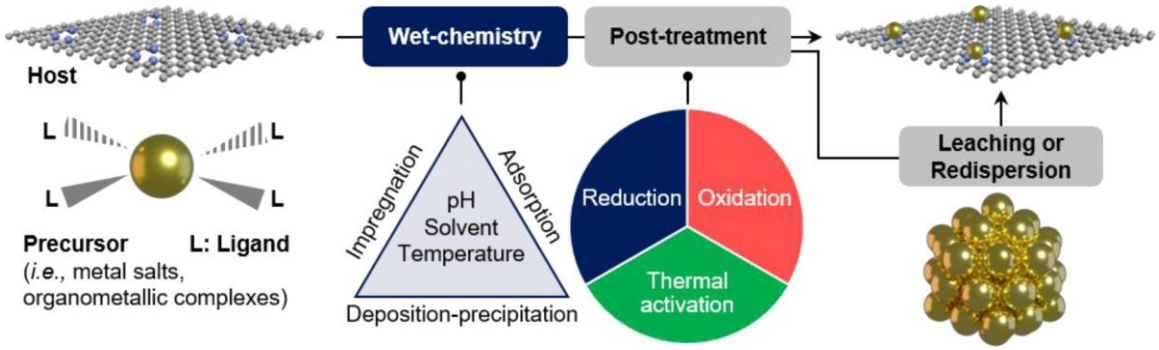

Figure 1.3. Overview of wet-chemistry approaches to synthesize SACs. Reprinted with permission from (2). Copyright (2020) American Chemical Society.

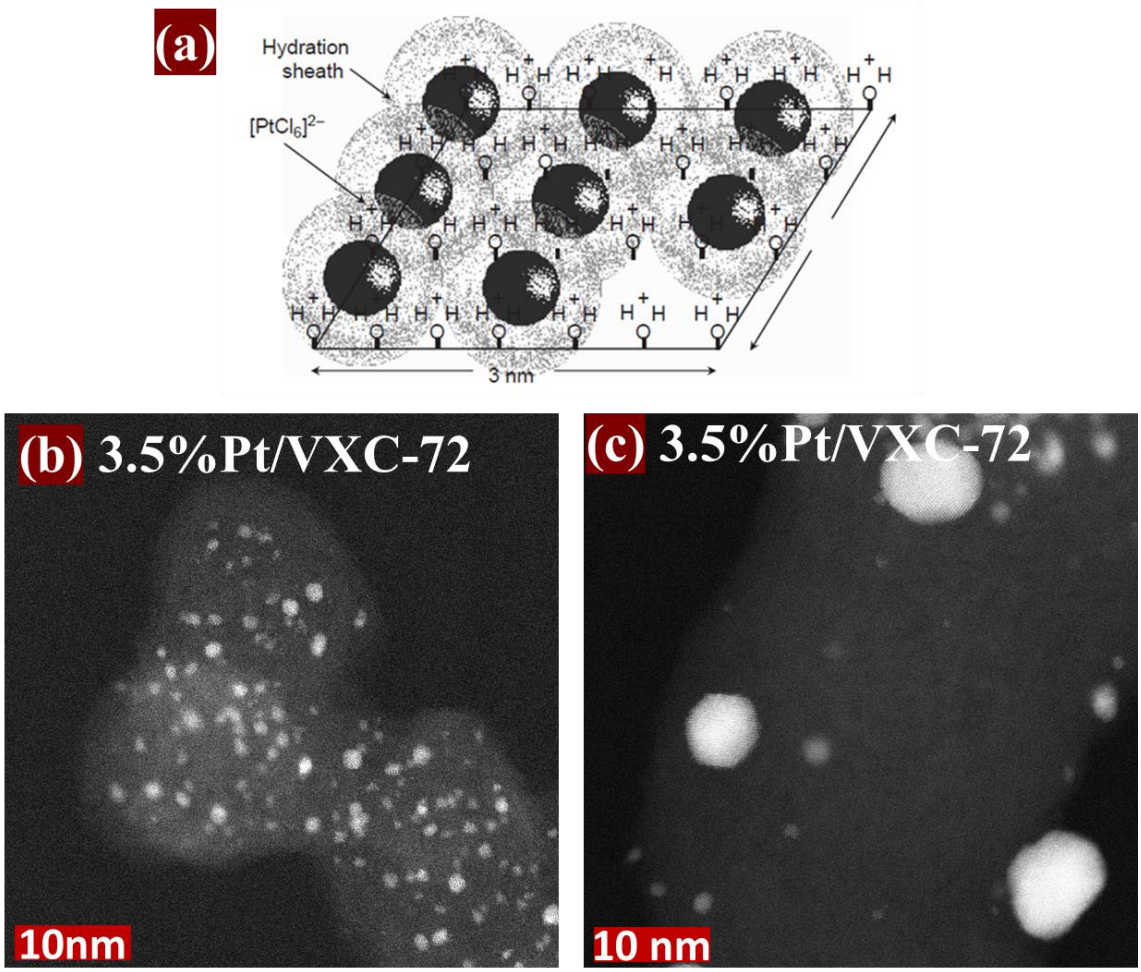

Figure 1.4. (a) Electrostatic adsorption, an adsorbed monolayer of sterically closed packed metal precursors (b) is transformed after drying and reduction into ultrasmall (< 2 nm) nanoparticles (c), or with incomplete drying, into much larger nanoparticles.

CHAPTER 2

A GENERAL, SCALABLE, AND SIMPLE SYNTHESIS METHOD

It is known that capillary forces cause inhomogeneity in the resulting catalysts using wet chemistry approaches. Sun et al. (X. Sun et al. 2020) used an effective approach to produce single-atom catalysts from exotic acetylacetonates precursors soluble in acetone (almost insoluble in water) and used low-boiling-point, low-polarity solvent such as acetone to impregnate 1 wt.% Pd/C, Pt/C, Ru/C, and Au/C materials through wet impregnation. They systematically investigated the synthesis of Au/C by wet impregnation of $HAuCl_4$ in aqueous solution, different mixtures of acetone/water, and pure acetone. The aqueous solution and mixtures resulted in Au nanoparticles, and pure acetone resulted in single-atom catalysts(X. Sun et al. 2020).

Why Water?

The standard precursors are soluble in water because of its high polarity among other solvents. In general, solvents with high dielectric constant (e.g., water) tend to dissolve and retain the ionic compounds by exerting an attractive force. However, solvents with low dielectric constants are not able to fully dissolve the catalyst precursors expelling the ionic precursors from the solution by exerting a repulsive force on them. This effect can be explained by substituting force exerted by a point charge into the Coulomb's law together with ionic interactions expressed as the valency, z, multiplied by the elementary

electron charge, -e. Therefore, the electrostatic free energy for charges separated by a distance equal to Bohr radius, r_b, is $G_{(r)} = \frac{z_1 z_2 e^2}{4\pi\varepsilon\varepsilon_0 r_b}$ where ε is the dielectric constant of solvent and ε_0 is the permittivity of free space (vacuum). In case of catalyst precursor with unlike ionic species if the free energy, $G_{(r)}$, is negative yielding an attractive force. If two like charges precursor ions are separated with a dielectric material (mostly water) the dielectric material diminishes the forces between charges by an extent equal to the dielectric constant of material. That is why it is important to use water as solvent because it readily dissolves the standard catalyst precursors due to its high dielectric constant (Donaldson and Alam 2008; Faghri and Zhang 2006a, 2006c).

Problem statement

We identified the problem of using water in the last step of synthesis during activation of the catalyst; when a small amount of water is left during drying, it may break up into small droplets. Because of high surface tension and large dielectric constant which exert an attractive force to the precursor ions and agglomerates the precursor ions together forms small crystallites that later lead to formation of nanoparticles during activation. The strong electrostatic adsorption (SEA) of the catalyst precursor ions onto the support substrate alter the interfacial tension of support-water interface resulting in much smaller droplets and consequently ultrasmall nanoparticles. This can be explained by surface pressure of adsorbed precursor ions $p_s = \sigma_{sv} - \sigma_{sv,a}$where $\sigma_{sv,a}$ is the interfacial tension with the absorbed substance present. Therefore, Young's equation (**Figure**) can be written as $\cos\theta = \frac{(\sigma_{sv} - p_s) - \sigma_{sl}}{\sigma_{lv}}$ which shows that the SEA changes the equilibrium contact angles and the solvent surface tension near the support surface (Faghri and Zhang 2006c).

Proposed Solution

To make single atom catalyst, water need to be displaced by a wetting solvent. Therefore, when a small amount of solvent left during activation, the solvent may spread over the support substrate surface and form a thin film containing precursor ions. A permanent nonuniformity of temperature and concentration at the solvent-gas phase interface results in a surface tension gradient. The high temperature interfacial areas or wetting solvent with small surface tension expands at the expense of an area with larger surface tension establishes a steady flow in the system called the Marangoni effect. Herein, we propose the use of The Marangoni effect as a driving force to displace water throughout the system after deposition of the catalyst precursor ions at incipient wetness condition. The surface tension of such system in equilibrium with the gas phase can be expressed as $\sigma = \sigma (T, x_1, x_2, \ldots, x_{N-1})$ where x_i represents the molar fraction of i_{th} component of the liquid phase. Thus, the change in surface tension can be expressed as $d\sigma = \left(\frac{\partial \sigma}{\partial T}\right)_{x_i} dT + \sum_{i=1}^{N-1} \left(\frac{\partial \sigma}{\partial x_i}\right)_{T, x_{j \neq i}} dx_i$. The Marangoni number for temperature change in the system during the activation of the catalyst expressed as $Ma = \frac{\zeta ({}^{d\sigma}/_{dT}) \delta^2}{\alpha_l \mu_l}$ where α_l is thermal diffusivity of the liquid, $\zeta = {}^{(T_w - T_\delta)}/_{\delta}$, μ_l is viscosity of liquid, and δ is the thin film thickness (Donaldson and Alam 2008; Faghri and Zhang 2006a, 2006c).

We established that the water is necessary to dissolve the precursor salts, but it causes the formation of nanoparticles during activation of the catalyst. To prevent the formation of water droplets and consequently agglomeration of the precursor ions, we proposed addition of a wetting solvent that forms a uniform thin film during activation of

the catalyst by the help from the Marangoni effect. One last important parameter that affect the dispersion of the catalyst precursor ions during activation is disjoining pressure. When a liquid film on a support substrate becomes very thin, the intermolecular attractive forces pull the liquid to the liquid film. The disjoining pressure can be considerably effective as long-range intermolecular forces in the range of 0.2 to 10 nm spacing regardless of the medium between the species originating in van der Waals forces including London dispersion and electrostatic interactions. The disjoining pressure becomes more significant in case of ultra-thin liquid films because the liquid-vapor interface is closer to the solid surface which can be explained by $P_d(\delta) = -\frac{2A_H}{\pi(n-2)(n-3)}\delta^{3-n}$. A_H is a constant coefficient called the Hamaker constant that relates the interactive van der Waals energy to the distant of separation between the two molecules where the interactive forces are independent of intervening media. The interactions between the particles are relative to the refractive index n and the dielectric constant ε. The Hamaker constant take account for both temperature dependent forces like Keesom and Debye polar molecular forces and temperature independent forces like London dispersion forces resulting from the orbiting electron frequency, ν, and the refractive index, n. The Hamaker constant may be related to the interfacial tension between the two surfaces separated by intermolecular distance, δ. In summary, the fluid properties such as density, volatility, viscosity, van der Waals forces, and molecular electrical interacting forces control the spreading. The pressure required to lift the liquid from solid is the disjoining pressure which is a product of attractive van der Waals forces, the electrostatic forces, and hydration forces that suggest that in the equilibrium thin film (**Figure**) containing precursor ions, the liquid molecules adhere to the solid (Donaldson and Alam 2008; Faghri and Zhang 2006c, 2006a).

Hypotheses and Objectives

The following proposed syntheses of single atom catalyst on support substrates, are simple, fast, generalizable, and readily scalable at standard incipient wetness conditions, and also, results in much higher densities than currently achieved in the state-of-the-art single atom catalysts. The current synthesis approaches are mainly based on ultra-low densities of SACs (Tieu et al. 2021; Resasco and Christopher 2020; Jing Zhang et al. 2021; Kou et al. 2020) or using exotic catalyst precursors (X. Sun et al. 2020; Jing Liu et al. 2018; Alexeev and Gates 2000; Kou et al. 2020). Here, we identified the problem in the standard synthesis procedures with the water drying step in which high surface tension of water and the force that water (high dielectric constant) exerts to precursor ions and retain them in solution form the agglomerated precursors and result in formation of nanoparticles. Error! Reference source not found.**2.3** shows the difference among the standard industrial catalyst synthesis method resulting in large and nonuniform nanoparticles, the sophisticated strong electrostatic adsorption (SEA) resulting in ultrasmall and uniform nanoparticles, and the proposed synthesis method producing single atom catalysts. Our developed technology provides a simple solution to produce high densities of single atom catalyst on a wide range of insoluble support substrates.

The four hypotheses were tested in the following work, are including the fundamental understanding of synthesis procedure in which:

1. Polar solvent with high dielectric constant that is capable of dissolving high concentrations of the catalyst precursor's salt for high metal loadings.
2. After impregnation, replace high polar solvent with low polar wetting solvent to facilitate the formation of thin film solvent.

3. Reduce without exposure to water in the air to prevent moisture adsorption by precursors ions and the support substrate.
4. If precursor is to be expose to air (moisture), we add chelating agent immiscible in water to prevent precursor agglomeration on a water adsorbed surface.

The proposed work demonstrated the generalizability of our developed methods by studying the syntheses by different solvents, support substrates, and metals as catalyst. Hence, it could usher a new era of industrial applications due to its simplicity and scalability. New technologies are emerging in the field of SACs including partial oxidation, selective hydrogenation, and complex organic synthesis (Datye and Guo 2021).

The present work helped understanding synthesis procedure in fundamental levels and investigated the viability of the synthesis method on different systems. The fast and easy synthesis method providing insights into new possibilities and will expand the single atom catalyst applications that are requiring new support systems. The systems we examined to study the effects of solvent are summarized in **table 2.1**. The primary support chosen is diamond nanoparticles in which consisting of only crystalline carbon with no functional groups on the surface. This expanded the versatility of our synthesis method into a wide range of support substrates regardless of the functional groups on the surface. The first three experiments were aiming to demonstrate the effect of second solvents with lower surface tensions and different dipole moments in spreading the catalyst precursor and forming SACs. The last two experiments were to evaluate the possibility of using only one wetting solvent and explore the formation of SACs with different loadings.

Preparation by Switched Solvent Synthesis (SwiSS) method

Although, the functional groups on the surface of the support substrates are beneficial because other than providing anchoring sites for the single atoms, they would help to make the solvent more wetting and help with uniform spreading the precursor ions through electrostatic adsorption. Different functional groups would provide different environments for anchored single atoms and results in variable properties including oxidation state, stability, and functionality. Also, the standard industrial supports are included to show case the synthesis and function of the resulted single atom catalysts in both thermo-catalytic and electro-catalysis applications. The VXC-72 carbon based industrial support was chosen for evaluation in the oxygen reduction reaction catalyst (ORR). The TiO_2 supported Pd and Pt SACs were evaluated in partial oxidation of 1-phenylethanol into acetophenone. Electrochemical measurement carried out in three electrode cell using ring-rotating disk electrode as well as a cathode in anion exchange membrane fuel cells (AEMFCs).

Results and Discussions

The current synthesis approaches are mainly based on ultra-low densities of SACs (Tieu et al. 2021; Resasco and Christopher 2020; Jing Zhang et al. 2021; Kou et al. 2020) or using exotic catalyst precursors (X. Sun et al. 2020; Jing Liu et al. 2018; Alexeev and Gates 2000; Kou et al. 2020; Jin et al. 2021). Here, we identified the problem in the standard synthesis procedures with the water drying step in which high surface tension of water and the force that water (high dielectric constant) exerts to precursor ions and retain them in solution form the agglomerated precursors and result in formation of nanoparticles. Error! Reference source not found. shows the difference among the standard industrial

catalyst synthesis method resulting in large and nonuniform nanoparticles, the strong electrostatic adsorption (SEA) resulting in ultrasmall and uniform nanoparticles, and the proposed synthesis method producing single atom catalysts. Our developed technology provides a simple solution to produce high densities of single atom catalyst on a wide range of insoluble support substrates. The fast and easy synthesis method is providing insights into new possibilities and will expand the single atom catalyst applications that are requiring new support systems. Although, the functional groups on the surface of the support substrates are beneficial because other than providing anchoring sites for the single atoms, they could help to make the solvent more wetting and help with uniform spreading the precursor ions through electrostatic adsorption. Different functional groups would provide different environments for anchored single atoms and results in variable properties including oxidation state, stability, and functionality.

Aberration corrected scanning transmission electron microscopy (AC-STEM) in most cases made possible the identification of individual atoms based on the Z-contrast. In some cases, when the support substrate is conductive and there is enough difference in atomic number between the elements in the system, it may be possible to characterize the SACs using Z-contrast imaging. **Figure 2.4(A)** shows the AC-STEM image of 2%Pt/Diamond prepared by switched solvent method using acetone as second solvent. Acetone has a dipole moment of 2.88 D larger than that of water so its molecules interact with precursor's ions stronger than water. It seems that acetone replaces water in the system. In addition, acetone has much lower surface tension and viscosity than water with higher wetting properties which results in well dispersed single atom catalyst. This result could be explained by formation of the thin liquid film containing precursor ions and

disjoining pressure. In the case of ethanol as the second solvent, because of the lower ethanol dipole moment of 1.66 D than water, it is not expected for ethanol to be able to replace the hydration sheath of the precursor's ions. Also, ethanol and water are both forming hydrogen bonding and the viscosity of ethanol is slightly higher than water. However, ethanol has much lower surface tension than water so it can act as a wetting solvent to some extent. The resulted catalyst for 2%Pt/Diamond using ethanol as the second solvent shown in **figure 2.4(B)**. There are single atoms, dimers, trimers, clusters, and ultra-small nanoparticles formed which are much smaller species in comparison to **figure 2.4(C)** representing 2%Pt/Diamond prepared with only water as solvent at incipient wetness condition.

Temperature programmed desorption of CO (CO-TPD) is a characterization tool to distinguish between SACs and catalysts containing nanoparticles. The preliminary results in **figure 2.4(D)** demonstrate the difference in CO desorption temperature from SACs and sample containing nanoparticles. The top (blue) curve shows CO desorption temperature from the 2%Pt/Diamond catalyst is about 350K and the bottom curve belongs to the CO desorption at almost 480K from 2%Pt/Diamond catalyst containing nanoparticles. Because a large fraction of Pt atoms is inside the nanoparticles and are not accessible to adsorb CO, the intensity of the CO desorption peak is much smaller than the ones containing single atoms and clusters with almost all accessible Pt atoms. The middle curve resulted from the catalyst with all different species in **figure 2.4(B)** shows three CO desorption peaks. The peak at 350K is attributed to the single atoms and nanoparticles CO desorption peak at 580K while the peak at 400K could be attributed to the Pt dimers and trimers in the catalyst (Therrien et al. 2018).

The samples further characterized in XPS chamber but because the diamond support is not conductive, the neutralizer electron gun was necessary to compensate for the electron used in XPS measurements. However, the small size of the Pt single atoms and clusters led to shifts to lower binging energy in Pt 4f peaks because of electron overcompensation. So, we synthesized identical samples on conductive Volcan XC-72 that has a specific surface area close to that of diamond, 257 m^2/g. The AC-STEM images in **figure 2.4(E-G)** show the identical samples prepared using acetone, ethanol, and only water, respectively. The in situ XPS measurement of Pt 4f peaks of 2%Pt/VXC-72 containing nanoparticles demonstrated a Pt 4f peak at 71.2 eV (**figure 2.4(H)**-top curve) which is expected for nanoparticles reported in literature (Therrien et al. 2018). The Pt 4f peak for the sample with only single atoms is shown in **figure 2.4(H)**-bottom curve shifted to 72.5 eV. The sample containing single atoms and clusters demonstrated two Pt4f peaks at both 71.2 and 72.5 eV.

The water content of the system before activation is very important. To demonstrate the effect, we prepared a catalyst by switched solvent method using acetone as the second solvent. However, instead of activating the catalysts immediately, the catalyst was dried under the fume hood overnight like the procedure of commercial the incipient wetness method. **Figure 2.5(A)** shows the AC-STEM image of 2%Pt/VXC-72 that was dried and exposed to the room air (moisture) prior to activation at 170 ˚C. The in situ XPS spectra of the catalyst as received prior to activation, the catalyst in situ reduced at 170 ˚C, and the catalyst in situ reduced at 600 ˚C are demonstrated in **figure 2.5(B)**. The dried catalyst shows that different Pt species are present in the catalyst. After first in situ reduction, there is only one species formed and the Pt 4f peak position is in agreement with Pt nanoparticles

shown in **figure 2.5(A)**. To make sure that the Pt 4f peak is attributed to only nanoparticles, we reduced the sample at 600 ˚C and compared the Pt 4f peak positions. In conclusion, the switched solvent method is very sensitive to the moisture. The unreduced precursor ions are capable of adsorbing moisture from the surrounding air and forming crystallites upon drying and nanoparticles after activation. Thus, the catalyst should not be exposed to the atmosphere containing moisture prior to the activation.

The stability of these single atom catalysts was investigated by heating them to 300 ˚C under flow of 10%H_2 balance N_2. **Figure 2.5(C-F)** shows AC-STEM images of the catalyst including the particle size distribution. The diamond surface does not have any defects or functional groups, so the particle size distribution of sintered single atoms into nanoparticles has a large average particle size about 5 nm (**figure 2.5(C-D)**). There are lots of single atoms left in the 2%Pt/Diamond catalyst because the anchoring sites are not in proximity of all single atoms. However, the surface of Volcan XC-72 support contains defects everywhere on the surface including micropores which prevent sintering to some extent and single Pt atoms sinter into smaller nanoparticles with an average particle size about 1 nm (**figure 2.5(E-F)**).

The method is applicable to a variety of transition metals regardless of the ligands in the precursors. **Figure 2.6(A)** shows 1%Pd/Diamond prepared by switched solvent method using tetraamminepalladium nitrate as precursor. Also, 1%Cu/Diamond, 1%Ni/Diamond, and 1%Co/Diamond were synthesized from copper nitrate, nickel nitrate, and cobalt nitrate precursors, (**Figure 2.6(B-D)**) respectively. So, the synthesis method does not require any special ligand or anchoring functional group on the support.

The switched solvent method utilizes the basics of the science in wetting surfaces to produce single atom catalyst or small clusters. The outcome of this method depends on lots of parameters including dielectric constant, surface tension, viscosity, boiling point, hydrogen bonding and other physical properties of second solvent. Also, the ratio of the solvents, heating ramp, and activation process of the catalyst greatly effects the product which needs thorough studies to uncover the underlying effects of each parameter and their interactions.

Applications

Electrochemical Catalysis

The SwiSS method can produce ultrasmall nanoparticles by adjusting the 1:1 molar ratio of acetone to water. The catalysts prepared by SwiSS method showed outstanding performance in electrochemical evaluations in both AEMFC experiments. **Figure 2.7** demonstrates the electrochemical measurements of both 5%Pt/VXC-72 SAC (SwiSS) and 40%Pt/VXC-72 commercial. Part a show the RDE results for comparison between our catalyst and commercial catalyst. The average number of electron transfer is about 3.98 with very low peroxide yield about 1% that suggest the reaction pathway is through the desired 4 electron pathway (part b). In comparison with the commercial catalysts in AEMFC at the high standard industrial conditions by the US DOE, our 5%Pt/VXC-72 slightly outperformed the commercial AEMFC with almost 11 times less precious metal loading per unit area of electrode. The 5% Pt/VXC-72 SAC catalyst with the Pt loading of 0.045 mg Pt/cm^2 showed about 82% of voltage for 40% Pt/VXC-72 with the Pt loading of 0.48 mg Pt/cm^2 at 1000 mA/cm^2. The voltage of SAC was about 92% at higher current

density of 2000 mA/cm^2.The peak power density of both catalysts are the same in the AEMFC (part c). The durability of our catalyst catalyst was evaluated by running the AEMFC for 250 h at the harsh condition of constant 600 mA/cm^2 current density (part d).

Figure 2.8 represents the difference between the catalyst prepared by dry impregnation (**Figure 2.8(A)**) and the SwiSS method (**Figure 2.8(B)**). Both catalysts contain same amount of Pt but the active surface area per unit mass of the SwiSS catalyst is much higher consequently less amount of the catalyst is needed to gain the same performance (**Figure 2.7(C)**) as the commercial catalyst with 40% Pt/VXC-72 shown in **figure 2.8(C)**. The Pt loading of the SwiSS catalyst is 15.7 times lower than the commercial cell with the same performance at milder operational condition. To improve the catalyst performance even more, the microporous VXC-72 was replaced with a mesoporous N-doped carbon (**figure 2.8(D)**). The anode side Pt-Ru bimetallic catalysts are shown in **figure 2.9**. A visual example of the problem that water causes during drying and activation is shown in **figure 2.9(A)** for the dry impregnation of Pt on nitrogen doped carbon support. As explained before, the drying step with the present of only water causes inhomogeneity and sintering of metals. However, the SwiSS method catalyst shown in **figure 2.9(B)** resulted in a uniform, well alloyed, and ultrasmall nanoparticles. Other than very high (60%Pt-Ru) content of precious metals, the commercial catalyst (**figure 2.9(C)**) and dry impregnation catalyst are not well alloyed. The well alloyed catalysts made by SwiSS method maximized the synergistic effects of bimetallic active centers proven to be promoting for the HOR reaction. Another improvement in this work was to make the ultrasmall active centers on commercial VXC-72 support accessible in the reaction media. The ultrasmall sub nanometer particles made by SwiSS method can easily fit inside the

micropores of the VXC-72. Water is the HOR product and part of the reaction media blocking micropores during reaction. Consequently, active centers inside the micropores are not accessible. To make the active centers accessible, the N-C support with only mesopores were selected to make the catalyst by SwiSS method. The AEMFC performance of two HOR catalysts of 4%Ru2%Pt/VXC-72 and 4%Ru2%Pt/N-C shown in **figure 2.10**. The optimized AEMFC performance for the catalyst with mesoporous support outperformed the commercial catalyst with the precious 12.7 times lower metal loading per cm^2 (**figure 2.11**). In summary, **figure 2.11** represents the performance of anode and cathode catalysts prepared by SwiSS method in comparison with a completely commercial AEMFC.

Table 2.1. Summary of proposed single atom catalysts prepared with different solvents.

Cat\Sol.	Solvent 1 (dipole moment)	Solvent 2 (dipole moment)
Pt/Diamond	Water (1.85)	Acetone (2.88)
		Ethanol (1.69)

	Acetone (2.88)	---

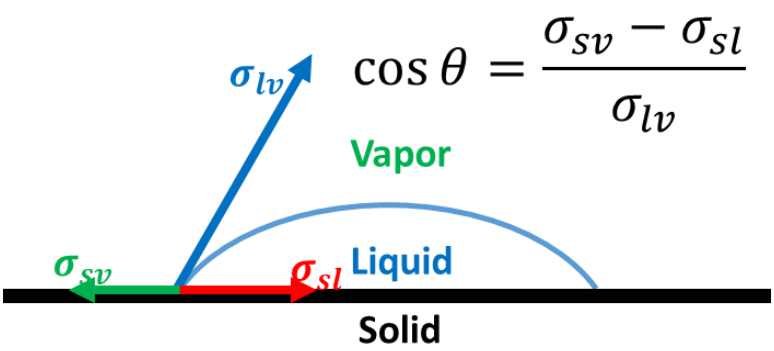

Figure 2.1. Basic equation for contact angle by Young (1805).

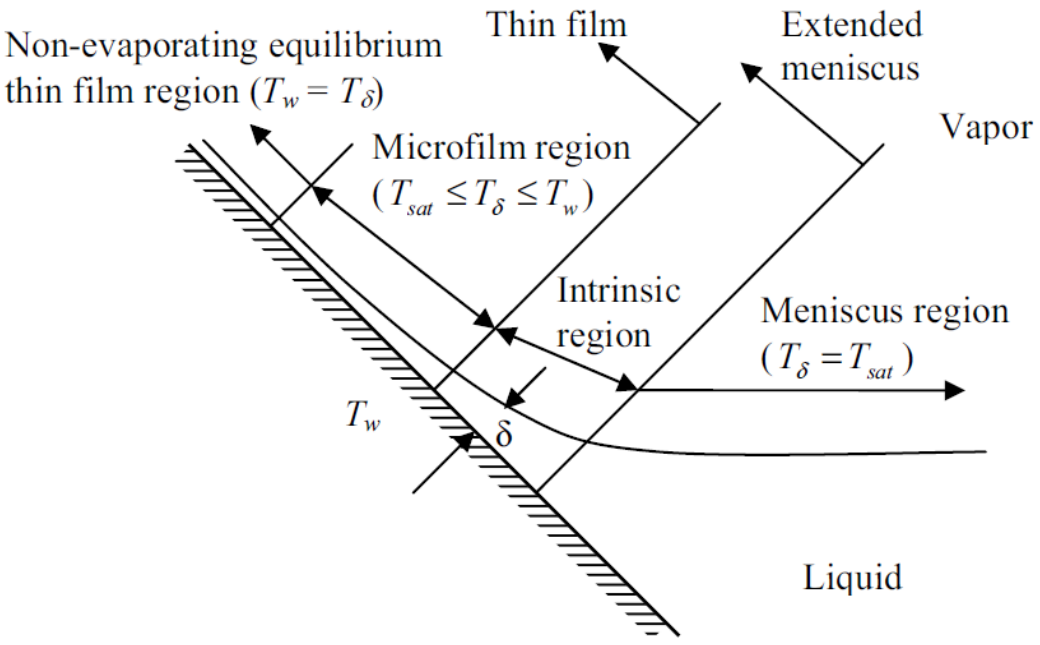

Figure 2.2. Thin film liquid on the support substrate (39).

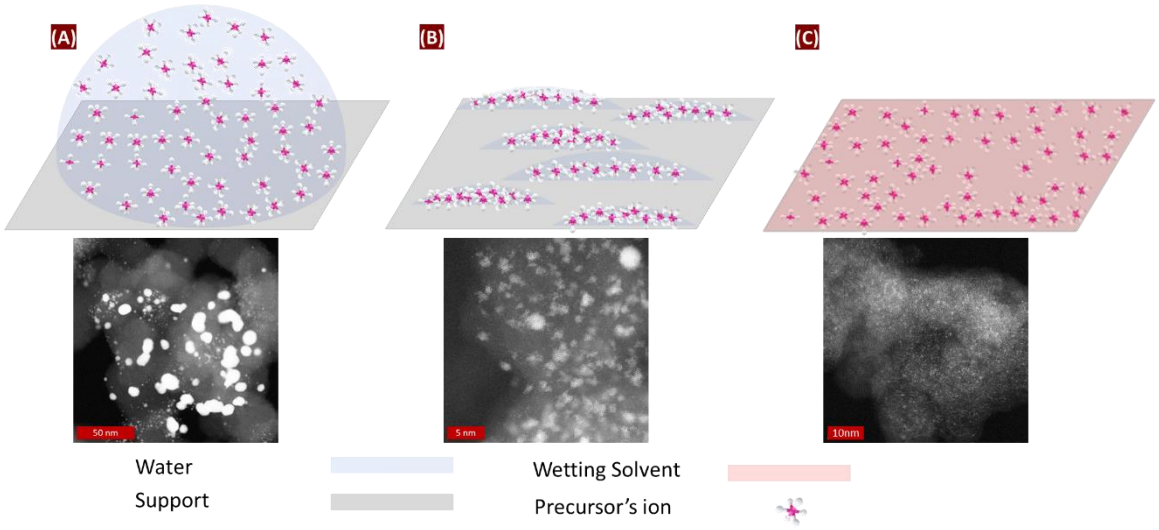

Figure 2.3. Schematic of last step of drying where a small amount of solvent remained in different synthesis methods, (A)impregnation, (B) strong electrostatic adsorption, and (C) use of a wetting solvent to produce isolated precursor's ions. All AC-STEM images contain 7.7%Pt/VXC-72.

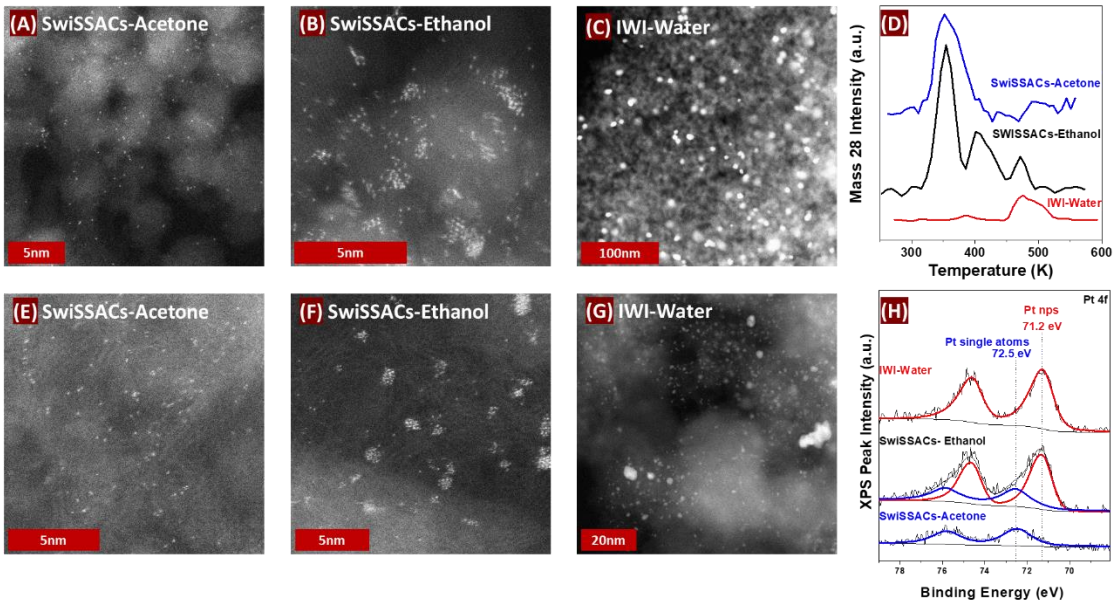

Figure 2.4. Switched solvent effect AC-STEM images of (A) 2%Pt/Diamond switched solvent with acetone, (B) 2%Pt/Diamond switched solvent with ethanol, (C) 2%Pt/Diamond prepared at incipient wetness, and CO-TPD of (A), (B), and (C) samples. AC-STEM images of (E) 2%Pt/VXC-72 switched solvent with acetone, (F) 2%Pt/VXC-72 switched solvent with ethanol, (G) 2%Pt/VXC-72 prepared at incipient wetness, and corresponding XPS spectra of (E), (F), and (G) samples.

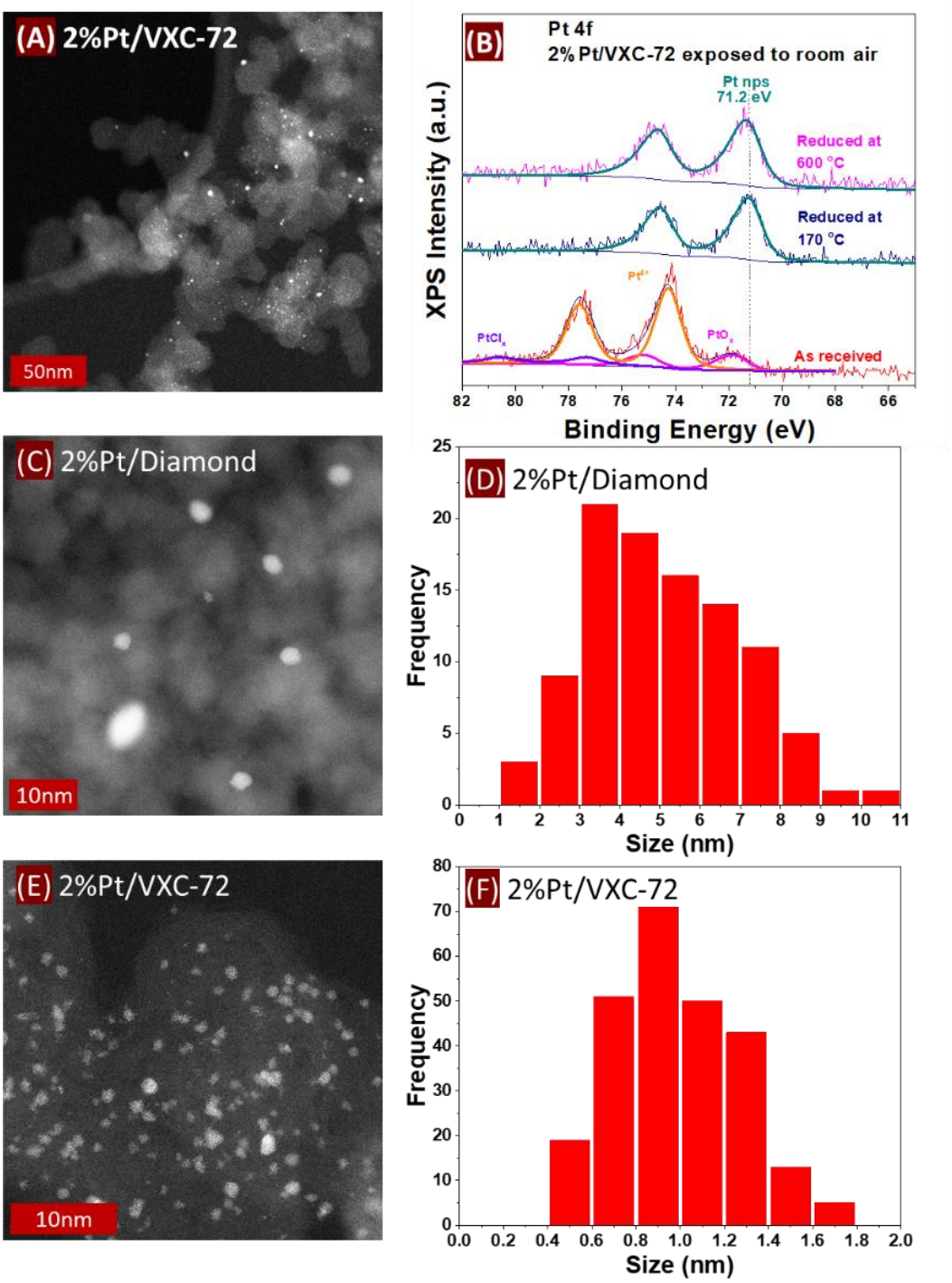

Figure 2.5. Stability of catalysts (A) AC-STEM image of 2%Pt/VXC-72 exposed to room air (moisture) overnight before activation, (B) XPS spectra of 2%Pt/VXC-72 as received, in situ reduced at 170 ˚C, in situ reduced at 600 ˚C, (C) AC-STEM image of 2%Pt/Diamond, (D) particle size distribution activated at 300 ˚C for 3h, (E) AC-STEM image of 2%Pt/VXC-72, and (F) particle size distribution activated at 300 ˚C for 3h.

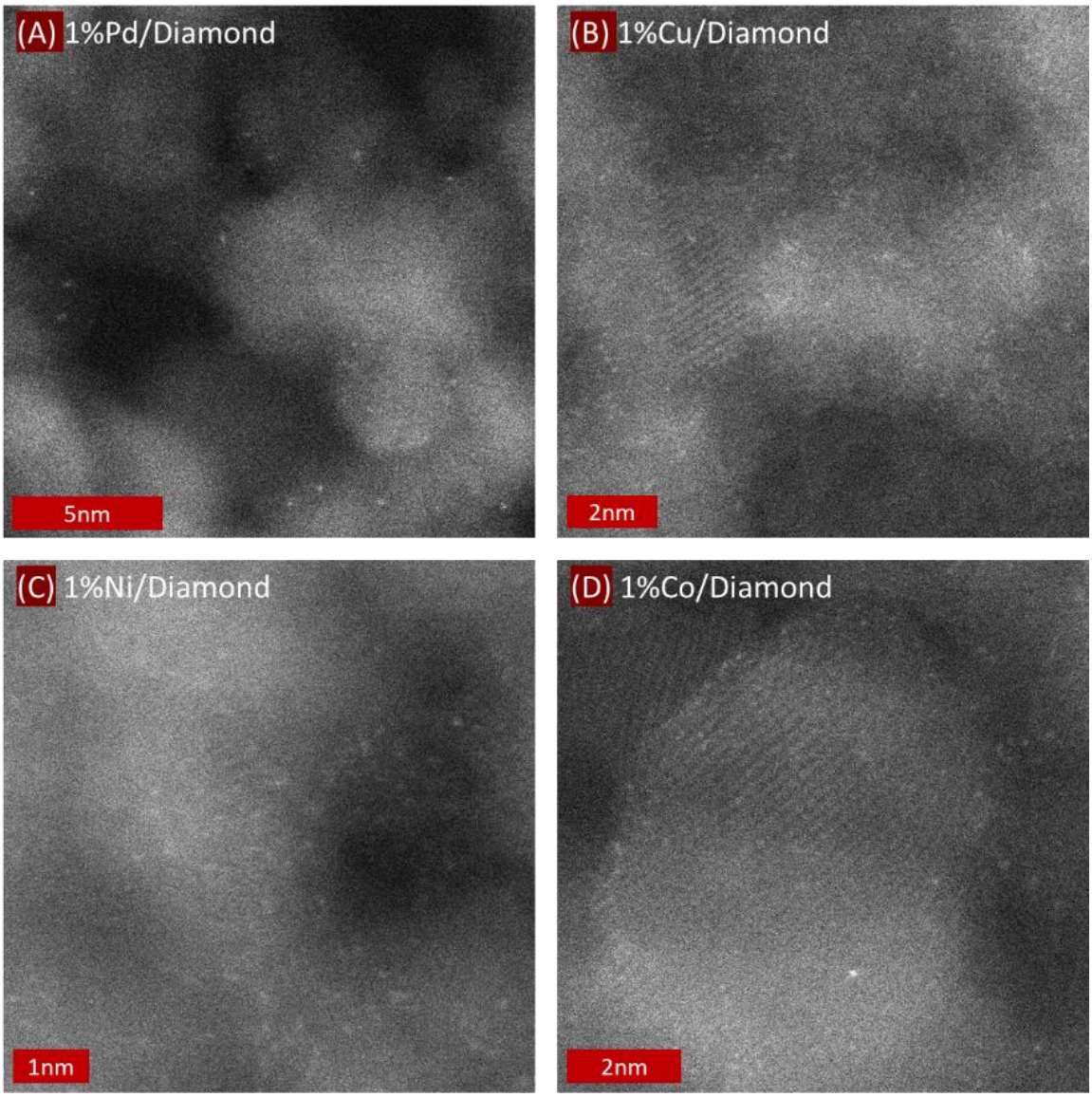

Figure 2.6. Versatility of the switched solvent method. (A) 1%Pd/Diamond, (B) 1% Cu/Diamond, (C) 1% Ni/Diamond, and (D) 1% Co/Diamond**.**

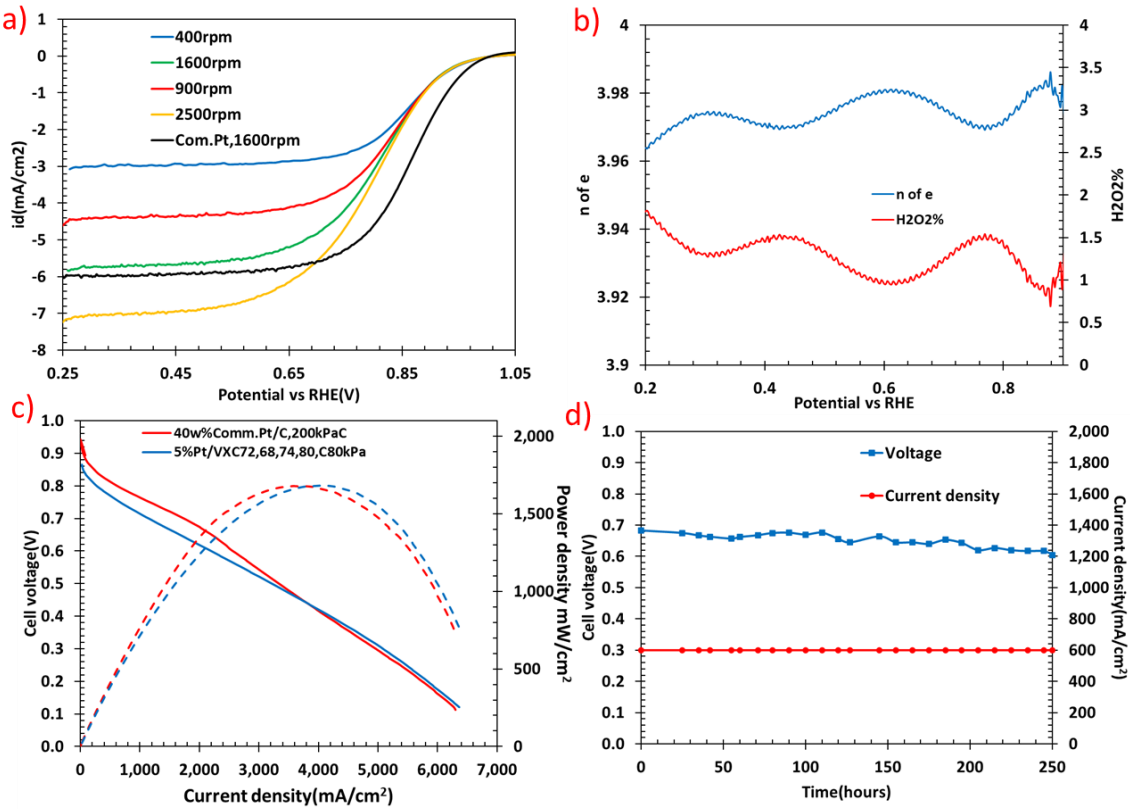

Figure 2.7. Electrochemical measurements, a) RDE of 5%Pt/VXC-72 SAC (SwiSS) and 40%Pt/VXC-72 commercial, b) average number of electron transfer and peroxide yield (RRDE), c) polarization curves and power density curves for both SAC(SwiSS) and commercial catalyst.

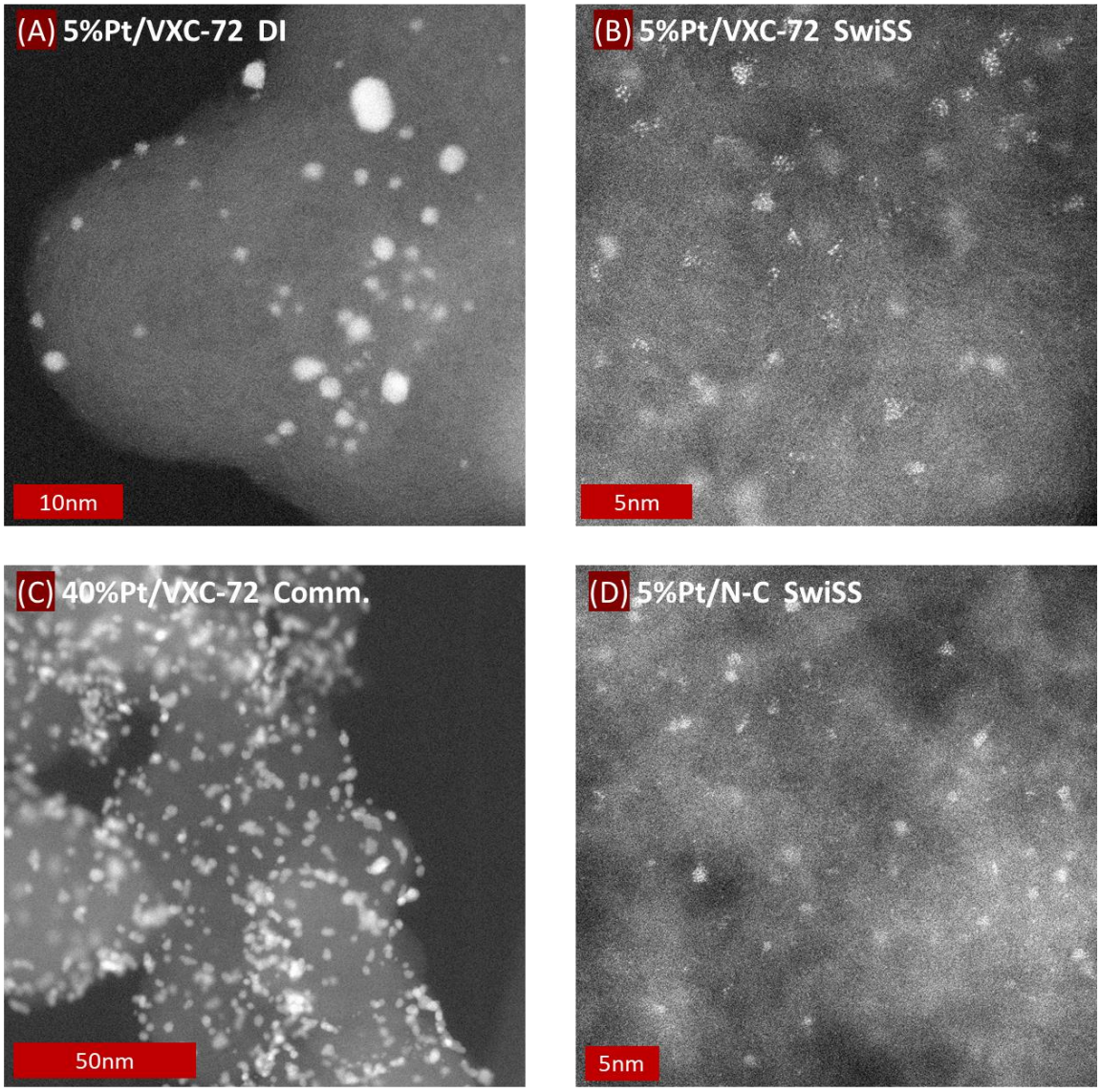

Figure 2.8. Cathode catalyst, (A) 5%Pt/VXC-72, dry impregnation, (B) 5%Pt/VXC-72, SwiSS, (C) 40%Pt/VXC-72 commercial catalyst, (D) 5%Pt/N-C, SwiSS.

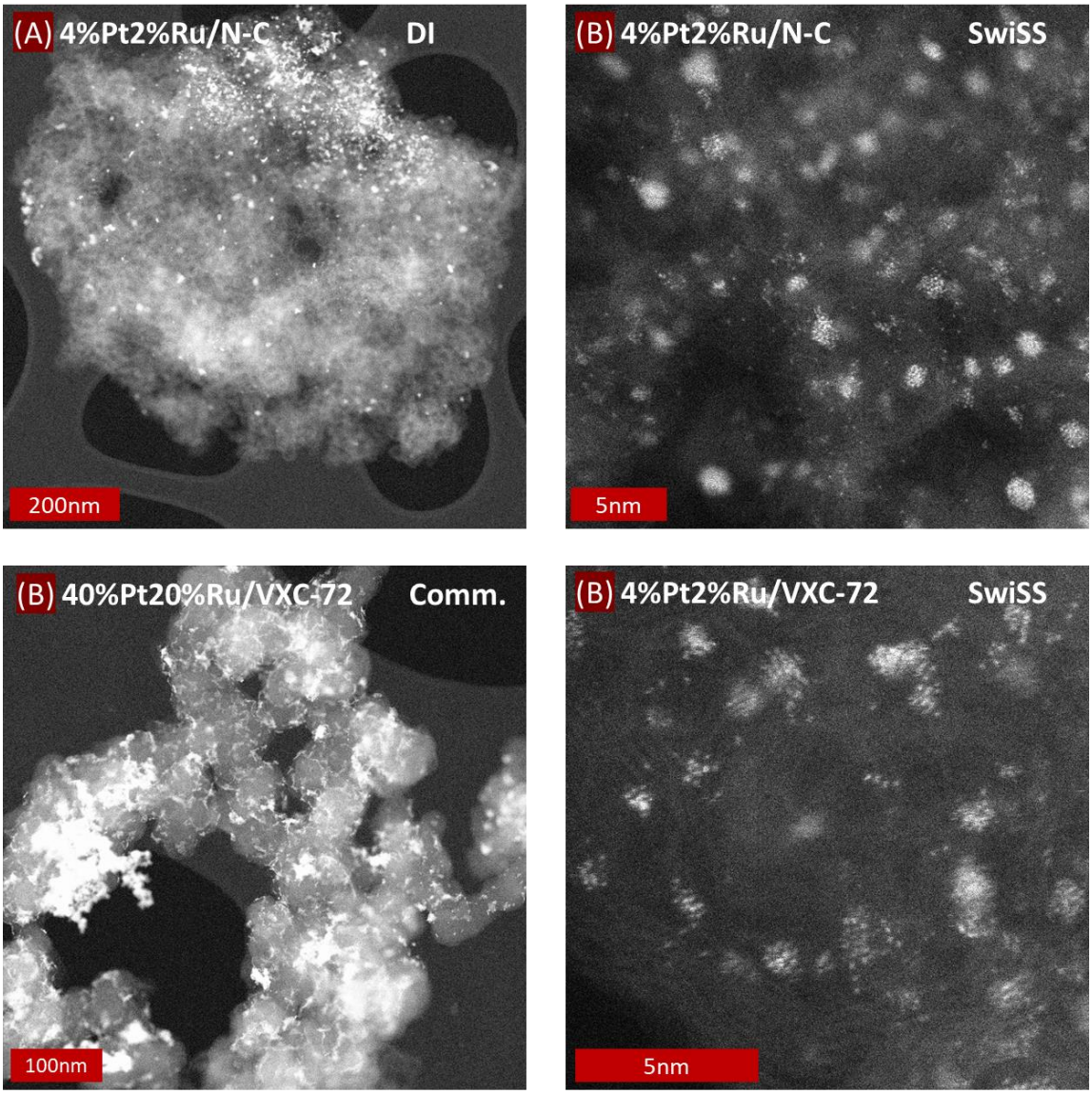

Figure 2.9. Anode catalysts, (A) 4%Pt2%Ru/N-C, dry impregnation, (B) 4%Pt2%Ru /N-C, SwiSS, (C) 40%Pt20%Ru /VXC-72 commercial catalyst, (D) 4%Pt2%Ru /VXC-72, SwiSS.

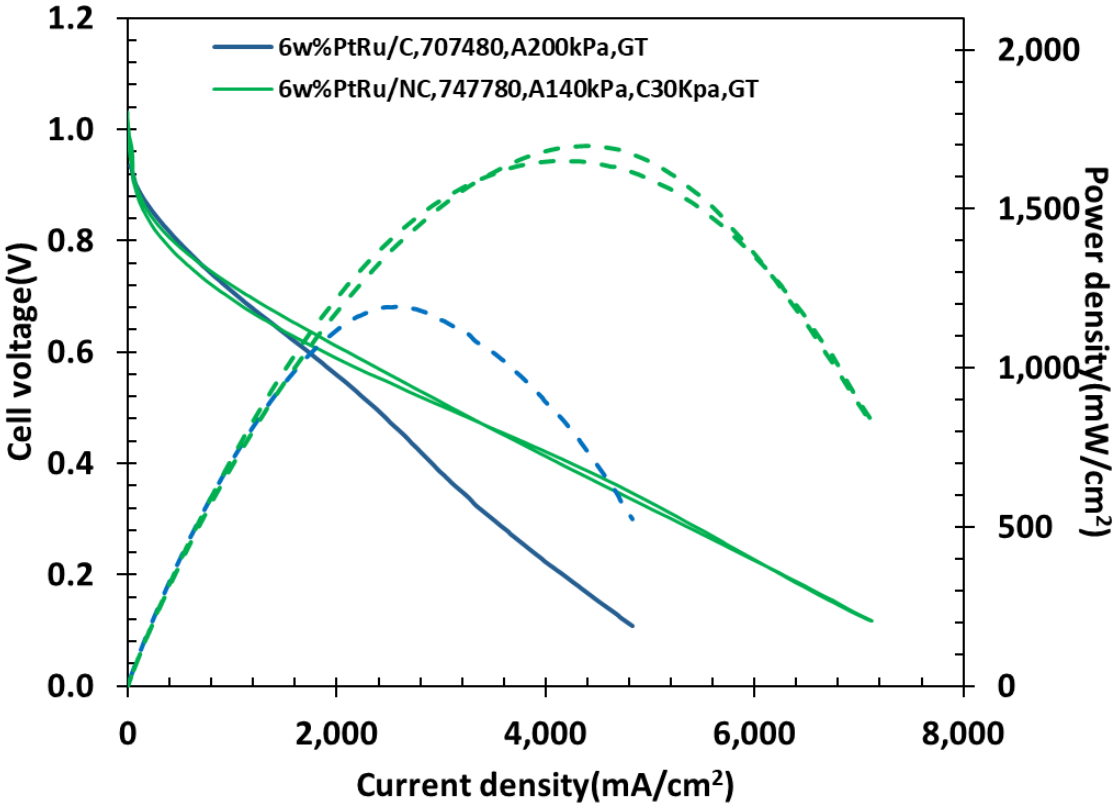

Figure 2.10. Pore size effect of the catalyst support on the performance of AEMFCs.

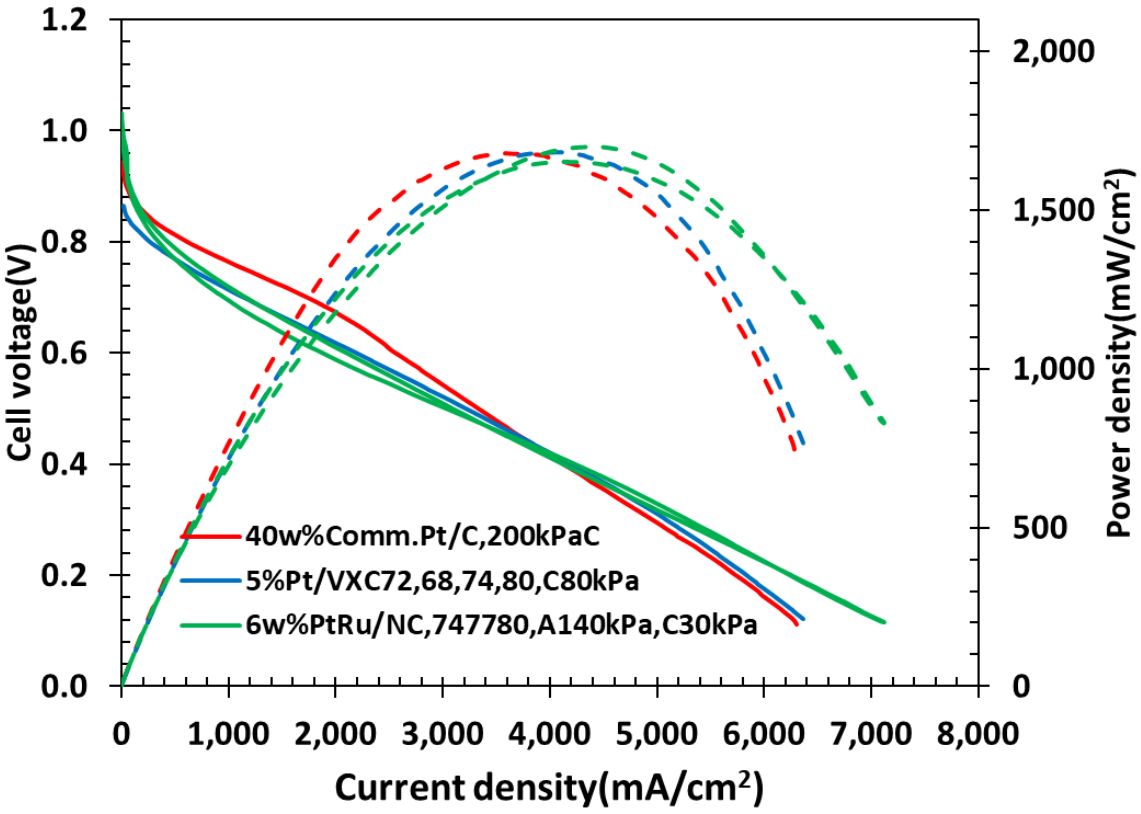

Figure 2.11. Polarization curves and power densities of AEMFCs with 40%Pt/C commercial, 5%Pt/C SwiSS, and 6%Pt-Ru/N-C SwiSS catalysts.

CHAPTER 3

THE SIMPLE SYNTHESIS OF HIGHLY METAL LOADING SINGLE ATOM CATALYSTS VIA CHELATE FIXATION (CHEFI)

New catalytic technologies are ever-growing, considering that 90% of all chemical processes employ some type of catalyst, whether they be homogeneous or heterogeneous in nature (Kaiser et al. 2020). Supported single-atom catalysts (SACs) are at the frontier of catalysis research, promising the combined advantages of homogeneous (e.g., well-defined site, high selectivity) and heterogeneous (e.g., high stability, easy separation) catalysts (Kaiser et al. 2020; Datye and Guo 2021; Samantaray et al. 2020; Jincheng Zhang, Yang, and Liu 2021; Singh et al. 2021; K. Qi, Chhowalla, and Voiry 2020; Mitchell and Pérez-Ramírez 2020). Such well-defined materials have the potential to provide unique catalytic performance due to the intimate electronic interaction between the isolated active site and a given support material. Examples of such materials include preferential oxidation of CO in hydrogen-rich fuel reported on a 2wt% Pt SAC (S. Cao et al. 2020), highly active, selective, and coke-resistant Rh single-atom catalyst dispersed in Cu for low-temperature nonoxidative propane dehydrogenation(Hannagan et al. 2021; Shijia Sun et al. 2021), and a stable heterogeneous single-atom Pd catalyst supported on graphitic carbon nitride for Suzuki coupling (Z. Chen et al. 2018). A general limitation in these studies has been the inability to produce loadings of accessible single atoms that are relevant to industrial applications (L. Chen et al. 2021). In addition, in order to produce and retain isolated single

metal atom sites in the resulting materials, novel and/or complicated synthesis methods have been employed (Y. Chen et al. 2017; Zhong et al. 2019; C. Gao et al. 2018; Sa et al. 2016; Jiang et al. 2019; Ge et al. 2020; Shuhui Sun et al. 2013; Wei et al. 2017; Yao et al. 2019; Adabi et al. 2021). To fully exploit the potential for commercial applications of SACs, the development of scalable and facile synthesis methods that can produce high loadings of isolated active sites is required.

There are many synthetic methods available to deliver metal precursors to catalytic supports (i.e., oxides, carbon). For example, strong electrostatic adsorption (SEA), ensures an even distribution of metal ions on the support surface through control of solution pH (Spieker et al. 2003; Wong et al. 2017a; Jiao and Regalbuto 2008; Lambert et al. 2009). This method can reliably produce small metal nanoparticles (xiong et al. 2020; B.A.T. Mehrabadi et al. 2019), as well as isolated single atoms if the metal loading is low enough (Resasco and Christopher 2020; DeRita et al. 2017). However, at loadings greater than ~0.1 wt%, activation of such catalysts (i.e, through calcination and/or reduction treatments) results in cluster and nanoparticle formation (Jing Zhang et al. 2021; Resasco and Christopher 2020). One strategy to achieve high single metal atom loadings involves the use of chelating agents that complex with the metal precursor and are then pyrolyzed (sometimes along with other organic components) to produce a carbon material with single metal atoms dispersed throughout. However, there are some concerns that not all of the single atoms in such a carbon support matrix are accessible (Kaiser et al. 2020; W. Chen et al. 2020), and the approach is limited to carbon supports.

Recently, Hutchings and co-workers reported promising results using non-aqueous organic solvents to deliver metal salt and organometallic precursors to a carbon support

surface. They were able to achieve single atom species up to a loading of 1 wt% for Au, Pt, Pd and Ru, and demonstrated their efficacy for acetylene hydrochlorination. Due to the instability of the employed precursors in aqueous solution, "extra dry" organic solvents had to be employed (X. Sun et al. 2020). Indeed, solution removal at the last step of the incipient wetness impregnation before the catalyst activation has been reported to form crystallites because of weak interactions and redistribution of precursors ions (Kumar et al. 2004; Sietsma et al. 2006; Haukka, Lakomaa, and Suntola 1999). Even in the case of SEA, incomplete drying of the adsorbed precursors on the support during activation (**Figure A1**) results in the formation of large nanoparticles.

We hypothesized that formation of reduced metal clusters and particles (as opposed to single isolated atoms), even when starting with well-dispersed, adsorbed precursors obtained with SEA, is significantly influenced by the presence of water (**Figure 3.1(A)**). In addition to any bulk water that might remain in support pores even after drying, there is also a significant amount of water associated with each precursor in the form of a hydration sheath (Hao, Spieker, and Regalbuto 2003; Santhanam et al. 1994; Regalbuto 2016). For example, $PtCl_6^{2-}$ is known to retain one hydration sheath, while $Pt(NH_3)_4^{2+}$ is known to retain two hydration sheaths, even upon drying at room temperature. In order to retard (or eliminate) the negative influence of such water on the formation of supported single atoms, a chelating agent was introduced immediately following the precursor adsorption step. This chelating agent, 8-hydroxyquinoline (8-HQ), has a high affinity for transition metals (Mlahi et al. 2015; Martín 2018; Rohini, Paul, and Luxami 2020; Prachayasittikul et al. 2013), and has been shown to adsorb on a variety of carbon surfaces for application in metal extraction (Ravindran et al. 1999; Sheikhmohammadi et al. 2017; Guo et al. 2015).

We surmised that 8-HQ, which is not soluble in water, will anchor the metal precursor on the support surface (**Figure 3.1(B)**). The strong metal-8-HQ interaction coupled and high boiling point of 8-HQ (267˚C), would then allow the metal ion to be reduced with H_2, while avoiding formation of clusters or nanoparticles. [A comparison of SEA with this new chelate fixation (CheFi) method, with SEA alone, for Pt on VXC-72 and TiO_2 support substrates is provided in **Figure A2**. It can be seen that there is significant particle/cluster formation for the SEA sample upon reduction in H_2 at 300˚C, albeit with a very tight particle size distribution (**Figure A1(B)**). However, for the CheFi sample, the sample primarily consists of isolated single atoms, along with few agglomerates as dimers, trimers, etc. It was further found that SEA was not necessary for the CheFi method to be successful. A set of experiments conducted at pH 2.9 over a VXC-72 support (where maximum SEA of the Pt precursor occurs) and 9 (the point of zero charge of the VXC-72 where there is no SEA) shows identical results (**Figure A3(A-B)**). In addition, contrary to SEA, the CheFi synthesis method proved successful at high ionic strength using both anionic and cationic Pt precursors (**Figure A3(C-D)**).]

In this contribution, we demonstrate that this proposed chelate fixation (CheFi) method produces high densities (up to at least ~1 atom/nm^2) of isolated single atoms of Pt on a variety of carbon supports (blacks, activated carbon, diamond), as well as TiO_2 and SiO_2. In addition, the method has been demonstrated for other catalytically important transition metals (e.g., Ir, Ru). The results open up a simple, cheap and scalable method to produce SACs, for both fundamental catalysis studies and practical industrial applications.

Aberration corrected scanning transmission electron microscopy (AC-STEM) has been used to characterize the samples. **Figure 3.2(A-F)** show the images of CheFi-prepared

0.8%Pt/VXC-72, 3.5%Pt/VXC-72, and 7.7%Pt/VXC-72 corresponding to densities of 0.1, 0.45 and 1.0 atom/nm^2. With a reduction temperature of 170°C (**Figure 3.2(A-C)**) the atoms are seen to be completely isolated, while a higher reduction at 300°C causes a small amount of agglomeration at the highest metal loading (**Figure 3.2(F)**). Applying 1 atom/nm^2 on a Norit ROX carbon with a surface area of 1200 m^2/g resulted in 30%Pt/C SACs shown in **Figure 3.2(G-H)**. The higher resolution images show well distributed single atoms. The zoomed inset emphasizes the contrast signal overlap from single atoms in different focal planes as a white haze below and above the single atoms in focus. The higher temperature reduction (300°C) again causes a slight amount of agglomeration (**Figure 3.2(H)**). As some blurring is caused by the three-dimensional sample not all being in the focal plane, this was further explored. **Figure A4** shows the same area with either the left-hand focused (**Figure A4(A)**) or the right-hand (**Figure A4(B)**). Atoms are clearly resolved when any section of the sample is brought into focus. Such imaging strongly suggests that the metal atoms are not only present on the outer surface of the support, but within the support pore framework.

Further characterization has been performed with XPS and CO-temperature programmed desorption. The in-situ XPS measurement of Pt 4f peaks of 2%Pt/VXC-72 prepared by standard dry impregnation before reduction in hydrogen is shown in **figure A5(A)**, and contain several species of Pt, including PtO_x at 72 eV, Pt^{4+} at 72.9 eV, and $PtCl_6$ at 75.7 eV. After an in situ reduction at 300˚C only one Pt species peak at 71.2 eV is observed, and is associated with the Pt 4f of metallic Pt nanoparticles (Therrien et al. 2018). Indeed, reduction of the sample to 600˚C resulted in the same position of the Pt 4f peak, confirming it as a reference for Pt nanoparticles. A 2%Pt/VXC-72 catalyst prepared

using CheFi showed different species of Pt in as received sample demonstrated in **figure 3.3(A)** and after in situ reduction at 170˚C, 300˚C, and 600˚C Pt 4f peak showed up at the characteristic position of 71.2 eV for nanoparticles and 72.4 eV for single atoms. Before reduction at 600˚C, the catalyst was reduced at 170˚C, with the XPS spectrum shown in **figure 3(A).** This corresponds to STEM images (**figure A5(B)**) revealing only single Pt atoms, with the associated Pt 4f peak shifted to 72.4 eV (Huabin Zhang et al. 2018). The small peak at 70.9 eV is attributed to formation of single atom Pt carbide atoms (Vu et al. 2011). The sample reduced at 300˚C demonstrated two Pt 4f peaks at both 71.2 and 72.4 eV, associated with nanoparticles and single atoms, as seen in the associated STEM images (**figure A5(C)**). The 30% Pt/C_{Norit} fresh catalyst was slightly more oxidized than the fresh 2% Pt/VXC-72 shown in **figure 3.3(B)**. The 30% Pt/C_{Norit} catalyst reduced at 100˚C resulted in a single specie associated with single atoms while reduction at 170˚C resulted in coordination of single atoms together because of high density of single atoms (**figure 3.2(G)**). A higher temperature reduction at 300˚C resulted in coordination of all Pt atoms and formation of very small clusters shown in **figure 3.2(H)**.

Temperature programmed desorption of CO (CO-TPD) can further distinguish between SACs and catalysts containing nanoparticles (Hulva et al. 2021). The results in **figure 3.3(C)** demonstrate the difference in CO desorption temperature from SACs and catalyst containing both SACs and nanoparticles. The bottom (black) curve shows CO desorption profile from the 2%Pt/VXC-72 catalyst that was first reduced at 170˚C. A main CO desorption peak appears at 350K, and is attributed to desorption from single Pt atoms (Therrien et al. 2018). A small shoulder at 400 K can be attributed to the Pt carbide in the catalyst(Therrien et al. 2018), consistent with the XPS results (Vu et al. 2011). The top

(blue) curve shows the CO desorption profile for the 2%Pt/VXC-72 catalyst reduced at 300˚C. Desorption peaks are observed at 350K and 480K, and arise from single atoms and nanoparticles, respectively. These observations are once again consistent with the AC-STEM images of the catalyst treated at 170˚C (**figure A5(B)**) and 300˚C (**figure A5(C)**). Since a large fraction of Pt atoms is inside the nanoparticles and are not accessible to adsorb CO, the intensity of the CO desorption peak is much smaller than the peak from single atoms. **Figure 3.3(D)** (blue) demonstrate CO-TPD of 30% Pt/C_{Norit} reduced at 100˚C resulting in majority of single atom confirming the XPS results (**figure 3.3(B)**). Further reduction at 170˚C resulted in the majority of Pt atoms coordination into dimers, trimers, and ultrasmall clusters resulted in CO desorption at higher temperatures (**figure 3.3(D)** dark green). The CO-TPD of 30% Pt/C_{Norit} reduced at 300˚C showed formation of more small nanoparticles (**figure 3.2(H)**) resulted in CO desorption at slightly higher temperature close to the CO desorption temperature from nanoparticles (**figure 3.3(D)** light green).

Because the chelating agent is not soluble in water a polar solvent like acetone is needed to dissolve the chelating agent and with a dipole moment higher than water, replaces water to facilitate the chelating process. The presence of water in the system exerts a repulsive force on the chelated complex of metal ion to the more stable surface of the solid support during activation and results in immobility of the catalyst precursor complex.

The CheFi method appears to be applicable to a variety of transition metals, regardless of the presence of ligands in the precursors. The 8-HQ can chelate metal ions (Martín 2018; Zborowski et al. 2013; Guo et al. 2015) or metal ion complexes with ligands(Warr et al. 2009; Uysal et al. 2017; Carson et al. 2015). For example, **Figure A6**

shows the platinum NMR taken during 8-HQ interaction with hexachloroplatinate anion. The results show a peak for platinum at 224.1 ppm suggest the chelating agent chelate the metal ion complex as well. A catalyst using the platinum nitrate as precursor on nanodiamond is shown in **figure 3.4(A)**.

The CheFi method appears to be very versatile with respect to both supports and metals. In addition to VXC-72 (i.e., carbon black) and Norit ROX (activated carbon), Figure 4B shows a representative STEM image for 1% Pt on nanodiamond. The result shows that single Pt atoms can be produced on a support that has no surface functional groups. Silica and titania are two other common industrial oxide support substrates, and CheFi also yielded isolated Pt atoms (**figure 3.4(C) (figure A7),** and **figure 3.4(D),** respectively). With different metals, **Figures 3.4(E) and 3.4(F)** show VXC-72-supported catalysts containing 3.5%Ir and 1.8%Ru prepared by the CheFi method.

In conclusion, the CheFi method is a simple, fast, and readily scalable synthetic strategy to produce SACs utilizing pre-existing support substrates. Perhaps most exciting is that the CheFi method is extremely simple, scalable, and can be applied to a wide variety of precursors regardless of the presence of ligands, charge, and ionic strength of the synthesis media.

FTIR

The Fourier transform Infrared spectroscopy using CO as a probe bonding with SACs. In general, as a probe, room temperature chemisorption of CO can be utilized to determine the characteristics of the catalyst surface via FTIR. At low coverage, it shows a single band at 1920 cm^{-1}, and it shifts to higher frequencies with an increase in coverage. Investigations on Pd single crystal surfaces showed that the coordination number of surface

sites has a role in determining the band position. Dipole-dipole coupling mode leads to a continuous shift of absorption band to higher frequencies with increasing in coverage. At low coverages, a combination of dipole-dipole coupling and indirect effects via the host is responsible for the shift in frequencies. However, a direct molecular repulsion affects the chemisorption band so strongly that it covers the other effects at higher coverages. An increase in coverage of CO molecules on the surface causes a decrease in back donation into 2π orbital of the CO. Consequently, the adsorption energy decreases, and the CO stretch frequency shifts to higher wavenumbers. In the case of SACs, the isolated atoms are far from each other, and the back donation will be minimum from a single atom, so the CO stretch frequencies on SACs are expected to shift to the higher wavenumbers. The CO stretch frequency for clusters/nanoparticles are expected to appear at lower wavenumbers. The effect of support substrate will be considerable in the position of the CO stretch frequency on single atom metals in the catalyst. **Figure** shows in situ FTIR spectra both during reduction and CO adsorption on 0.98%Pt/Diamond SAC prepared by CheFi. In part a, stack of spectra every 10˚C starting from 30˚C-300˚C in-situ reduction of the catalyst revealed that almost all the chelating agent peaks removed at 170˚C. The CO adsorption carried out following the reduction. After saturation by CO, the system purged with N_2 until the gas phase CO removed and stable adsorbed CO remained (part b). The CO-FTIR study confirmed the results from XPS and CO-TPD which confirms presence of both single atoms and clusters/nanoparticles in SAC reduced at 300˚C.

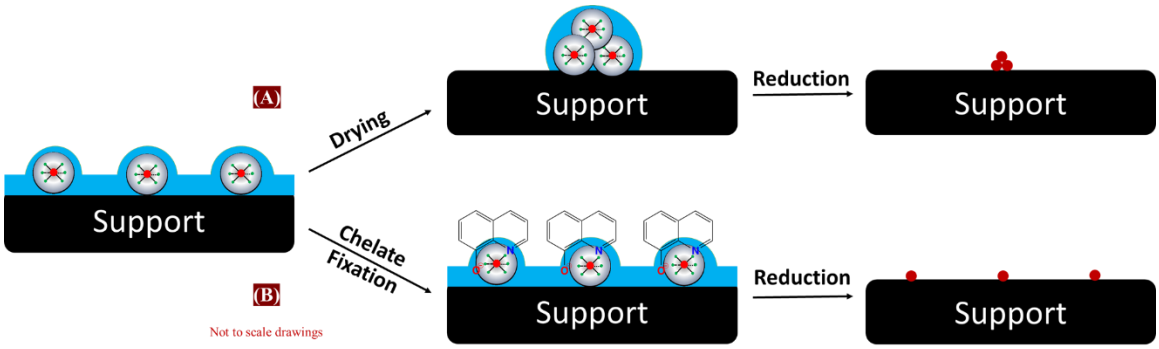

Figure 3.1. Schematic of hypothesis and synthesis methods, (A) effect of water during drying and activation of the catalyst, (B) chelate fixation during drying and activation.

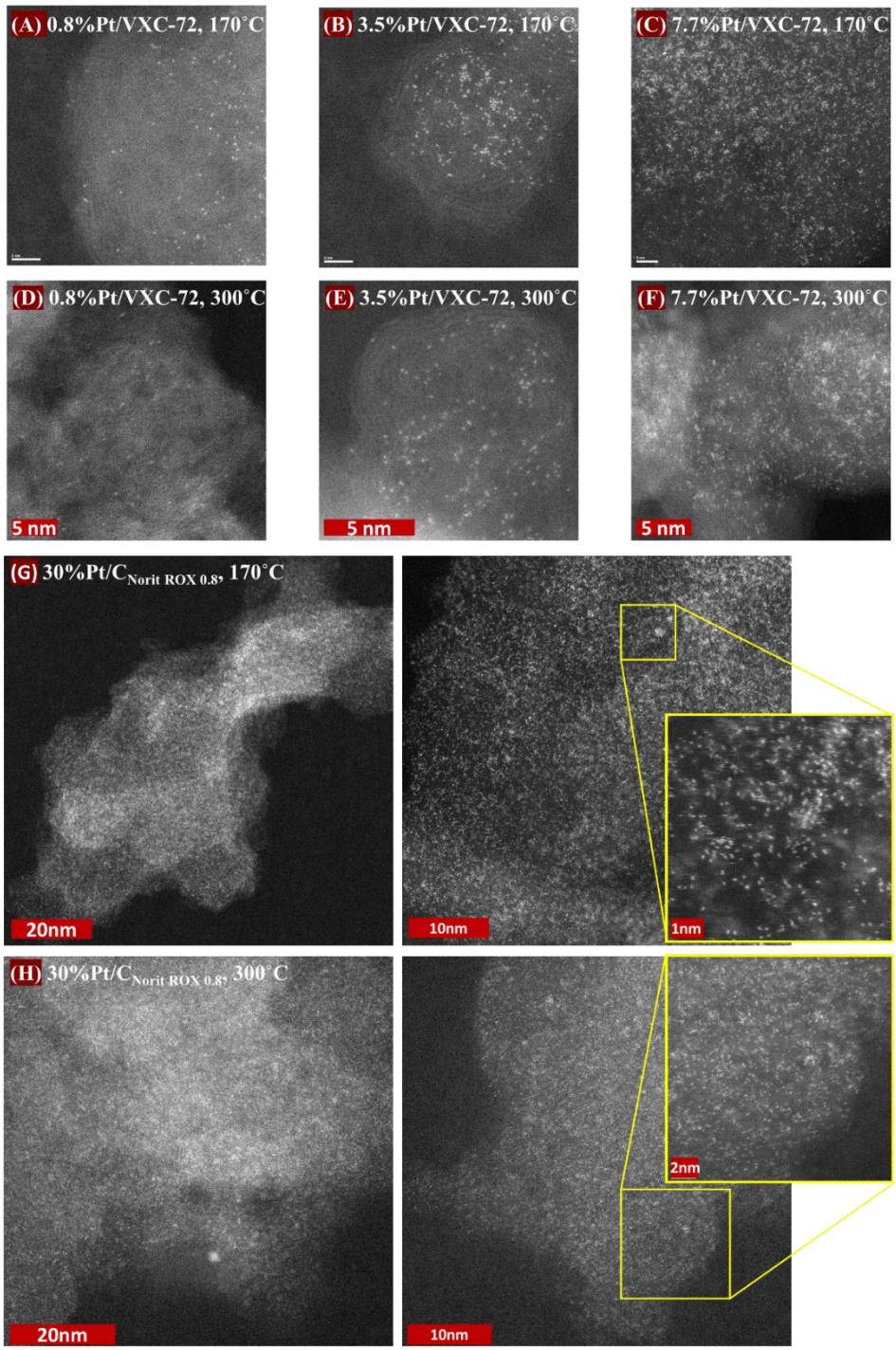

Figure 3.2. Various densities of single atom supported catalysts. AC-STEM images of 0.8%Pt/VXC-72 CheFi, 3.5%Pt/VXC-72 CheFi, 7.7%Pt/VXC-72 (1 Pt atom/nm^2) CheFi reduced at (A-C) 170˚C, and (D-F) 300˚C, 30%Pt/C_{Norit} (1 Pt atom/nm^2) CheFi-reduced at (G) 170˚C, and (H) 300˚C.

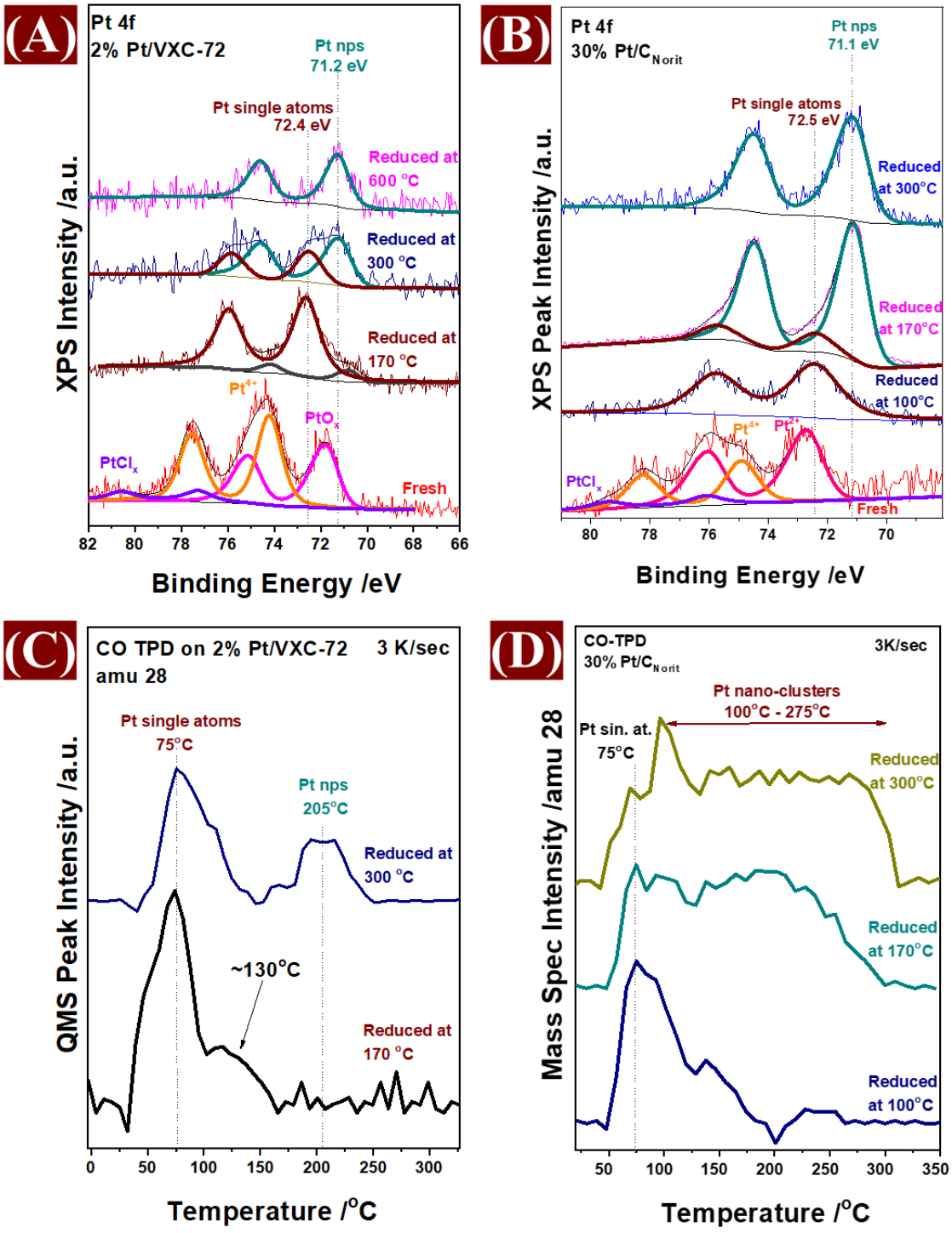

Figure 3.3. In Situ XPS studies & CO TPD, In situ XPS spectra of (A) fresh, reduced at 170˚C, 300˚C, and 600˚C 2%Pt/VXC-72 CheFi, (B) fresh, reduced at 100˚C, 170˚C, and 300˚C 30%Pt/ C CheFi, (C) CO-TPD of 2%Pt/VXC-72 CheFi in situ reduced at 170˚C and 300˚C, (D) CO-TPD of 30%Pt/ C CheFi in situ reduced at 100 ˚C , 170˚C and 300˚C.

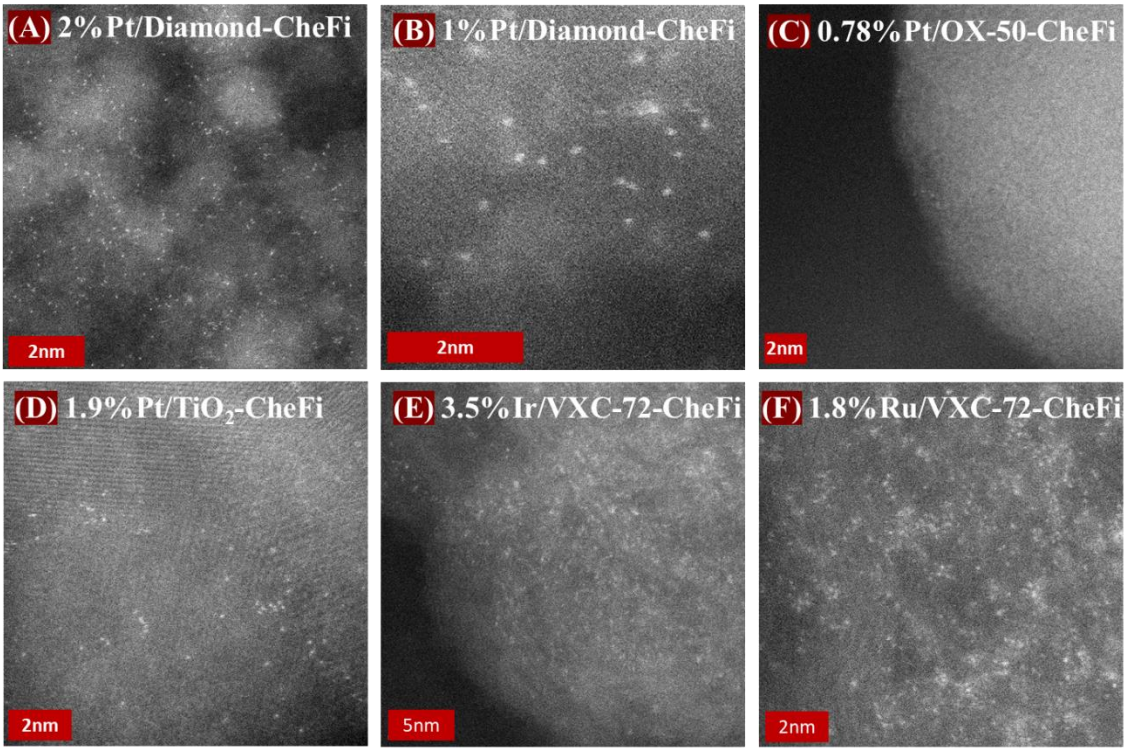

Figure 3.4. Versatility of the CheFi method. (A) 2%Pt/Diamond (platinum nitrate precursor), (B) 1% Pt/Diamond, (C) 0.78% Pt/SiO_2, (D) 1.9% Pt/TiO_2, 3.5%Ir/VXC-72, and 1.8%Ru/VXC-72**.**

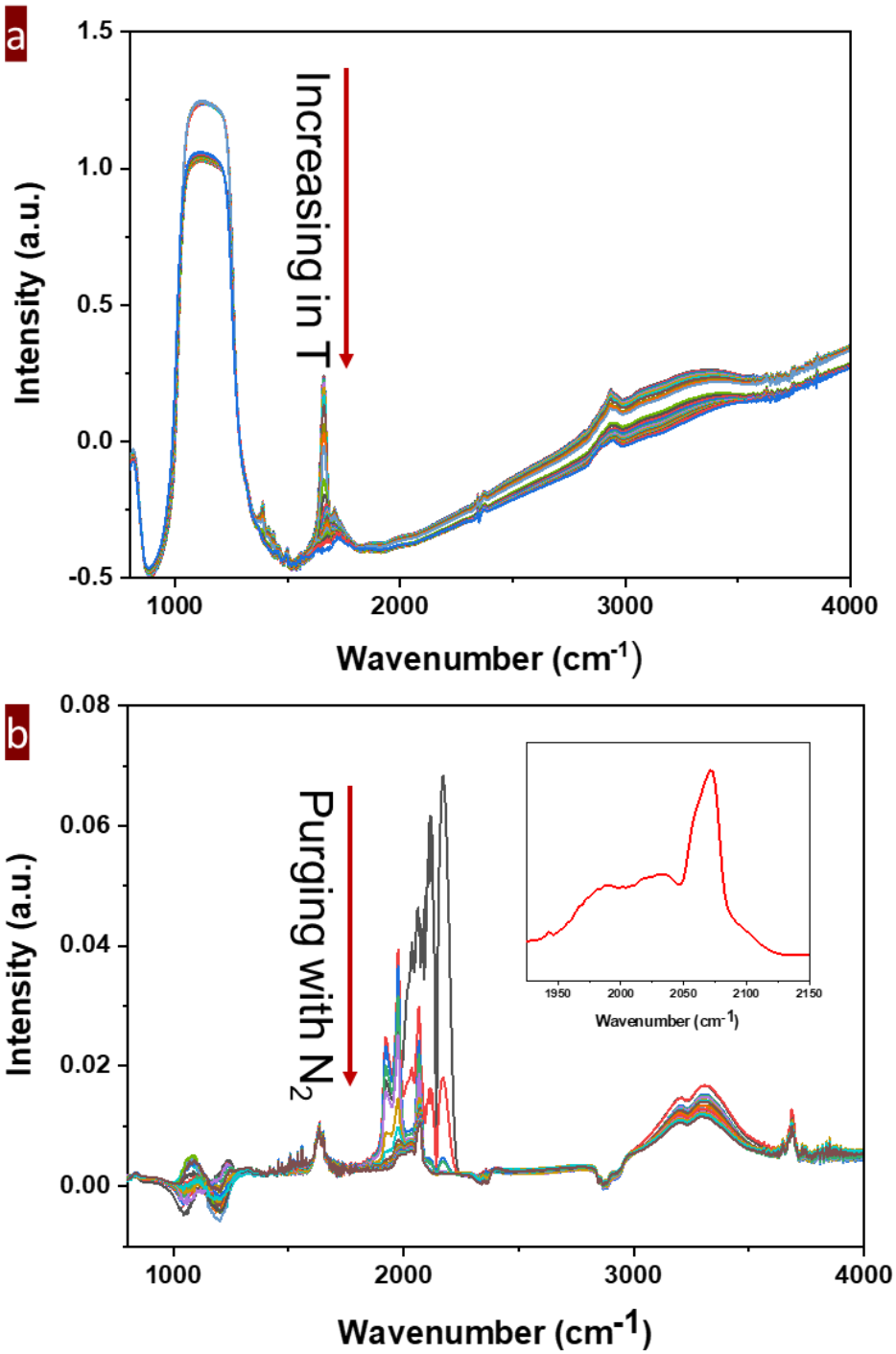

Figure 3.5. In situ FTIR spectra of 0.98%Pt/Diamond a) in situ reduction under 10%H_2/N_2 and b) CO adsorption and purging with N_2 to remove gas phase CO, adsorbed CO remaining (in set).

CHAPTER 4

EVALUATION OF PALLADIUM/GOLD DILUTE LIMIT ALLOY FOR PARTIAL OXIDATION OF 1-PHENYLETHANOL

Introduction

Useful chemicals are widely synthesized by homogeneous transition metal-catalyzed reactions. However, the aggregation and precipitation of atomically dispersed catalysts cause considerable loss of activity(Enache et al. 2006). For example, palladium-based catalysts, while being some of the most versatile, are known to aggregate to form Pd black(Iwasawa et al. 2004). This has spurred interest in the heterogenization of atomically dispersed Pd catalysts to impart stability and facilitate recyclability.

Supported atomically dispersed Pd on La-modified Al_2O_3 first time reported (2001) as an active catalyst for CO oxidation reaction. However, sintering of Pd single atoms under reaction conditions with temperatures higher than 100 °C was an issue. The sintered Pd particles could be dispersed again by calcination at 700 °C in air(Peterson et al. 2014). The activity of Pt and Au single-atom catalyst reported being much higher than the Pd single-atom catalyst. However, a recent study has shown that CeO_2 supported Pd single-atom catalyst has high activity for CO oxidation because of interactions between PdO_x species and CeO_2 in the catalytic cycle(Abbet et al. 2001; L. Liu and Corma 2018; Spezzati et al. 2017; Su et al. 2018).

As a probe, room temperature chemisorption of CO can be utilized to determine the characteristics of the catalyst surface via FTIR. At low coverage, it shows a single band at 1920 cm^{-1}, and it shifts to higher frequencies with an increase in coverage. Investigations on Pd single crystal surfaces showed that the coordination number of surface sites has a role in determining the band position. Dipole-dipole coupling mode leads to a continuous shift of absorption band to higher frequencies with increasing in coverage. At low coverages, a combination of dipole-dipole coupling and indirect effects via the host is responsible for the shift in frequencies. However, a direct molecular repulsion affects the chemisorption band so strongly that it covers the other effects at higher coverages. An increase in coverage of CO molecules on the surface causes a decrease in back donation into 2π orbital of the CO. Consequently, the adsorption energy decreases, and the CO stretch frequency shifts to higher wavenumbers.

Selective oxidation of alcohols on heterogeneous catalysts has been reported with high activity and selectivity using supported nanoparticles such as Pd, Au, Pt, etc(Davis, Ide, and Davis 2013; Abad et al. 2005; Enache et al. 2006). Iwasawa et al. investigated Pd based homogeneous catalysts to decrease metal aggregation and precipitation in alcohol oxidation processes(Iwasawa et al. 2004). Later, Enache et al. studied the oxidation of primary alcohols to aldehydes using a heterogeneous bimetallic Au-Pd supported catalyst (Enache et al. 2006). The isolated single atoms are shown as active sites for oxidation of the alcohols. Hackett et al.(Hackett et al. 2007) made supported single Pd atoms for selective oxidation of allylic alcohols. A strong size effect on TOFs in crotyl alcohol oxidation observed from single Pd atoms to Pd nanoparticles. The difference in TOFs was as large as two orders of magnitude in case of mesoporous alumina support. The highest

TOF belongs to isolated single Pd atoms while preserving an excellent selectivity. The partial oxidation of allylic alcohols can be carried out by supported Au catalyst resulting in very high selectivity towards carbonyl compound products. In comparison, the supported isolated Pd single atoms catalyst (4400 h^{-1} at 60 °C) has much higher activity with slightly less selectivity (~90%) than the supported Au catalyst (538 h^{-1} at 120 °C) with very high selectivity (99%) towards carbonyl compound products. The lifetime of the Pd single-atom catalyst for selective oxidation of allylic alcohols was not mentioned but the lifetime of the Au nanoparticle catalysts was very long(Abad et al. 2005; L. Liu and Corma 2018; Hackett et al. 2007).

An isolated metal atom in a second metal particle might lead to a unique bimetallic catalyst. The lattice mismatch, steric isolation, electronical effect of the host particle, and bimetallic catalytic interactions provide coordinatively unsaturated active centers that might be a heterogeneous mimic of a homogeneous catalyst. A rational advanced method of catalyst preparation is strong electrostatic adsorption (SEA) (Wong et al. 2017b; Bahareh Alsadat Tavakoli Mehrabadi et al. 2019). The SEA is a simple and scalable rational method for catalyst preparation. It offers a better degree of control over the dispersion of catalysts resulting in very small and uniform nanoparticles. The result can further improve with tuning treatment conditions, ensuring the accessibility of active centers. The Single-atom alloy (SAA) catalysts or single-atom catalysts (SAC's) have been demonstrated superior performance for selective hydrogenation (Y. Cao et al. 2020; Lucci, Liu, et al. 2015; Boucher et al. 2013; Yang and Yang 2017; Pei et al. 2014; Fu and Luo 2013; Jilei Liu et al. 2017; Xinrui Cao, Fu, and Luo 2014; Aich et al. 2015; Xinxiang Cao et al. 2015; Lucci, Marcinkowski, et al. 2015; Simonovis et al. 2019; Jilei Liu et al. 2019),

selective oxidation (H. Li, Chai, and Henkelman 2019; Kim et al. 2018), alcohol dehydrogenation (Giannakakis et al. 2018), and C-H activation (Darby et al. 2018; Marcinkowski et al. 2018; Shan et al. 2018; H. Li, Chai, and Henkelman 2019), among other reactions (Greiner et al. 2018; Kruppe, Krooswyk, and Trenary 2017b; C.-H. Chen et al. 2019; Kruppe, Krooswyk, and Trenary 2017a; Thirumalai and Kitchin 2018; Nigam and Majumder 2018; Kim, Kim, and Lee 2018; Lucci et al. 2016; Xing et al. 2019; Shi et al. 2014; Z.-T. Wang et al. 2018).

In this study, we demonstrate the synthesis of a supported, dilute limit alloy of Pd in Au. Using the simple method of co-electrostatic adsorption(Wong et al. 2017b) with small amounts of Pd precursor relative to Au, Pd sites are isolated in the surface of silica-supported Au nanoparticles. Here we employ the partial oxidation of 1-phenylethanol, for which the selective product acetophenone will only occur over isolated Pd sites(Enache et al. 2006; Iwasawa et al. 2004). Site isolation is confirmed with in situ CO adsorption in an FTIR flow cell as well as measurements of catalytic reactivity.

Materials

Aerosil 300 amorphous silica (280 m^2/g, PZC 3.6) was used as support. Catalysts with different molar Pd:Au ratio of 3:1, 1:1, 1:3, 1:5, 1:14, 1:28, 1:53, and monometallic Pd and Au catalysts were synthesized. The Au precursor was synthesized using hydrogen tetrachloroaurate (III) hydrate 99.9% to make trichlorobis(ethylenediamine)gold(III). Tetraamminepalladium(II) chloride was used as a Pd precursor.

Strong Electrostatic Adsorption (SEA)

The catalyst was prepared using the simple and scalable method of strong electrostatic adsorption (SEA) (Wong et al. 2017b; Bahareh Alsadat Tavakoli Mehrabadi et al. 2019).

In situ FTIR Spectroscopy

A Fourier transform infrared spectroscopy (FTIR) model to develop a probe method of identifying the isolated catalytic sites in a single atom catalyst has been developed. The FTIR measurements were performed with a Thermo ELECTRON CORPORATION/NICOLET 4700 FTIR spectrometer system equipped with an MCT-B detector cooled by liquid nitrogen. A homemade in situ flow cell was used in conjunction with a gas switching manifold. All catalysts individually pressed into a 15 mg pellet and reduced in situ at 400 ˚C under 10% H_2 balance He atmosphere and cool down in the flow of He gas before CO adsorption. A background FTIR spectrum was taken on the surface of the catalyst pellet and set as the background for all spectra taken from that specific catalyst. The background was double-checked with collecting a spectrum that showed a flat line to make sure of the quality of the background prior to CO adsorption. A 1% CO balance He gas stream was used to saturate the surface of the catalysts and FTIR spectra were collecting frequently. Then, to remove gas-phase CO from pores of the catalyst pellet and the cell, pure N_2 gas was purged to the system and FTIR spectra collected frequently until equilibrium that there was no visible change in the intensity of the spectra.

1-Phenylethanol Partial Oxidation Reaction

The catalysts were evaluated for the oxidation of 1-phenylethanol (PE) in a 110 ml semi batch reactor (Autoclave Engineers) at 50 psig and 160 °C, with a stirring rate of 400

rpm. The reactor is only open to a small O_2 flow to maintain reaction pressure. In all cases, the initial reactor loading was 50 ml 1-phenylethanol and 106 mg catalyst. Much attention was placed on ensuring the safety of the reaction. The reactor is equipped with a rupture disk, as is standard for performing high pressure reactions. In addition, a needle valve was installed to control O_2 flow to the reactor. This valve is opened only to the level required to maintain the reaction pressure in the vessel. Thus, in the event of a thermal runaway, the reactor will quickly become starved of oxygen and the rate will be limited, providing the opportunity to shut the system down. No evidence of any uncontrolled reaction has been observed. The compositions of liquid reactant and products at various reaction times were measured using a gas chromatograph (HP 5890) coupled to an autosampler.

Results and Discussion

The FTIR data in **Figure 4.1** show the adsorbed CO spectra and deconvoluted peaks of various types of CO adsorption on the catalysts. CO adsorption favors non-linear adsorption on the surface of Pd. In the case of the bimetallic catalyst, the presence of the Au further promotes the nonlinear CO adsorption. **Figure** shows the CO adsorption spectra on the monometallic Pd catalyst and 1:3 molar ratio of Pd-Au bimetallic catalysts. The intensity of the nonlinear CO adsorption peaks is higher than linearly adsorbed CO that confirms the presence of the Au promotes nonlinear CO adsorption. Because of the difference in surface free energy, most of the Pd atoms are expected to be positioned on the surface of the bimetallic Au-Pd catalysts. There are DFT studies that suggest bridge mode adsorption of the CO on the interface of Au-Pd atoms. The bright red deconvoluted peak is assigned to the bridge adsorption of the CO on Au-Pd sites. The linear CO adsorption is more favored when the surface is saturated with CO or there are only isolated

Pd sites on the surface. On the monometallic Au surfaces, CO adsorption is almost negligible at room temperature.

The CO adsorption on monometallic Pd was used as a reference to fit the position and shape of peaks attributed to Pd. Au shows only a very small CO adsorption peak at 2130 cm^{-1} wavenumber. **Figure 4.2** demonstrates the shift in CO adsorption frequency at low Pd loading. The CO adsorption peaks on the bimetallic catalyst shift to lower wavenumbers in comparison with the monometallic Pd catalyst with the same amount of Pd. It may be due to the change in electronic interactions between Au and Pd atoms in the bimetallic catalyst which causes a resonance-like effect by increasing charge transfer to the C-O bond that leads to a decrease in frequency. In the bimetallic catalyst, the position and intensity of the peaks changed significantly with a decrease in the amount of Pd in the catalysts, while keeping the Au loading constant. **Figure 5.3** shows the isolated sites to non-isolated sites peak area by decreasing the Pd:Au molar ratio. This analysis confirms that almost all multi-coordinated forms of CO adsorption on Pd disappeared at the dilute limit of Pd/Au. The spectra and deconvoluted peaks of CO adsorption on all catalysts are shown in **Figure 4.4**.

The CO adsorption FTIR spectra in **Figure** deconvoluted to get detailed insight on linear and nonlinear adsorbed CO on the surface of each catalyst. The linearly adsorbed CO on the dilute limit Pd-Au/SiO_2 catalyst showed four different peaks shifting with the change in coverage and the Pd:Au ratio. There are two broader peaks attributed to the nonlinearly adsorbed CO at 1893 and 1943 cm^{-1}. The linear peaks are downshifting with time after purging the CO saturated catalyst with pure N_2. The first linear peak at the highest wavenumber assigned to the linearly adsorbed CO on single Pd atoms on the

support or single Pd atoms in a super small cluster of Au with a few numbers of Au atoms. Based on the literature and the data from very low loading of Pd on SiO_2, the Pd atoms are considered as coordinatively unsaturated. Therefore, Pd atoms adsorb CO stronger than the CO atoms associated with larger nanoparticles with higher electron density. Consequently, withdrawing electron density from the C-O bond causes an inductive effect that injects electron from oxygen into the C-O bond. Because of electron deficiency and inductive effects, the C-O bond becomes stronger, and the peak shows up at higher wavenumber relative to the other peaks. The intensity of this peak is very low because of the very small percentage of Pd atoms are placed individually on the support or small Au clusters. So, this peak is almost negligible relative to the other peaks at CO saturated spectra.

The next three peaks that are present in all spectra attributed to the linearly adsorbed CO on the Pd atoms at different conditions and positions. It's been reported in several studies that the intensity of these peaks decreases with decreasing wavenumber. In order to study the effect of the coverage, the collected spectra deconvoluted from CO saturation until the equilibrium with respect to time and the results are shown in **Figure** . It is assumed that the adsorbed CO are at the most stable state with no intramolecular effects forcing CO molecules to get adsorbed linearly. The nonlinear CO adsorption is the most favorable and stable form. Therefore, it is highly likely that the linearly adsorbed CO at equilibrium are adsorbed on the isolated Pd atoms. All three linearly adsorbed CO peaks downshifted in wavenumbers until steady at equilibrium. However, the intensity of peaks with lower wavenumbers showed a sudden decrease right after switching to the pure N_2 and then a sudden increase in intensity after a short period of time and later started decreasing

gradually. The intensity of the linear adsorbed CO with higher wavenumber decreases steadily until constant at equilibrium.

Catalyst Evaluation with 1-Phenylethanol Partial Oxidation Reaction

The preliminary results of the probe reaction are shown in Error! Reference source not found.. Significant amounts of acetophenone were produced at a Pd/Au ratio of 1:5, and this amount (per Pd site) increased further as the ratio of Pd/Au decreased. Evaluation of the complete series is underway. The turnover frequencies TOFs on the basis of total metal and Pd are reported in Error! Reference source not found. for all catalysts. The TOF is very low in case of single metal catalyst in comparison with bimetallic catalysts. It has been reported that the support has a substantial effect on the reactivity of the catalyst. A few supports Al_2O_3, TiO_2, Carbon, Fe_2O_3, and SiO_2 are listed from the most to least influential in term of reactivity of the catalysts. The TiO_2 supported catalyst showed the best activity and selectivity(Enache et al. 2006). In order to examine the activity of the isolated Pd sites, the least influential support SiO_2 was utilized to synthesize all of the single atom alloy catalysts. The bimetallic Pd-Au/SiO_2 catalysts TOFs increased from 31 h^{-1} to 4654 h^{-1} as the ratio of Pd:Au decreased from 1:5 to 1:53.

Figure 4.9 shows the concentration of the only oxidation product acetophenone for single metal silica supported catalysts and two bimetallic catalysts with 1:5 and 1:14 Pd-Au ratios. The amount of bimetallic catalysts in each reaction setup were adjusted to have 0.64 mmol of Pd in the reaction media. The results in Error! Reference source not found. shows that the Pd-Au catalyst with the 1:14 ratio is more active with the same amount pf Pd present in the reaction media because of more isolated active sites. Therefore, as the number of isolated Pd sites increases, the catalyst becomes more active. The mechanistic

step of Pd-Au bimetallic interaction that facilitated the partial oxidation of 1-phenylethanol at low temperature is shown in **Figure 4.6** (Rodriguez, Williams, and Monnier 2014). The activity of monometallic Pd or Au is very low in comparison with the bimetallic catalysts. This suggests that similar to the homogeneous catalyst that becomes deactivated via forming Pd black by having two or more Pd atoms agglomerated together, the activity of the catalyst depends on the number of isolated sites.

Table 4.1. TOFs of catalysts with different Pd content.

Catalyst	**Pd** (10^{-3} **mol/L)**	**Au** (10^{-3} **mol/L)**	**TOF$_{total-metal}$** (h^{-1})	**TOF$_{Pd}$** (h^{-1})
Pd	19.4	0	0.5	0.5
Au	0	24.75	0.4	0.4
1:5 Pd:Au	3.2	20.4	5.2	31
1:14 Pd:Au	1.8	25.8	4.4	68
1:28 Pd:Au	1	25.8	31	833
1:53 Pd:Au	0.4	24.75	74	4654

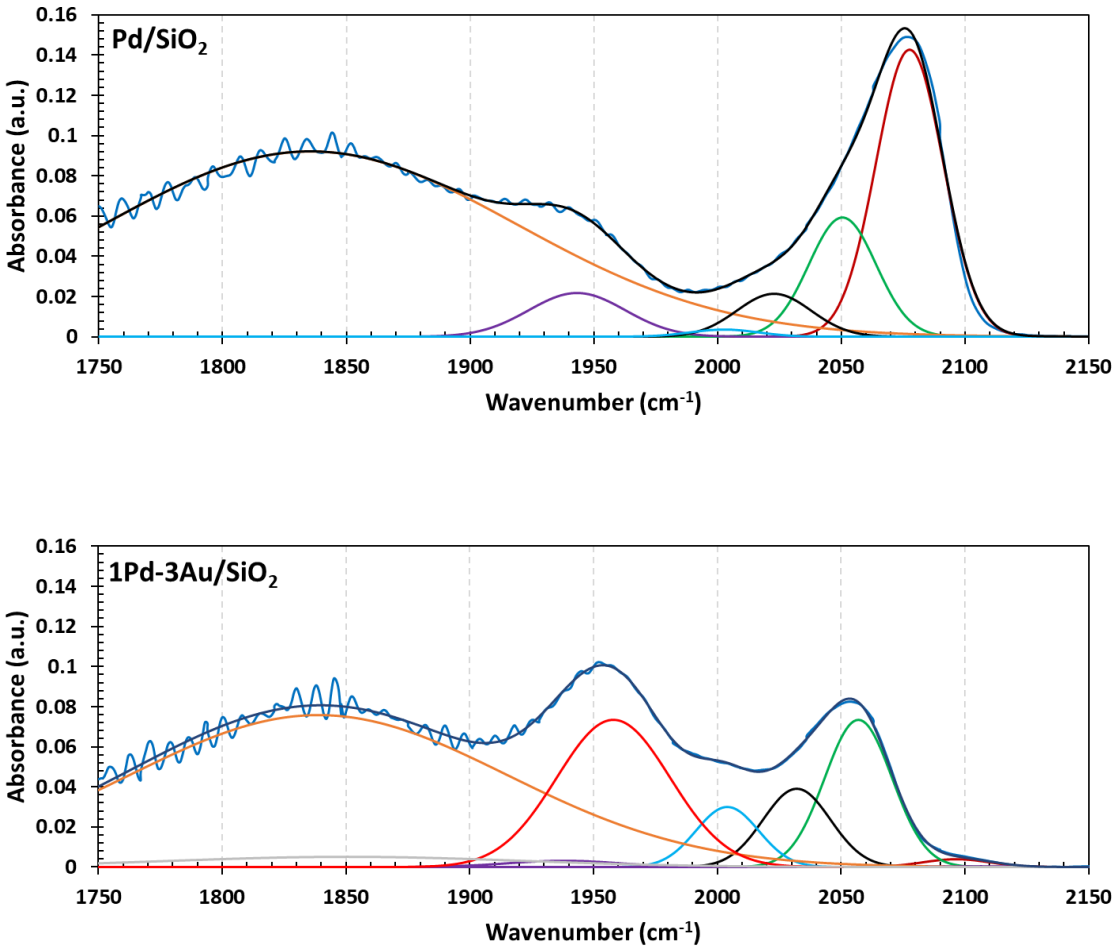

Figure 4.1. CO adsorption spectra of monometallic Pd and bimetallic Au-Pd catalysts.

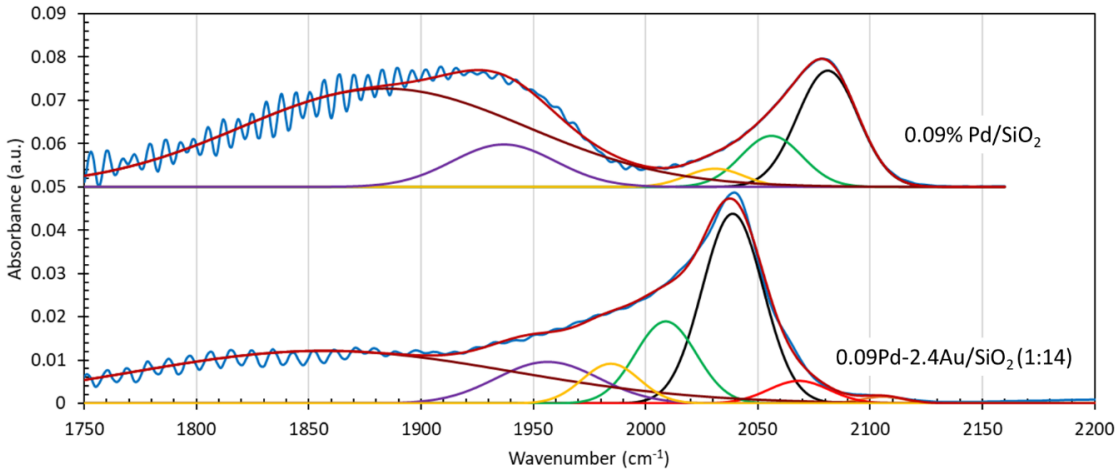

Figure 4.2. Shift of CO adsorption peaks between Pd and Pd-Au catalysts with same amount of low Pd loading.

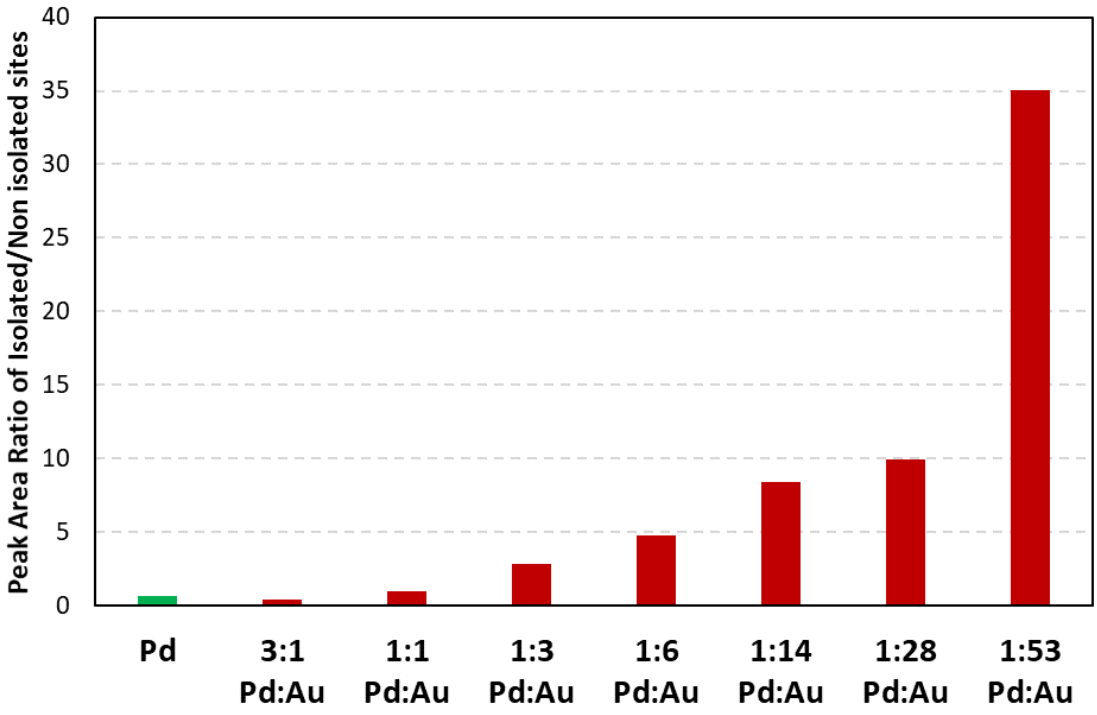

Figure 5.3. CO adsorption deconvoluted peak area ratio of isolated sites to non-isolated sites

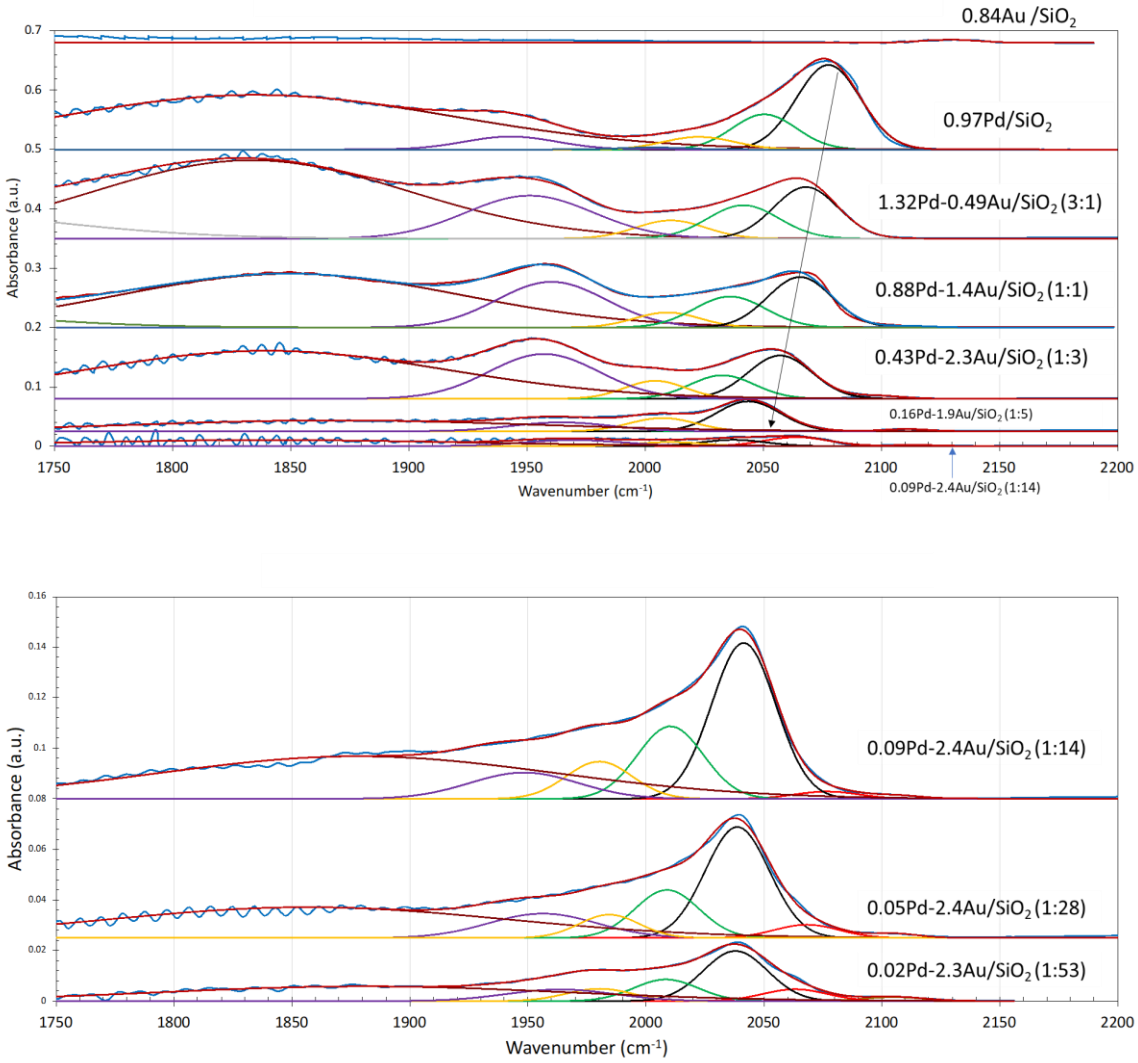

Figure 4.4. CO adsorption spectra of all catalysts.

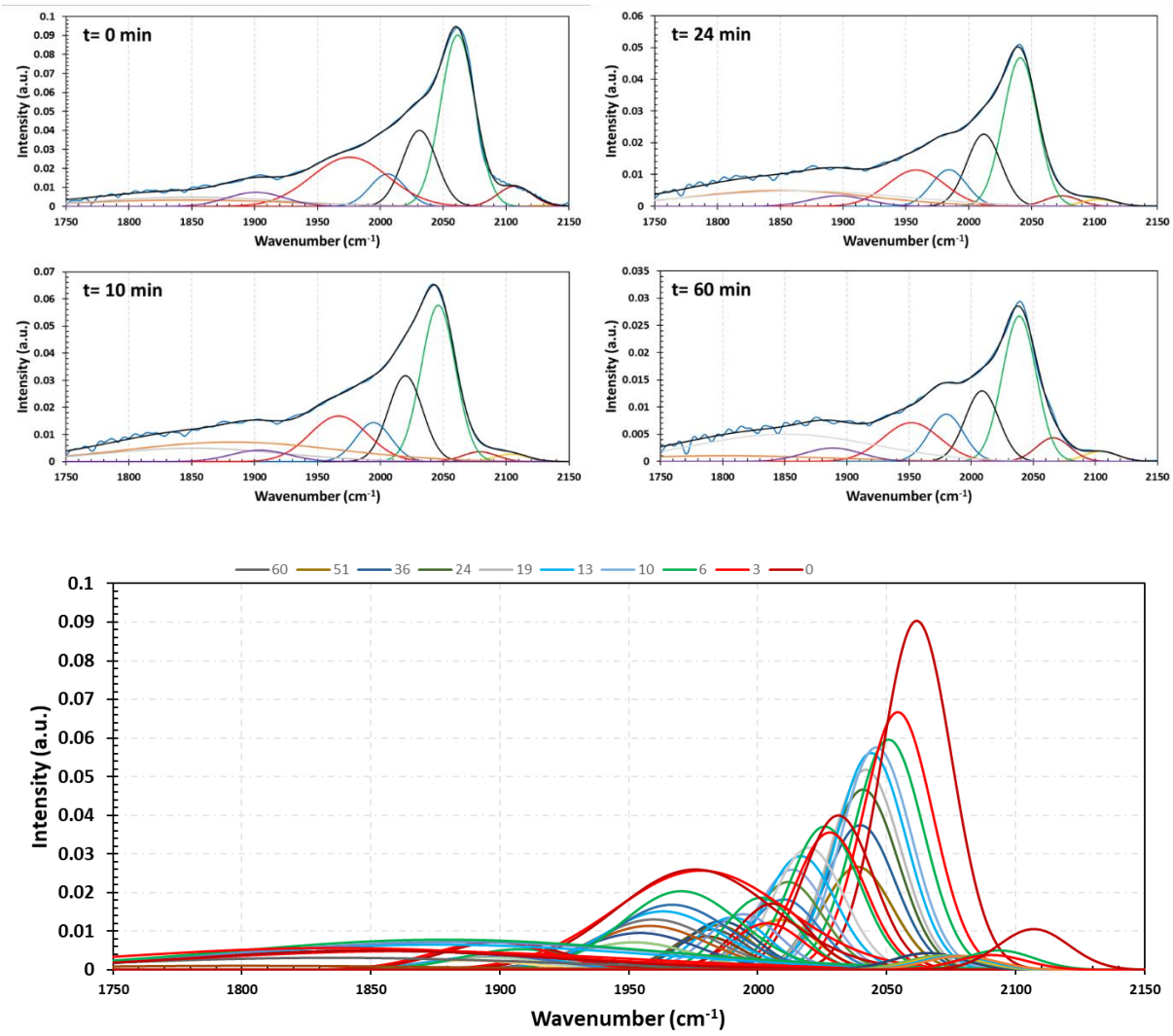

Figure 4.5. CO adsorption spectra on 1:53 Pd-Au/SiO_2 catalyst vs. time.

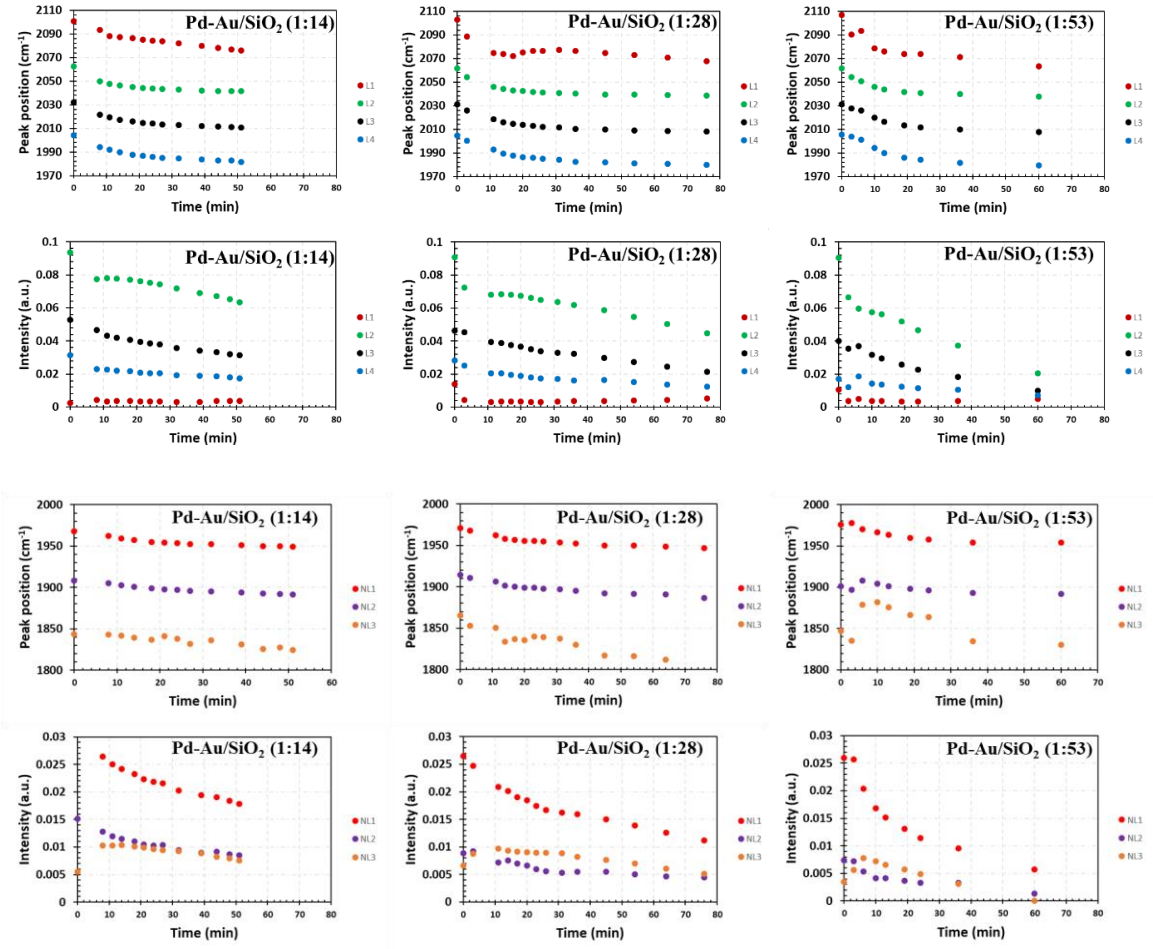

Figure 4.6. Linear and non-linear peaks position and intensity vs. time for dilute limit alloy catalysts.

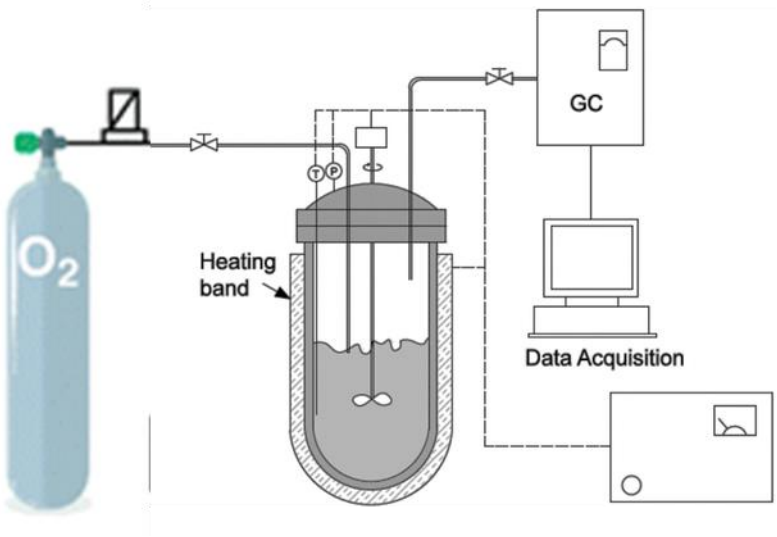

Figure 4.7. Reactor schematic for partial oxidation of 1-phenylethanol.

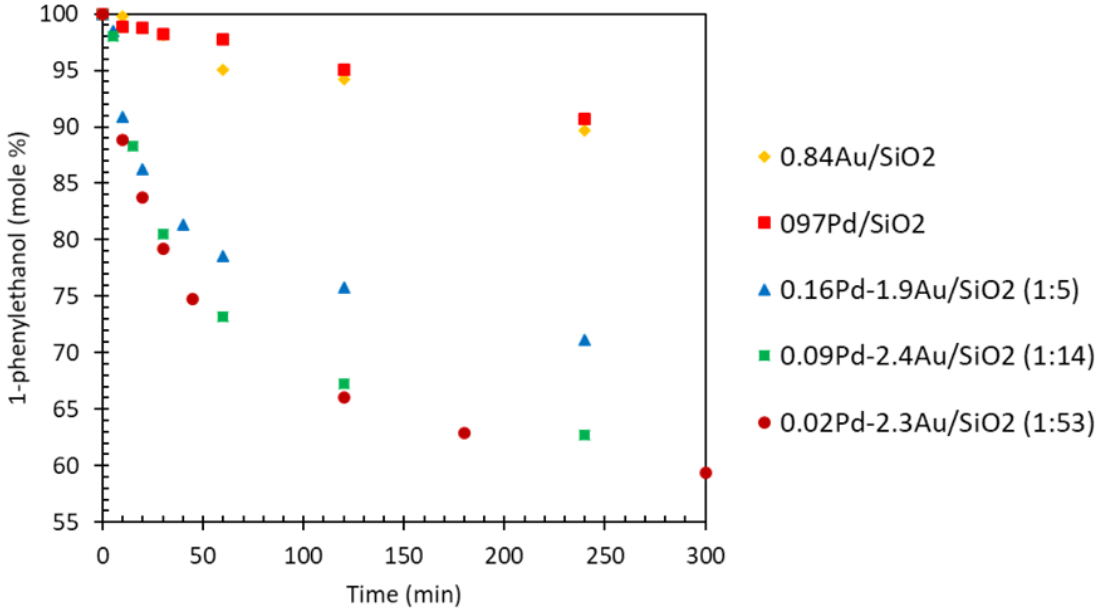

Figure 4.8. Reaction data of 1-phenylethanol partial oxidation using different catalysts.

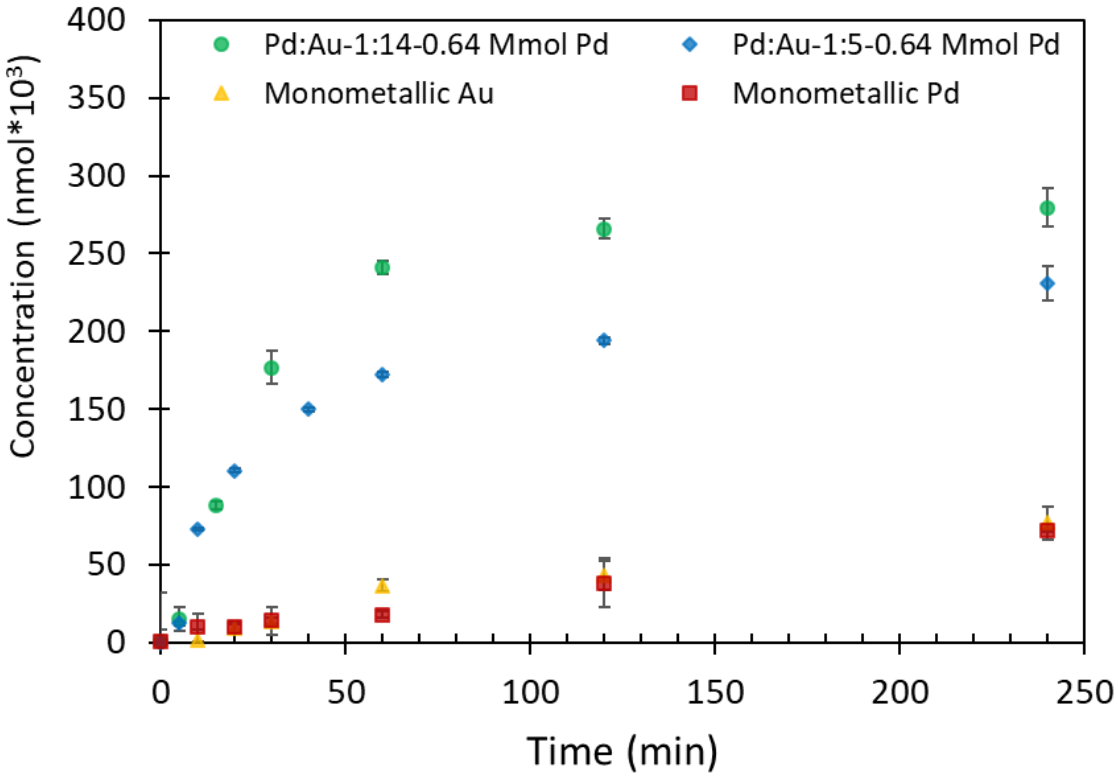

Figure 4.9. Production of acetophenone using the same amount of Pd in the reactor with different catalysts.

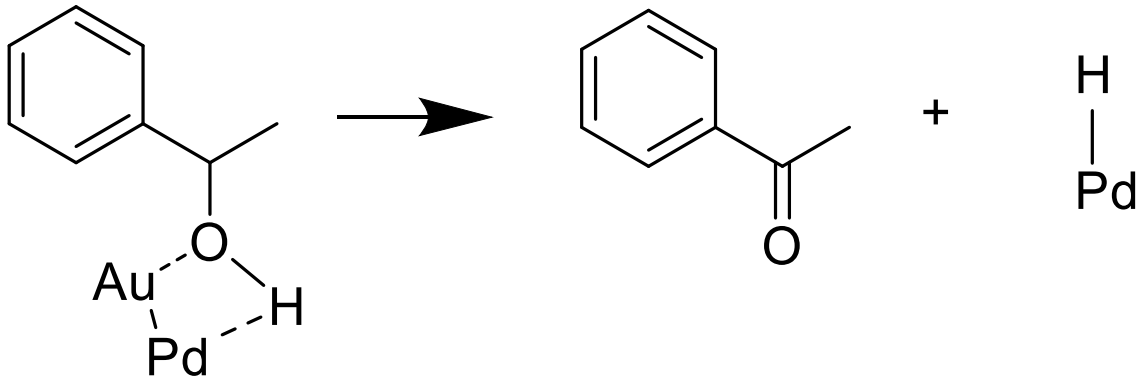

Figure 4.6. Proposed mechanistic step of bimetallic interaction of 1-phenylethanol on Pd-Au single atom alloy site during partial oxidation.

CHAPTER 5

RATIONAL SYNTHESIS OF MODEL CATALYSTS FOR SELECTIVE OXIDATION OF HYDROCARBONS

Summary

Ruthenium based catalysts with 3wt.% ruthenium content were synthesized by a variety of synthetic methods. The structure and physical properties of the catalysts were analyzed using a range of microscopic and spectroscopic approaches. New bimetallic copper-ruthenium and tin-ruthenium complexes were prepared and impregnated onto a silica support. The resulting catalysts displayed considerable promise for the partial oxidation of hydrocarbons to higher value-added chemicals. Catalytic tests demonstrated the Ru_6/SiO_2 cluster derived catalyst had a relatively high activity, as well as the highest selectivity towards acetophenone. The Ru_6/SiO_2 cluster-derived catalyst, with the highest TOF, formed rod shape particles that provided a particular facet for the oxidation reaction. The XPS results indicated that the carbide in the $Ru_6C(CO)_{16}/SiO_2$ cluster remained in the structure during the activation of the catalyst. Copper, which was introduced to the $(CH_3CN)_2Cu_2Ru_6C(CO)_{16}$ cluster, promoted the adsorption of oxygen, resulting in higher synergistic activity and spherical structure of the catalyst particles. The bimetallicRu_3Cu_1/SiO_2 SEA (Strong electrostatic Adsorption) catalyst was the most stable

and dispersed catalyst with high activity. The activity and the selectively of the cluster derived catalyst decreased by adding tin to the cluster, despite the rod-shaped structure.

Introduction

Phenyl ketones are important functionalized molecules that are primarily produced by Friedel-Crafts reactions, employing acid halides or acid anhydrides. The process requires stoichiometric amounts of the $AlCl_3$ catalyst and produces a large quantity of waste that makes it undesirable on large scales. Partial oxidation of alkylbenzenes using more environmentally friendly and efficient methods that employ, for example, O_2 as oxidants are being studied. Acetophenone (AP) is an essential intermediate in the production of important chemicals such as pharmaceuticals, resins, perfumes, alcohols, and esters. As such, there are many studies exploring environmentally friendly methods for producing acetophenone using both highly active and selective homogeneous and heterogeneous catalysts. Several attempts have been made using catalysts with tert-butyl hydroperoxide (TBHP) or hydrogen peroxide (H_2O_2) as oxidants. However, less expensive and more available oxidants like oxygen (particularly in the form of air) would be more preferable (Takahashi et al. 2017; H. Wu, Zhao, and Hu 2018; Sartori and Maggi 2006; López Nieto and Solsona 2018; Luo et al. 2016; J. Xu et al. 2016; Armstrong et al. 2016; Valange and Védrine 2018; Rafelt and Clark 2000; Raji, Chakraborty, and Parikh 2012).

Selective oxidation is a valuable method for preparing higher value chemicals from abundant, inexpensive simple hydrocarbons (Webb, Bolaño, and Gunnoe 2010). Controlled selective oxidations require the use of specialized catalysts. Copper ions in low oxidation states are well known for their ability to activate molecular oxygen (Elwell et al. 2017; Cook et al. 2018; Khivantsev et al. 2018). Nanoparticles of copper, silver, and gold

have recently been shown to be effective catalysts for selective oxidation reactions (Groothaert et al. 2005). Some copper-iron and copper-palladium bimetallic catalysts have been found to be even better than pure gold for certain selective oxidation reactions (J. Xu et al. 2016; Xavier, Chacko, and Yusuff 2004). Very few bimetallic copper-ruthenium oxidation catalysts have been investigated to date. However, such catalysts might be expected to perform well because Ru based catalysts have been reported to be very stable and resist coking due to the enhancement in the oxidation of CH_x fragments, which are adsorbed on the Ru active site (Sengodan et al. 2018). W. Wang, Ran, and Shao (2011) reported that a 3 wt% Ru/Al_2O_3 showed excellent operation stability in solid oxide fuel cell operating on methane and RuO_x interaction with the support in the as-synthesized catalyst (W. Wang, Ran, and Shao 2011).

Adsorbed oxygen can be classified into two types. First type is electrophilic oxygen species including oxide (O^-), superoxide (O_2^-), and peroxide (O_2^{2-}) which are responsible for complete oxidation. Second type is identified as lattice oxygen refers to the oxide ion (O^{2-}) which is responsible to carry out partial oxidation. This oxide ion has its full complement of electrons so it reacts with electron-poor portion of the molecule (Oyama 1996b). In ethylbenzene partial oxidation, the oxide ion reacts with ethyl group because the benzene ring is electron rich. It is highly likely that ethylbenzene adsorbs at oxide ion sites on the catalyst surface through the electron-poor ethyl group(Dadyburjor, Jewur, and Ruckenstein 1979; Oyama 1996a; Fathizadeh et al. 2018).

There is a relationship between the metal-oxygen bonds strength and the catalyst activity, selectivity, and the reactivity of surface oxygen species. The catalysts surface gets reduced by the adsorption of hydrocarbon and re-oxidized by oxygen without apparent

damage to the surface. The reduction of the catalyst by hydrocarbon is a surface reaction followed by diffusion of oxygen in the lattice of the catalyst. The gaseous oxygen replaces the consumed oxygen in the lattice. A proper catalyst for partial oxidation provides limited amount of oxygen sufficient to form desired products but less than enough for complete oxidation. To maintain a reasonable rate of reaction, a continuous supply of lattice oxygen is needed. Therefore, first step in selective oxidation is converting gaseous oxygen into lattice oxygen(Dadyburjor, Jewur, and Ruckenstein 1979).

The objective of this project is to understand how advanced methods of rational catalyst synthesis will control the structure, reactivity, and stability of heterogeneous bimetallic catalysts for selective oxidation of ethylbenzene. New bimetallic copper-ruthenium and tin-ruthenium complexes have been prepared and impregnated onto a silica support. The resulting catalysts have been shown to have considerable promise for the partial oxidation of hydrocarbons to higher value-added chemicals. Partial oxidation catalysts have been synthesized with a wide variety of preparation methods, but these methods lack the ability to control the atomic distribution of the true bimetallic nature of the catalyst, uniform particle size, and controlled synergistic effect of bimetallic catalysts. In this study, we employed what is generally called rational catalyst synthesis to prepare novel catalysts. Ultimately, ethylbenzene partial oxidation (**Figure 5.1**) is used as a target reaction with which to evaluate performance of the bimetallic catalysts.

Instrumentation

Infrared spectra were recorded on a Nicolet IS10 Midinfrared FT-IR spectrophotometer. ^{1}H NMR was recorded on a Varian Mercury 300 spectrometer operating at 300 MHz, respectively. All NMR spectra were recorded using solutions in

CD_2Cl_2 in 5mm sample tubes. All electron microscopy images were taken using a JEOL JEM-2100F Aberration Corrected Scanning Transmission Electron Microscope equipped with Fischione high angle annular darkfield detector (HAADF).

Reagents

$Ru_3(CO)_{12}$ was purchased from STREM Chemicals. $[Cu(MeCN)_4][BF_4]$ was purchased from Sigma Aldrich. $Ru(NH_3)_6Cl_3$ and $Cu(NO_3)_2$ were purchased from Alpha Aesar chemical manufacturing company. All reagents were used without further purification. $Ru_6C(CO)_{17}$ and $Ru_5C(CO)_{15}$ were prepared according to previously reported procedures.(Nicholls and Vargas 1983) $(CH_3CN)_2Cu_2Ru_6C(CO)_{16}$(J. S. Bradley et al. 1982) and $HRu_5C(CO)_{15}SnPh_3$(Adams et al. 2002b) were prepared according to previously reported procedures.(J. S. Bradley et al. 1982; Adams et al. 2002a) The support used was SiO_2 Evonik AEROSIL 300.

General Catalyst preparation

For a given catalyst preparation, the precursor complex was dissolved in 20mL of tetrahydrofuran in a 100mL flask. To this was added the appropriate amount of silica powder. This mixture was stirred vigorously for 4h and the resultant slurry was slowly dried by removal of the solvent under vacuum. All SiO_2 supported catalysts were subjected to thermal removal of the ligands at the selected temperature for activation by heating under vacuum. All Ru-containing catalysts prepared contained 3wt% Ru. The table described below shows the calculated amount of precursor complex and silica powder used in each catalyst preparation.

$Ru(NH_3)_6Cl_3$ and $Cu(NO_3)_2$ precursors were used for catalysts preparation with the SEA method(Bahareh Alsadat Tavakoli Mehrabadi et al. 2018; Wong et al. 2017b) and dry

impregnation methods. The catalysts were classified with constituent metal(s) symbols with no suffix for the cluster derived catalysts. The suffix SEA and DI were used for catalysts prepared with the SEA method and dry impregnation method, respectively. There is a cluster derived catalyst with a physical mixture of impregnated precursors that is shown with a "Phys. Mix." suffix. In the case of bimetallic catalysts, the molar ratio of the constituent metals was used as an identification for composition.

Catalyst evaluation

The catalysts were evaluated for the oxidation of ethylbenzene in a 110 ml semi batch reactor (Autoclave Engineers) at 150 psig and 150°C, with a stirring rate of 300 rpm. The reactor is only open to a small O_2 flow to maintain reaction pressure. In all cases, the initial reactor loading was 50 ml ethylbenzene (EB) and 50 mg catalyst. Much attention was placed on ensuring the safety of the reaction. The reactor is equipped with a rupture disk, as is standard for performing high pressure reactions. In addition, a needle valve was installed to control O_2 flow to the reactor. This valve is opened only to the level required to maintain the reaction pressure in the vessel. Thus, in the event of a thermal runaway, the reactor will quickly become starved of oxygen and the rate will be limited, providing the opportunity to shut the system down. No evidence of any uncontrolled reaction has been observed. The compositions of liquid reactant and products at various reaction times were measured using a gas chromatograph (HP 5890) coupled to an autosampler (**Figure 5.22**).

Computational Calculations

Figure 5.3 demonstrates the results of computational calculation for different species of Ru based catalyst for C-H bond activation. The C-H bond activation on Ru follows a two-state pathway suggesting that the empty 5s orbital providing energetically

favorable pathway (**Figure 5.3(A)**). The minimum activation energy for Ru_1 and Ru_6 calculated 0.14 eV (2μb path) and 0.76 eV (8μb path), respectively. In the case of ruthenium oxide, the calculations shoed a single state reactivity with a minimum activation energy associated with empty 5s orbital of Ru (**Figure 5.3(B-C)**). The overall results showed that the Ru^{+1} is the most active specie among two atom clusters and Ru_6 cluster is associated with higher activation energy (**Figure 5.3(D)**).

Results and Discussions

Catalyst activation

The precursor-impregnated supports were first examined using temperature-programmed methods to determine a suitable activation procedure. Temperature-programmed reduction (TPR) in H_2, oxidation (TPO) in O_2, and decomposition (TPD) in He, were explored for all the materials. Some representative examples are shown in **Figure** for the case of the $Ru_6C(CO)_{16}$, $(CH_3CN)_2Cu_2Ru_6C(CO)_{16}$, $Ru_3(CO)_{12}$, and $(CH_3CN)_4Cu(I)BF_4$ precursors. The TPO (red curve) has a higher intensity because all of precursors contain carbon in their ligand structures. So, the concentration for CO_2 is larger in comparison with TPR and TPD. There are two main peaks for $Ru_6C(CO)_{16}/SiO_2$ because of carbide and carbonyl ligands. There are three large peaks plus a shoulder on the first peak for CO_2 in the TPO curve of $(CH_3CN)_2Cu_2Ru_6C(CO)_{16}/SiO_2$. This is due to different carbon-containing ligands. Indeed, just one peak of CO_2 appears in the TPO curve for the $Ru_3(CO)_{12}/SiO_2$ catalyst, coming from the carbonyl group in the cluster structure. The results for TPD (green curve) show very similar results, albeit with less intensity plus some additional CO_2 coming off the surface at slightly higher temperatures for each catalyst. This may be due to the starvation of oxygen and using oxygen from the support structure

to oxidize carbon containing ligands at higher temperatures. The TPR (blue curve) results don't have high intensity peaks because reduction with hydrogen is more likely to happen in the absence of oxygen. Also, reduction with hydrogen is more favorable to happen at lower temperatures than taking oxygen from the support structure, which needs more energy and consequently higher temperatures.

While the oxidation technique shows promising results for activation of the catalysts, it also may affect the initial rate of the reaction since the catalyst might be fully oxidized. Catalysts were thus all activated at 400°C for 3 hrs in flowing He to ensure complete ligand removal.

Catalyst characterization

In-situ XPS results (**Figure**) demonstrated a small shift in C 1s, Ru peak from 281.5 eV to 280.9 eV representing less oxidized Ru after thermal treatment. According to the computational calculation less oxidized Ru specie expected to have lower activation energy for C-H bond activation. The result showed that during thermal treatment show that the carbide ligands remain in the clusters, likely maintaining their structure to some extent. The calculations of activation energy showed much lower activation energy for Ru carbide in comparison with the Ru6 clusters. However, in-situ FT-IR results in **Figure 5.6** show that other ligands, like carbonyl groups, are eliminated due to the thermal treatment providing a clean surface for the reaction to proceed.

Catalysts were examined using XRD before and after activation. As an example, **Figure 5.7** shows the powder XRD patterns for Ru_6/SiO_2, Ru_6Cu_2/SiO_2, Ru_3/SiO_2, and Cu/SiO_2 catalysts. As seen, there are no significant diffraction peaks prior to activation (other than for the SiO_2 support at $2\theta = 25^{\circ}$). After activation at 400°C for 3 hrs in flowing

He, there are several peaks resulting from various crystallites of Ru being formed. Analysis of these various peaks using the Scherrer equation suggests that there are particle sizes ranging between 2-15 nm for Ru_6Cu_2/SiO_2. The situation is similar for 3 wt% Ru_6/SiO_2. In contrast, for 3 wt% Ru_3/SiO_2, the XRD size range was found to vary up to 90 nm, suggesting that the carbide-free precursors are less stable to sintering upon activation. In the case of the 3 wt% Cu/SiO_2 catalyst, the XRD suggests that there are only very small (< 1nm) crystallites after treatment.

Figure 5.8 shows the STEM images of catalysts. Ru_6/SiO_2 cluster derived catalyst showed large rod shape particles confirming XRD results with sharp peaks. This provides specific facets while XPS results showed there is carbide on the surface of the catalyst even after activation treatment. The bimetallic Ru_6Cu_2/SiO_2 cluster derived catalyst formed small spherical particles along with some agglomerated particles. The small particles provide higher surface area with more active sites due to bimetallic nature of the catalyst. The dry impregnation Ru/SiO_2 DI catalyst presented all three small spherical, large agglomerated, and rod shape particles at once. The metal loading in all catalysts was 3 wt% and the Ru/SiO_2 DI catalyst has fairly larger particles in comparison with the other catalysts, so it has less surface sites in comparison with other catalysts. The smallest monodisperse particles belong to the bimetallic Ru_3Cu_1/SiO_2 SEA, which has the highest metallic surface area among all these catalysts. A similar cluster derived bimetallic catalyst with separate clusters made of physically mixed $Ru_6C(CO)_{16}$ + $(CH_3CN)_4Cu(I)BF_4$ clusters formed large nonuniform particles under the same treatment and conditions. So, the active surface area is smaller relative to the other catalysts. Monometallic Ru_3/SiO_2 cluster-derived catalyst formed a blend of small spherical and large triangular particles with lower

surface area in comparison with other catalysts with the same ruthenium loading. Finally, small spherical particles were observed for bimetallic Ru_5Sn/SiO_2 cluster derived catalysts with a core of ruthenium and a partial shell of tin.

Catalytic performance and comparison

Parameters of kinetic models are estimated using pseudo-first order reaction models, with reaction rate constants found using least square fitting method, as described in detail in the Supporting Information. For example, fitting results for Ru_5/SiO_2, Ru_5Sn/SiO_2, Ru_6/SiO_2 and Ru_6Cu_2/SiO_2 are shown in **Figure 5.9.**

The results listed in **Table 5.2** show that bimetallic catalysts are more active than monometallic catalysts because the second metal promotes more reaction pathways. For example, Ru_6/SiO_2 catalyst selectively promoted the first reaction. However, when copper was added to the cluster, it resulted in the promotion of the second reaction while k_1 for the first reaction is almost the same as the monometallic Ru_6/SiO_2 catalyst. The increase in k_2 comes from a bimetallic synergistic effect in Ru_6Cu_2/SiO_2 because Cu/SiO_2 itself promotes the third reaction. Dry impregnation catalysts show the same trend, but they are less active because of larger particle sizes and wider size distribution, and consequently have less active surface area. This behavior is in agreement with crystallite size distribution from XRD results. The larger Ru size distribution promotes the third reaction, and smaller Ru particle size distribution promotes first reaction. The catalyst derived from $Ru_5C(CO)_{15}$ clusters is less active than the catalysts derived from $Ru_6C(CO)_{16}$ clusters. The Ru_5Sn/SiO_2 catalyst shows less activity than Ru_5/SiO_2 because of different sizes, shapes, and facets of active sites. Adding Sn to the cluster poisons the catalyst and affects the selectivity of the

catalyst**.** The bimetallic Ru_5Sn/SiO_2 catalyst has slightly smaller crystallite size distribution than Ru_5/SiO_2. The same trend is observed between Ru_6Cu_2/SiO_2 and Ru_6/SiO_2.

The Ru_6/SiO_2 cluster-derived catalyst formed rod shape particles that provide a special facet for the oxidation reaction. According to the parameter estimation results, this catalyst has proven to be the most selective catalyst toward direct conversion of ethylbenzene to acetophenone. The turnover frequency of Ru_6/SiO_2 cluster derived catalysts is highest among all catalysts. The bimetallic cluster derived Ru_6Cu_2/SiO_2 catalyst has small spherical particles in addition to some large, sintered particles. The activity of this catalyst is highest in term of reaction rate, which is due to a synergistic effect of bimetallic particles. The Ru_6/SiO_2 cluster derived catalyst promotes direct conversion of ethylbenzene to acetophenone, while the copper catalyst promotes the reaction path with 1-phenyl ethanol as an intermediate to the acetophenone. In the case of the bimetallic cluster derived catalyst, the sum of the reaction rate constant for the direct and indirect conversion of ethylbenzene is higher than each pathway individually. This suggests that the bimetallic cluster derived Ru_6Cu_2/SiO_2 catalyst provides higher activity because of synergistic bimetallic effects. However, it shows smaller particles than the Ru_6/SiO_2 cluster derived catalyst with a higher rate of conversion for ethylbenzene, but it has 2.7 times lower TOF (**Table 5.3**) in comparison with monometallic Ru_6/SiO_2 catalyst. The dry impregnation Ru/SiO_2 DI catalyst shows the formation of all sorts of shapes observed in all catalysts. It contains spherical, rod, and sintered shape particles all in one. The activity of this catalyst is slightly lower than cluster derived catalysts. The Ru_3Cu_1/SiO_2 SEA catalyst represents a uniform distributed particle size with spherical particles. Regardless of the high surface area of the Ru_3Cu_1/SiO_2 SEA catalyst, it has almost the same activity

as the Ru_6/SiO_2 and Ru_6Cu_2/SiO_2 catalyst. In the case of Ru_3Cu_1/SiO_2 SEA, it was not confirmed that the reaction condition is not mass transfer limited because of the design limitation. In slightly higher agitation speeds, a centrifuge effect separated the catalyst particles from the reaction media to the wall and top of the reactor resulting in a decrease in the performance of the process. Because of the much higher surface area in this catalyst in comparison with the rest of catalysts, there may be mass transfer limitation in adsorption of gaseous oxygen that limits the formation of the lattice oxygen.

Conclusions

The cluster derived Ru_6/SiO_2 catalyst had a high selectivity for ethylbenzene partial oxidation towards acetophenone, while the Ru_6Cu_2/SiO_2 cluster derived catalyst had a higher activity because of its higher surface area and the synergistic effect of the bimetallic catalyst. The interaction between $Ru_6C(CO)_{16}/SiO_2$ and carbide that was revealed through XPS may explain the formation of a rod-shaped structure. This structure provides a special facet that selectively promotes the direct reaction pathway to acetophenone formation with a high TOF. The Ru_5Sn/SiO_2 catalyst showed that tin can poison the catalyst, which has a negative bimetallic effect on the activity of the catalyst, regardless of the rod-shaped structure. The Ru_3Cu_1/SiO_2 SEA catalyst had a highly dispersed particle size distribution. It displayed much better stability and agglomeration resistance than all other catalysts. The dry impregnation catalysts, as benchmark catalysts, showed relatively lower activity than the cluster derived catalysts and SEA catalyst. The physical mixture of the cluster derived catalyst showed the lowest activity, which emphasizes the effect of the synthesis method and synergistic effect of the bimetallic catalyst.

Table 5.1. Calculated amount of precursor complex and silica powder.

Sample No.	Sample contains (**3% Ru metal by weight on SiO_2 support**)	Amount of metal precursor complex added (mg)	Amount of SiO_2 added (mg)
1.	$HRu_5C(CO)_{15}SnPh_3$ / SiO_2	38.25	500
2.	$Ru_3(CO)_{12}$ / SiO_2	31.6	500
3.	$(CH_3CN)_4Cu(I)BF_4$ / SiO_2	74.3	500
4.	$Ru_6C(CO)_{17}$ / SiO_2	27.1	500
5.	$(CH_3CN)_2Cu_2Ru_6C(CO)_{16}$ / SiO_2	31.6	500
6.	$Ru_5C(CO)_{15}$ / SiO_2	27.8	500

Table 5.2. Parameter Estimation for all catalysts using pseudo first order reaction model. k_1, k_2, k_3, and k_4 are reaction rate constants of ethylbenzene→acetophenone (k_1), ethylbenzene→1-phenylethanol (k_2), 1-phenylethanol→acetophenone (k_3), and acetophenone→other products (k_4).

Precursor	Catalyst	k_1 (1/min) $*10^3$	k_2 (1/min) $*10^3$	k_3 (1/min) $*10^3$	k_4 (1/min) $*10^3$
$(CH_3CN)_2Cu_2Ru_6C(CO)_{16}$	Ru_6Cu_2/SiO_2	33.3	27.9	24.7	2.1
$Ru(NH_3)_6Cl_3$+$Cu(NO_3)_2$	Ru_6Cu_2/SiO_2 SEA	0.0	27.0	492.0	1.0
$Ru(NH_3)_6Cl_3$+$Cu(NO_3)_2$	Ru_6Cu_2/SiO_2 DI	28.1	12.6	27.3	3.3
$Ru_6C(CO)_{16}$	Ru_6/SiO_2	36.6	2.9	0.0	2.5
$Ru(NH_3)_6Cl_3$	Ru/SiO_2 DI	14.0	5.9	37.8	5.3
$(CH_3CN)_4Cu(I)BF_4$	Cu/SiO_2	0.7	15.2	138	4.3
$Ru_6C(CO)_{16}$+$(CH_3CN)_4Cu(I)BF_4$	Ru_6Cu_2/SiO_2 PM	11.4	0.7	0.0	2.0
$Ru_3(CO)_{12}$	Ru_3/SiO_2	1.5	3.0	34.2	12.2
$Ru_5C(CO)_{15}$	Ru_5/SiO_2	14.0	14.0	54.0	4.0
$HRu_5C(CO)_{15}SnPh_3$	Ru_5Sn/SiO_2	4.0	13.0	14.0	0.0

Table 5.3. TOF and chemisorption particle diameter for selected catalysts.

Precursor	Catalyst	TOF	Particle diameter (nm)
$(CH_3CN)_2Cu_2Ru_6C(CO)_{16}$	Ru_6Cu_2/SiO_2	19.7	2.1
$Ru(NH_3)_6Cl_3$+$Cu(NO_3)_2$	Ru_6Cu_2/SiO_2 SEA	17.8	3.2
$Ru(NH_3)_6Cl_3$+$Cu(NO_3)_2$	Ru_6Cu_2/SiO_2 DI	13.3	3.6
$Ru_6C(CO)_{16}$	Ru_6/SiO_2	30.6	3.0

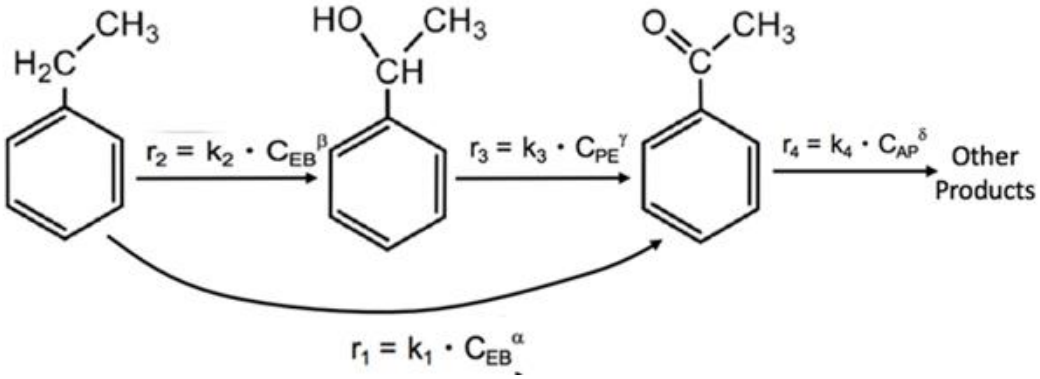

Figure 5.1. Ethylbenzene partial oxidation.

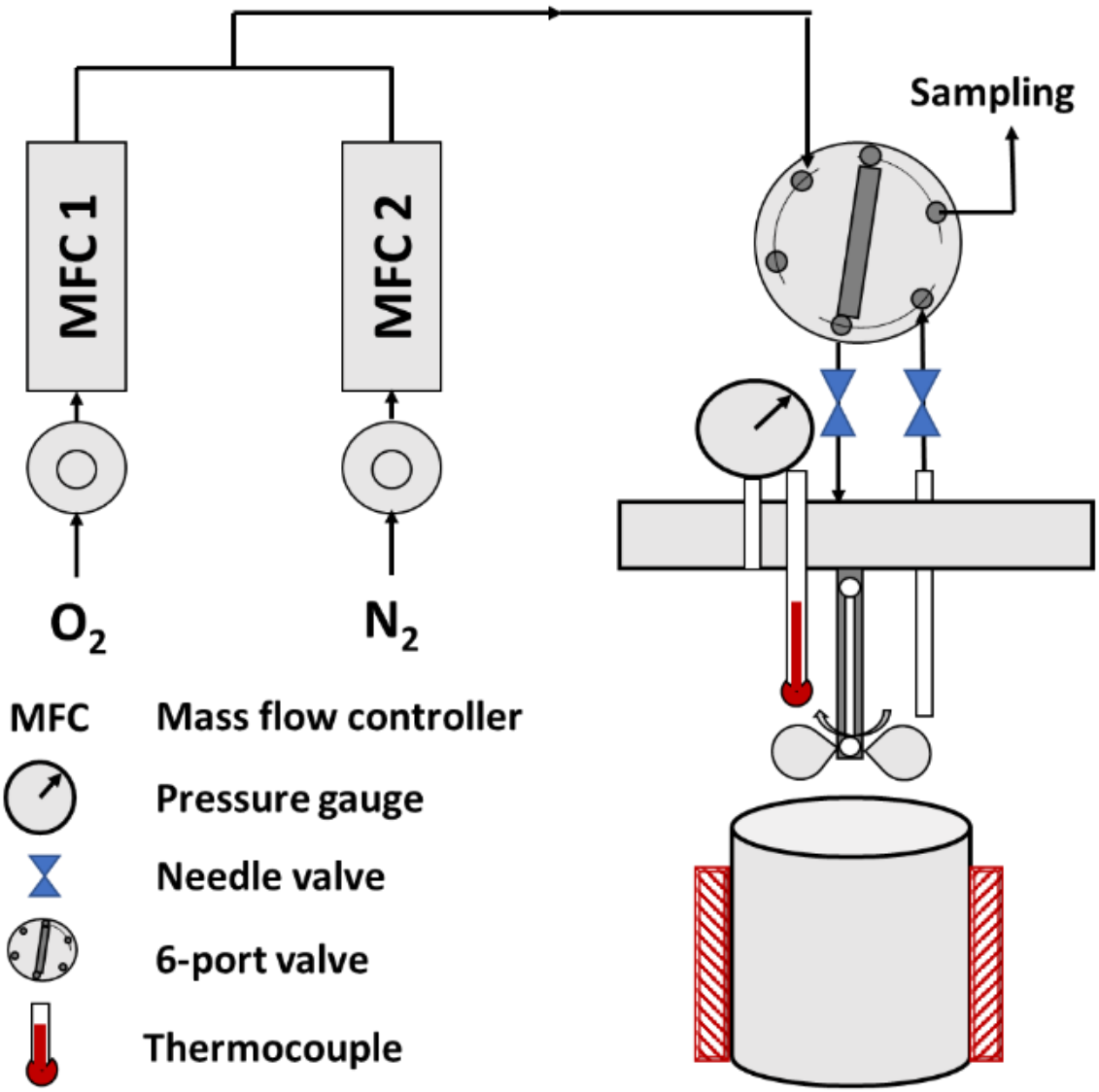

Figure 5.2. **Schematic** of the semi batch reactor setup.

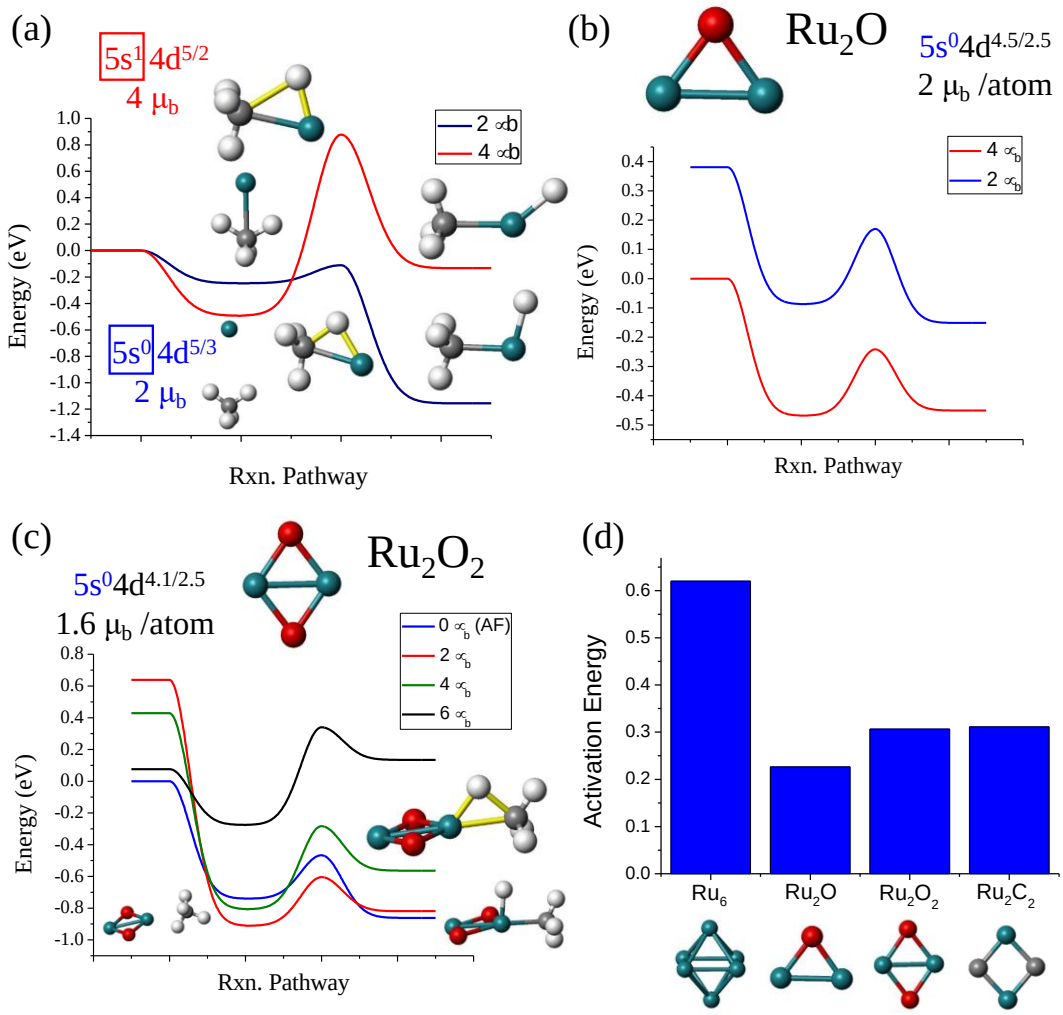

Figure 5.3. DFT calculations of activation energy for C-H bond activation of a) Ru, b) Ru_2O, c) Ru_2O_2, and d) comparison of different Ru species.

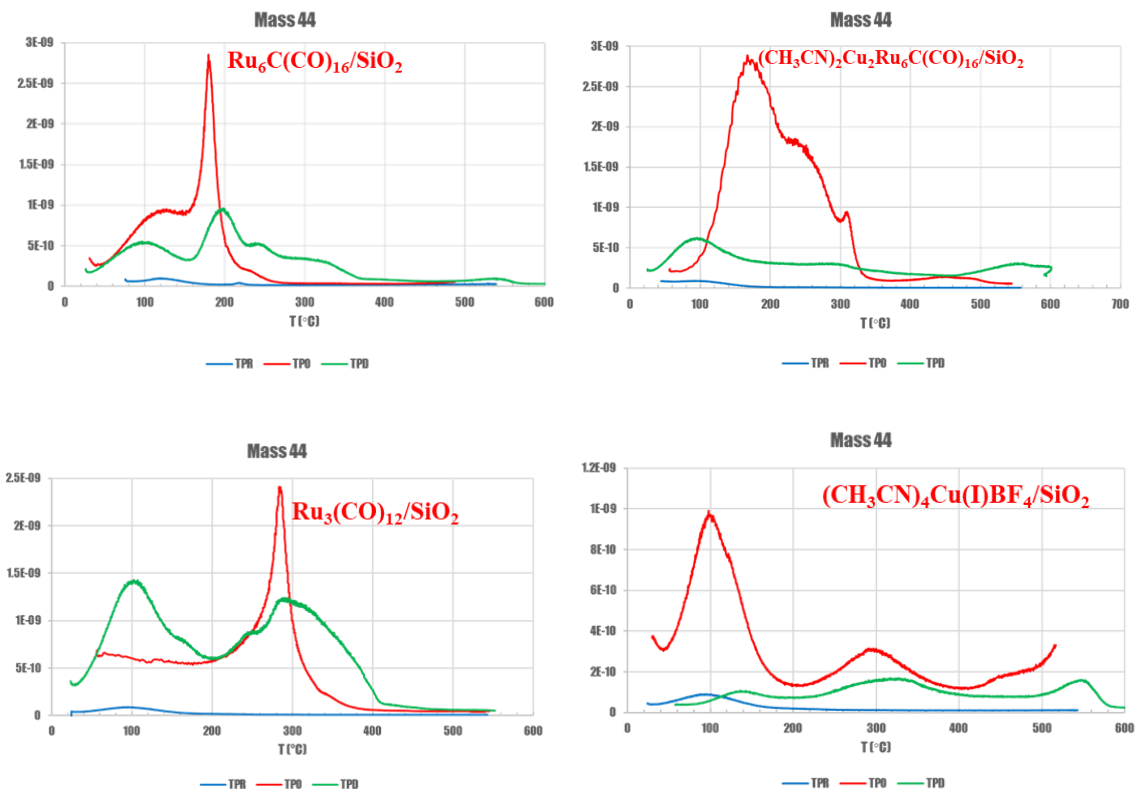

Figure 5.4. TPD, TPO, and TPR results for $Ru_6C(CO)_{16}/SiO_2$, $(CH_3CN)_2Cu_2Ru_6C(CO)_{16}/SiO_2$, $Ru_3(CO)_{12}/SiO_2$, and $(CH_3CN)_4Cu(I)BF_4/SiO_2$.

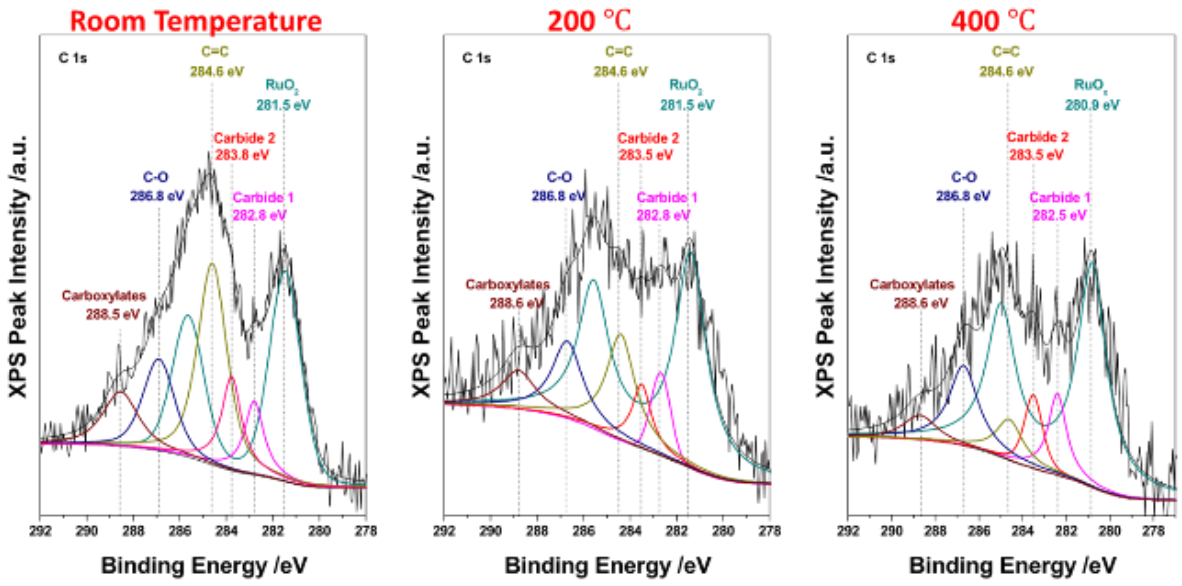

Figure 5.5. XPS spectra of $Ru_6C(CO)_{16}/SiO_2$ and Ru_6/SiO_2 activated in situ at 200°C and 400 °C.

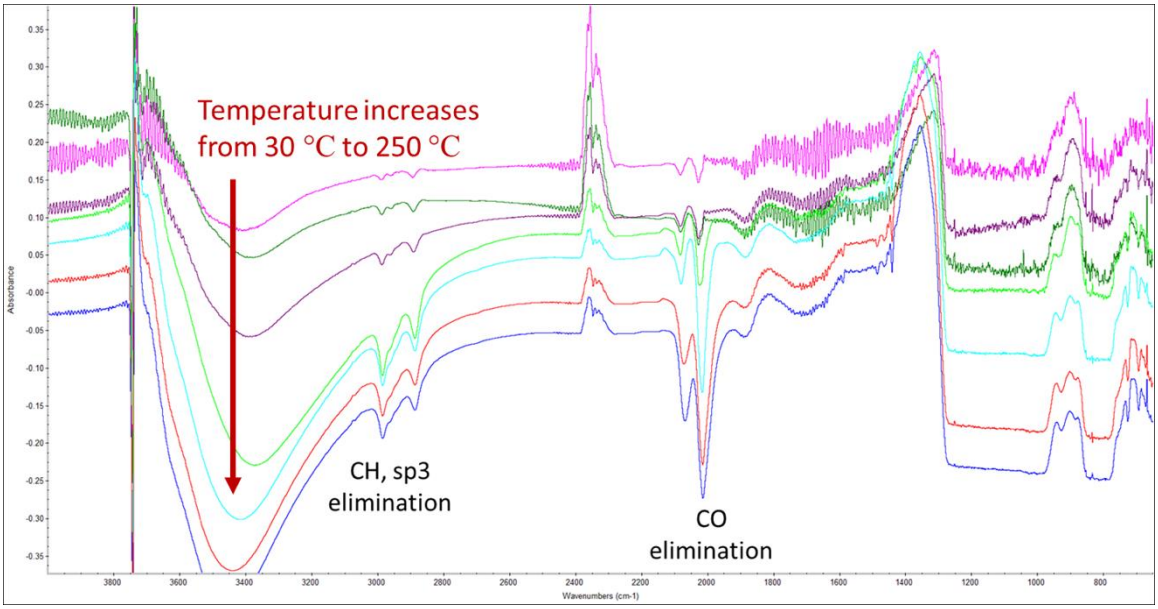

Figure 5.6. FT-IR spectra of in situ activated Ru_6Cu_2/SiO_2.

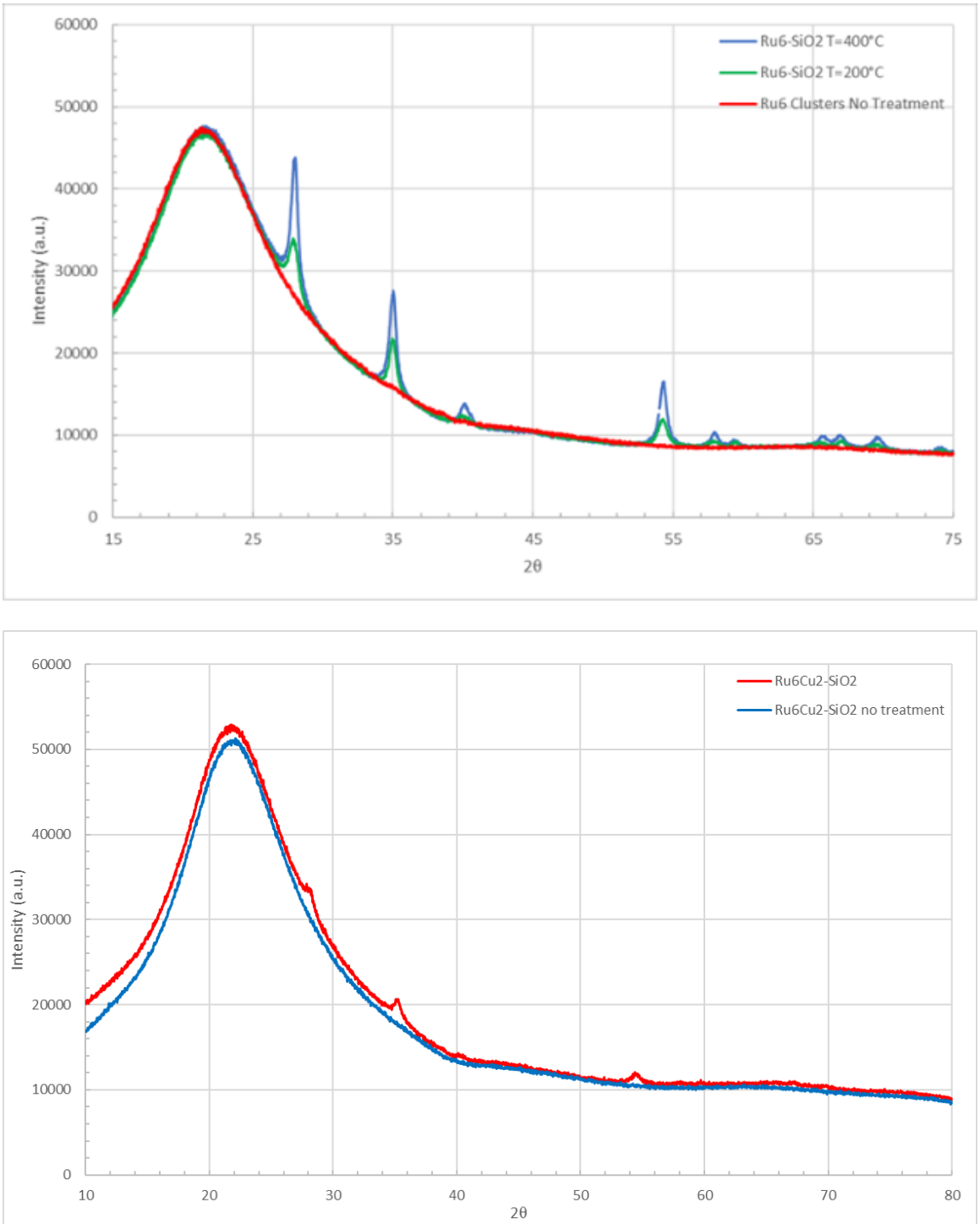

Figure 5.7. XRD spectra of (a) $Ru_6C(CO)_{16}/SiO_2$ and activated Ru_6/SiO_2 at 200 °C and 400°C, (b) $(CH_3CN)_2Cu_2Ru_6C(CO)_{16}/SiO_2$ and Ru_6Cu_2/SiO_2 catalyst activated at 400°C.

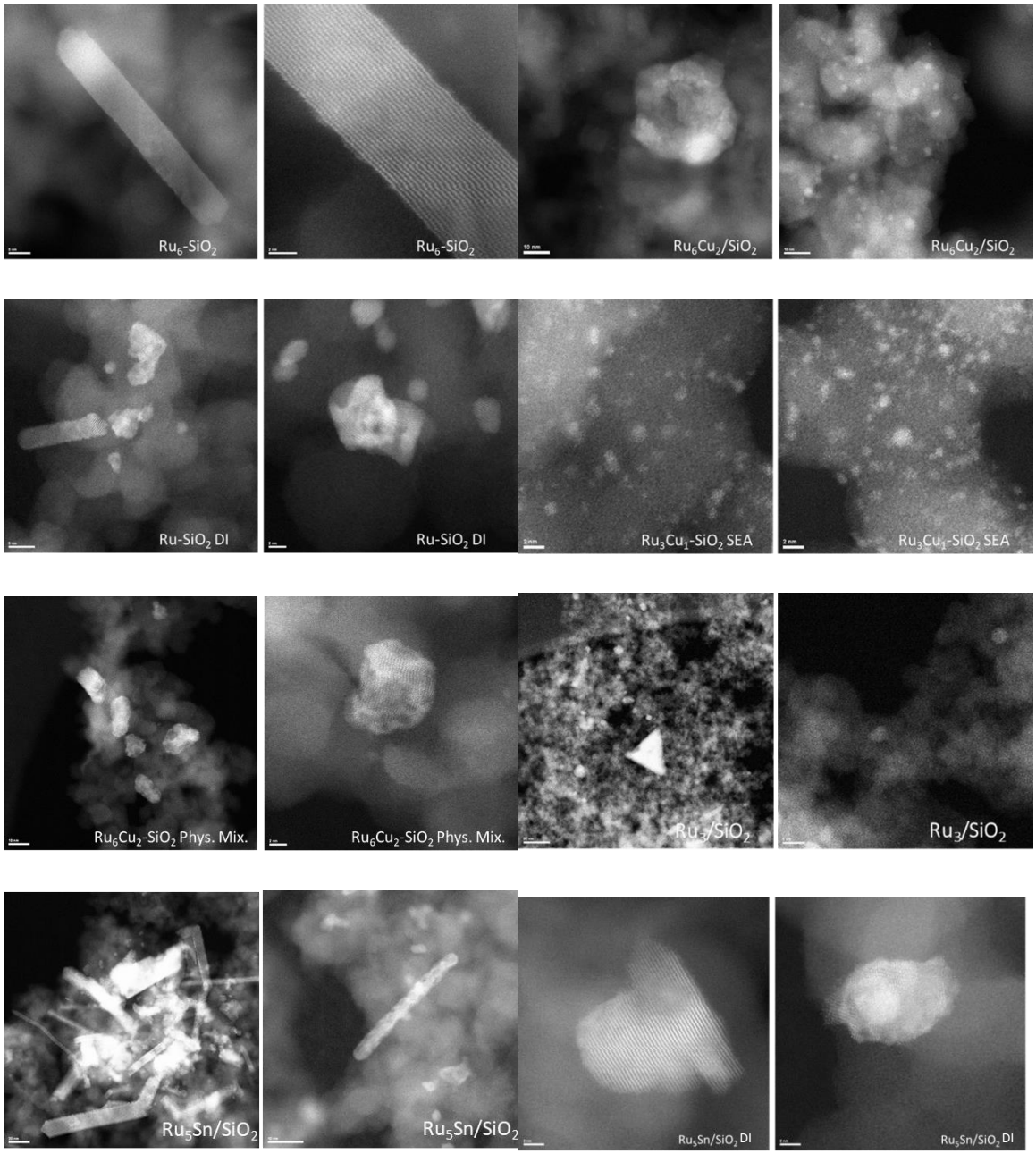

Figure 5.8. STEM images of Ru_6/SiO_2, Ru_6Cu_2/SiO_2, Ru/SiO_2 DI, Ru_3Cu_1/SiO_2 SEA, Ru_6Cu_2/SiO_2 Phys. Mix., Ru_3/SiO_2, Ru_5/SiO_2, and Ru_5Sn/SiO_2 DI.

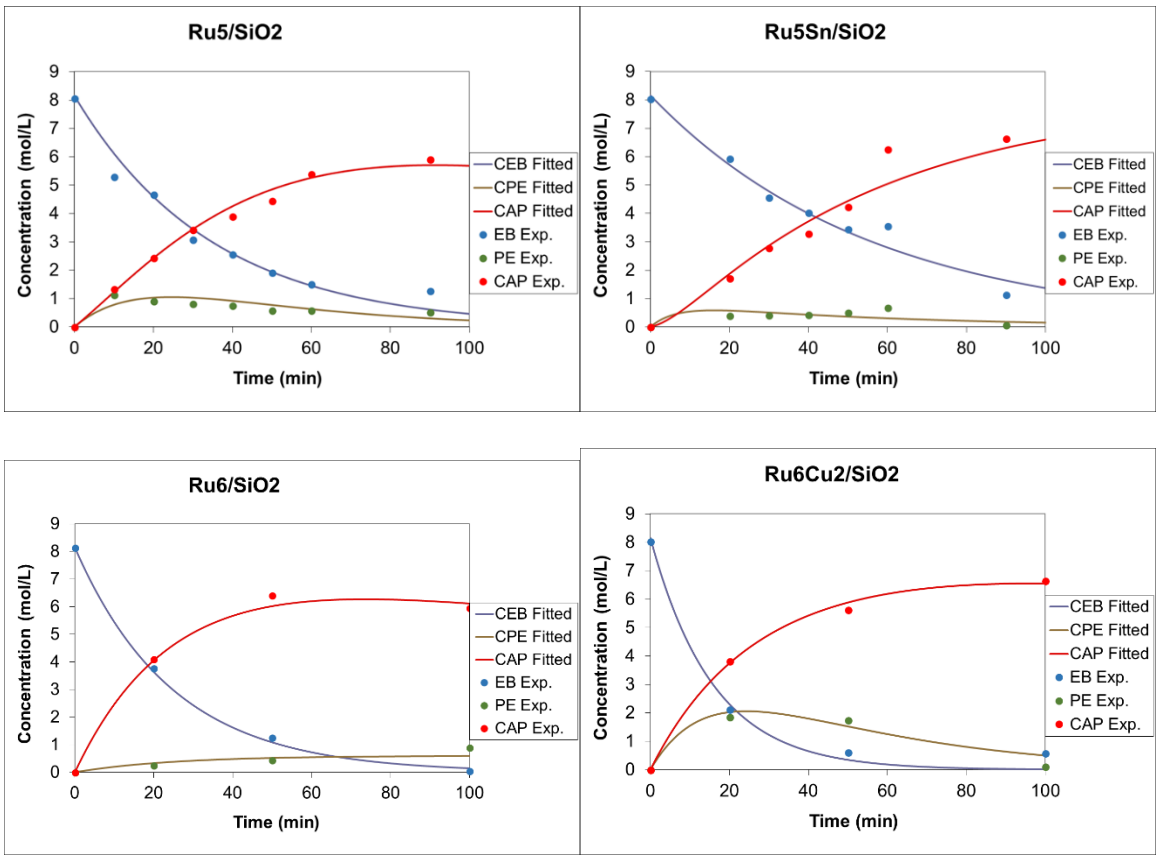

Figure 5.9. Ethylbenzene oxidation- Ru_5/SiO_2, Ru_5Sn/SiO_2, Ru_6/SiO_2, and Ru_6Cu_2/SiO_2 - Least Square Fitting.

References

Abad, Alberto, Patricia Concepción, Avelino Corma, and Hermenegildo García. 2005. “A Collaborative Effect between Gold and a Support Induces the Selective Oxidation of Alcohols.” *Angewandte Chemie International Edition* 44 (26): 4066–69. https://doi.org/10.1002/anie.200500382.

Abbet, S., U. Heiz, H. Häkkinen, and U. Landman. 2001. “CO Oxidation on a Single Pd Atom Supported on Magnesia.” *Physical Review Letters* 86 (26): 5950–53. https://doi.org/10.1103/PhysRevLett.86.5950.

Adabi, Horie, Abolfazl Shakouri, Noor Ul Hassan, John R Varcoe, Barr Zulevi, Alexey Serov, John R Regalbuto, and William E Mustain. 2021. “High-Performing Commercial Fe–N–C Cathode Electrocatalyst for Anion-Exchange Membrane Fuel Cells.” *Nature Energy* 6 (8): 834–43. https://doi.org/10.1038/s41560-021-00878-7.

Adams, Richard D, Burjor Captain, Wei Fu, and Mark D Smith. 2002a. “High Nuclearity Ruthenium−Tin Clusters from the Reactions of Triphenylstannane with Pentaruthenium Carbonyl Carbido Cluster Complexes.” *Inorganic Chemistry* 41 (21): 5593–5601. https://doi.org/10.1021/ic0204169.

———. 2002b. “High Nuclearity Ruthenium−Tin Clusters from the Reactions of Triphenylstannane with Pentaruthenium Carbonyl Carbido Cluster Complexes.” *Inorganic Chemistry* 41 (21): 5593–5601. https://doi.org/10.1021/ic0204169.

Ahn, Jaewan, Choongsik Bae, Paul S Weiss, and Il-Doo Kim. 2021. “Celebrating 50 Years of KAIST: Collective Intelligence and Innovation for Confronting Contemporary Issues.” *ACS Nano* 15 (2): 1895–1907. https://doi.org/10.1021/acsnano.1c01101.

Aich, Payoli, Haojuan Wei, Bridget Basan, A Jeremy Kropf, Neil M Schweitzer, Christopher L Marshall, Jeffrey T Miller, and Randall Meyer. 2015. “Single-Atom Alloy Pd–Ag Catalyst for Selective Hydrogenation of Acrolein.” *The Journal of Physical Chemistry C* 119 (32): 18140–48. https://doi.org/10.1021/acs.jpcc.5b01357.

Alexeev, O, and B C Gates. 2000. “EXAFS Characterization of Supported Metal-Complex and Metal-Cluster Catalysts Made from Organometallic Precursors.” *Topics in Catalysis* 10 (3): 273–93. https://doi.org/10.1023/A:1019184605678.

Armstrong, Robert, Graham Hutchings, Stuart Taylor, Robert D. Armstrong, Graham J. Hutchings, and Stuart H. Taylor. 2016. “An Overview of Recent Advances of the Catalytic Selective Oxidation of Ethane to Oxygenates.” *Catalysts* 6 (5): 71. https://doi.org/10.3390/catal6050071.

Babucci, Melike, Adisak Guntida, and Bruce C Gates. 2020. “Atomically Dispersed Metals on Well-Defined Supports Including Zeolites and Metal–Organic Frameworks: Structure, Bonding, Reactivity, and Catalysis.” *Chemical Reviews* 120 (21): 11956–85. https://doi.org/10.1021/acs.chemrev.0c00864.

Boucher, Matthew B, Branko Zugic, George Cladaras, James Kammert, Matthew D

Marcinkowski, Timothy J Lawton, E Charles H Sykes, and Maria Flytzani-Stephanopoulos. 2013. “Single Atom Alloy Surface Analogs in Pd0.18Cu15 Nanoparticles for Selective Hydrogenation Reactions.” *Physical Chemistry Chemical Physics* 15 (29): 12187–96. https://doi.org/10.1039/C3CP51538A.

Bulushev, Dmitri A, and Lyubov G Bulusheva. 2021. “Catalysts with Single Metal Atoms for the Hydrogen Production from Formic Acid.” *Catalysis Reviews*, February, 1–40. https://doi.org/10.1080/01614940.2020.1864860.

Cao, Sufeng, Yanyan Zhao, Sungsik Lee, Shize Yang, Jilei Liu, Georgios Giannakakis, Mengwei Li, et al. 2020. “High-Loading Single Pt Atom Sites [Pt-O(OH)<Em>_X</Em>] Catalyze the CO PROX Reaction with High Activity and Selectivity at Mild Conditions.” *Science Advances* 6 (25): eaba3809. https://doi.org/10.1126/sciadv.aba3809.

Cao, Xinrui, Qiang Fu, and Yi Luo. 2014. “Catalytic Activity of Pd-Doped Cu Nanoparticles for Hydrogenation as a Single-Atom-Alloy Catalyst.” *Physical Chemistry Chemical Physics* 16 (18): 8367–75. https://doi.org/10.1039/C4CP00399C.

Cao, Xinxiang, Arash Mirjalili, James Wheeler, Wentao Xie, and Ben W -L. Jang. 2015. “Investigation of the Preparation Methodologies of Pd-Cu Single Atom Alloy Catalysts for Selective Hydrogenation of Acetylene.” *Frontiers of Chemical Science and Engineering* 9 (4): 442–49. https://doi.org/10.1007/s11705-015-1547-x.

Cao, Yueqiang, Jonathan Guerrero-Sańchez, Ilkeun Lee, Xinggui Zhou, Noboru

Takeuchi, and Francisco Zaera. 2020. “Kinetic Study of the Hydrogenation of Unsaturated Aldehydes Promoted by CuPtx/SBA-15 Single-Atom Alloy (SAA) Catalysts.” *ACS Catalysis* 10 (5): 3431–43. https://doi.org/10.1021/acscatal.9b05407.

Carson, Innis, Kirstian J MacRuary, Euan D Doidge, Ross J Ellis, Richard A Grant, Ross J Gordon, Jason B Love, et al. 2015. “Anion Receptor Design: Exploiting Outer-Sphere Coordination Chemistry To Obtain High Selectivity for Chloridometalates over Chloride.” *Inorganic Chemistry* 54 (17): 8685–92. https://doi.org/10.1021/acs.inorgchem.5b01317.

Chang, Qing-Yu, Kai-Qi Wang, Zhi-Jun Sui, Xing-Gui Zhou, De Chen, Wei-Kang Yuan, and Yi-An Zhu. 2021. “Rational Design of Single-Atom-Doped Ga2O3 Catalysts for Propane Dehydrogenation: Breaking through Volcano Plot by Lewis Acid–Base Interactions.” *ACS Catalysis* 11 (9): 5135–47. https://doi.org/10.1021/acscatal.0c05454.

Chen, Cui-Hong, Deyao Wu, Zhe Li, Rui Zhang, Chun-Guang Kuai, Xue-Ru Zhao, Cun-Ku Dong, Shi-Zhang Qiao, Hui Liu, and Xi-Wen Du. 2019. “Ruthenium-Based Single-Atom Alloy with High Electrocatalytic Activity for Hydrogen Evolution.” *Advanced Energy Materials* 9 (20): 1803913. https://doi.org/10.1002/aenm.201803913.

Chen, Linxiao, Raymond R Unocic, Adam S Hoffman, Jiyun Hong, Adriano H Braga, Zhenghong Bao, Simon R Bare, and Janos Szanyi. 2021. “Unlocking the Catalytic Potential of TiO_2-Supported Pt Single Atoms for the Reverse Water–Gas Shift

Reaction by Altering Their Chemical Environment." *JACS Au* 1 (7): 977–86. https://doi.org/10.1021/jacsau.1c00111.

Chen, Weiming, Xuanli Luo, Thomas J A Slater, Yongfang Zhou, Sanliang Ling, Rui Bao, Jesum Alves Fernandes, Jianshe Wang, and Yi Shen. 2020. "General Synthesis of Single Atom Electrocatalysts via a Facile Condensation–Carbonization Process." *Journal of Materials Chemistry A* 8 (48): 25959–69. https://doi.org/10.1039/D0TA08115A.

Chen, Y, S Ji, Y Wang, J Dong, W Chen, Z Li, R Shen, L Zheng, Z Zhuang, and D Wang. 2017. "Isolated Single Iron Atoms Anchored on N-Doped Porous Carbon as an Efficient Electrocatalyst for the Oxygen Reduction Reaction." *Angew. Chem., Int. Ed.* 56: 6937.

Chen, Zupeng, Evgeniya Vorobyeva, Sharon Mitchell, Edvin Fako, Manuel A Ortuño, Núria López, Sean M Collins, et al. 2018. "A Heterogeneous Single-Atom Palladium Catalyst Surpassing Homogeneous Systems for Suzuki Coupling." *Nature Nanotechnology* 13 (8): 702–7. https://doi.org/10.1038/s41565-018-0167-2.

Cook, Brian J, Gianna N Di Francesco, Matthew T Kieber-Emmons, and Leslie J Murray. 2018. "A Tricopper(I) Complex Competent for O Atom Transfer, C–H Bond Activation, and Multiple O2 Activation Steps." *Inorganic Chemistry* 57 (18): 11361–68. https://doi.org/10.1021/acs.inorgchem.8b00921.

Dadyburjor, Dady B, S S Jewur, and Eli Ruckenstein. 1979. "Selective Oxidation of Hydrocarbons on Composite Oxides." *Catalysis Reviews* 19 (2): 293–350.

https://doi.org/10.1080/03602457908068057.

Darby, Matthew T, Romain Réocreux, E Charles. H Sykes, Angelos Michaelides, and Michail Stamatakis. 2018. “Elucidating the Stability and Reactivity of Surface Intermediates on Single-Atom Alloy Catalysts.” *ACS Catalysis* 8 (6): 5038–50. https://doi.org/10.1021/acscatal.8b00881.

Datye, Abhaya K, and Hua Guo. 2021. “Single Atom Catalysis Poised to Transition from an Academic Curiosity to an Industrially Relevant Technology.” *Nature Communications* 12 (1): 895. https://doi.org/10.1038/s41467-021-21152-0.

Davis, Sara E., Matthew S. Ide, and Robert J. Davis. 2013. “Selective Oxidation of Alcohols and Aldehydes over Supported Metal Nanoparticles.” *Green Chem.* 15 (1): 17–45. https://doi.org/10.1039/C2GC36441G.

DeRita, L, S Dai, K Lopez-Zepeda, N Pham, G W Graham, X Pan, and P Christopher. 2017. “Catalyst Architecture for Stable Single Atom Dispersion Enables Site-Specific Spectroscopic and Reactivity Measurements of CO Adsorbed to Pt Atoms, Oxidized Pt Clusters, and Metallic Pt Clusters on TiO2.” *J. Am. Chem. Soc.* 139: 14150.

Donaldson, Erle, and Waqi Alam. 2008. *Wettability*.

Elwell, Courtney E, Nicole L Gagnon, Benjamin D Neisen, Debanjan Dhar, Andrew D Spaeth, Gereon M Yee, and William B Tolman. 2017. “Copper–Oxygen Complexes Revisited: Structures, Spectroscopy, and Reactivity.” *Chemical Reviews* 117 (3): 2059–2107. https://doi.org/10.1021/acs.chemrev.6b00636.

Enache, Dan I., Jennifer K. Edwards, Philip Landon, Benjamin Solsona-Espriu, Albert F. Carley, Andrew A. Herzing, Masashi Watanabe, Christopher J. Kiely, David W. Knight, and Graham J. Hutchings. 2006. “Solvent-Free Oxidation of Primary Alcohols to Aldehydes Using Au-Pd/TiO2 Catalyst.” *Science* 311 (5759): 362–65. https://doi.org/10.1126/science.1120560.

Faghri, Amir, and Yuwen Zhang. 2006a. “2 - THERMODYNAMICS OF MULTIPHASE SYSTEMS.” In , edited by Amir Faghri and Yuwen B T - Transport Phenomena in Multiphase Systems Zhang, 107–76. Boston: Academic Press. https://doi.org/https://doi.org/10.1016/B978-0-12-370610-2.50007-6.

———. 2006b. “5 - SOLID-LIQUID-VAPOR PHENOMENA AND INTERFACIAL HEAT AND MASS TRANSFER.” In , edited by Amir Faghri and Yuwen B T - Transport Phenomena in Multiphase Systems Zhang, 331–420. Boston: Academic Press. https://doi.org/https://doi.org/10.1016/B978-0-12-370610-2.50010-6.

———. 2006c. “SOLID-LIQUID-VAPOR PHENOMENA AND INTERFACIAL HEAT AND MASS TRANSFER.” In *Transport Phenomena in Multiphase Systems*, edited by Amir Faghri and Yuwen B T - Transport Phenomena in Multiphase Systems Zhang, 331–420. Boston: Elsevier. https://doi.org/10.1016/B978-0-12-370610-2.50010-6.

Fan, Yu, Shange Liu, Yu Yi, Hongpan Rong, and Jiatao Zhang. 2021. “Catalytic Nanomaterials toward Atomic Levels for Biomedical Applications: From Metal Clusters to Single-Atom Catalysts.” *ACS Nano* 15 (2): 2005–37. https://doi.org/10.1021/acsnano.0c06962.

Fathizadeh, Mahdi, Konstantin Khivantsev, Travis J. Pyrzynski, Naomi B. Klinghoffer, Abolfazl (Nabi) Shakouri, Miao Yu, and Shiguang Li. 2018. “Bio-Mimetic Oxygen Separation via a Hollow Fiber Membrane Contactor with O 2 Carrier Solutions.” *Chemical Communications* 54 (68): 9454–57. https://doi.org/10.1039/C8CC01457D.

Fu, Qiang, and Yi Luo. 2013. “Catalytic Activity of Single Transition-Metal Atom Doped in Cu(111) Surface for Heterogeneous Hydrogenation.” *The Journal of Physical Chemistry C* 117 (28): 14618–24. https://doi.org/10.1021/jp403902g.

Gao, Chao, Shuangming Chen, Ying Wang, Jiawen Wang, Xusheng Zheng, Junfa Zhu, Li Song, Wenkai Zhang, and Yujie Xiong. 2018. “Heterogeneous Single-Atom Catalyst for Visible-Light-Driven High-Turnover CO2 Reduction: The Role of Electron Transfer.” *Advanced Materials* 30 (13): 1704624. https://doi.org/https://doi.org/10.1002/adma.201704624.

Gao, Dunfeng, Tianfu Liu, Guoxiong Wang, and Xinhe Bao. 2021. “Structure Sensitivity in Single-Atom Catalysis toward CO2 Electroreduction.” *ACS Energy Letters* 6 (2): 713–27. https://doi.org/10.1021/acsenergylett.0c02665.

Ge, Xiaoxiao, Peng Zhou, Qinghua Zhang, Zhonghong Xia, Shulin Chen, Peng Gao, Zhe Zhang, Lin Gu, and Shaojun Guo. 2020. “Palladium Single Atoms on TiO 2 as a Photocatalytic Sensing Platform for Analyzing the Organophosphorus Pesticide Chlorpyrifos.” *Angewandte Chemie* 132 (1): 238–42. https://doi.org/10.1002/ange.201911516.

Giannakakis, Georgios, Antonios Trimpalis, Junjun Shan, Zhen Qi, Sufeng Cao, Jilei Liu,

Jianchao Ye, Juergen Biener, and Maria Flytzani-Stephanopoulos. 2018. “NiAu Single Atom Alloys for the Non-Oxidative Dehydrogenation of Ethanol to Acetaldehyde and Hydrogen.” *Topics in Catalysis* 61 (5): 475–86. https://doi.org/10.1007/s11244-017-0883-0.

Greiner, M T, T E Jones, S Beeg, L Zwiener, M Scherzer, F Girgsdies, S Piccinin, M Armbrüster, A Knop-Gericke, and R Schlögl. 2018. “Free-Atom-like d States in Single-Atom Alloy Catalysts.” *Nature Chemistry* 10 (10): 1008–15. https://doi.org/10.1038/s41557-018-0125-5.

Groothaert, Marijke H, Pieter J Smeets, Bert F Sels, Pierre A Jacobs, and Robert A Schoonheydt. 2005. “Selective Oxidation of Methane by the Bis(μ-Oxo)Dicopper Core Stabilized on ZSM-5 and Mordenite Zeolites.” *Journal of the American Chemical Society* 127 (5): 1394–95. https://doi.org/10.1021/ja047158u.

Guo, Wenlu, Xiangguo Meng, Yan Liu, Liang Ni, Zhaoyong Hu, Rui Chen, Minjia Meng, Yun Wang, Juan Han, and Min Luo. 2015. “Synthesis and Application of 8-Hydroxyquinoline Modified Magnetic Mesoporous Carbon for Adsorption of Multivariate Metal Ions from Aqueous Solutions.” *Journal of Industrial and Engineering Chemistry* 21: 340–49. https://doi.org/https://doi.org/10.1016/j.jiec.2014.01.048.

H Sykes, E Charles, and Phillip Christopher. 2020. “Recent Advances in Single-Atom Catalysts and Single-Atom Alloys: Opportunities for Exploring the Uncharted Phase Space in-Between.” *Current Opinion in Chemical Engineering* 29: 67–73. https://doi.org/https://doi.org/10.1016/j.coche.2020.06.004.

Hackett, Simon F. J., Rik M. Brydson, Mhairi H. Gass, Ian Harvey, Andrew D. Newman, Karen Wilson, and Adam F. Lee. 2007. “High-Activity, Single-Site Mesoporous Pd/Al2O3 Catalysts for Selective Aerobic Oxidation of Allylic Alcohols.” *Angewandte Chemie International Edition* 46 (45): 8593–96. https://doi.org/10.1002/anie.200702534.

Hannagan, Ryan T, Georgios Giannakakis, Romain Réocreux, Julia Schumann, Jordan Finzel, Yicheng Wang, Angelos Michaelides, et al. 2021. “First-Principles Design of a Single-Atom–Alloy Propane Dehydrogenation Catalyst.” *Science* 372 (6549): 1444 LP – 1447. https://doi.org/10.1126/science.abg8389.

Hao, X, W A Spieker, and J R Regalbuto. 2003. “A Further Simplification of the Revised Physical Adsorption (RPA) Model.” *Journal of Colloid and Interface Science* 267 (2): 259–64. https://doi.org/https://doi.org/10.1016/S0021-9797(03)00644-1.

Haukka, S, E.-L. Lakomaa, and T Suntola. 1999. “Adsorption Controlled Preparation of Heterogeneous Catalysts.” In *Adsorption and Its Applications in Industry and Environmental Protection*, edited by A B T - Studies in Surface Science and Catalysis Dąbrowski, 120:715–50. Elsevier. https://doi.org/https://doi.org/10.1016/S0167-2991(99)80570-9.

Hu, Fenglian, Leipeng Leng, Mingyang Zhang, Wenxing Chen, Yanlong Yu, Jun Wang, J Hugh Horton, and Zhijun Li. 2020. “Direct Synthesis of Atomically Dispersed Palladium Atoms Supported on Graphitic Carbon Nitride for Efficient Selective Hydrogenation Reactions.” *ACS Applied Materials & Interfaces* 12 (48): 54146–54. https://doi.org/10.1021/acsami.0c13881.

Hulva, Jan, Matthias Meier, Roland Bliem, Zdenek Jakub, Florian Kraushofer, Michael Schmid, Ulrike Diebold, Cesare Franchini, and Gareth S Parkinson. 2021. "Unraveling CO Adsorption on Model Single-Atom Catalysts." *Science* 371 (6527): 375 LP – 379. https://doi.org/10.1126/science.abe5757.

Iwasawa, Tetsuo, Makoto Tokunaga, Yasushi Obora, and Yasushi Tsuji. 2004. "Homogeneous Palladium Catalyst Suppressing Pd Black Formation in Air Oxidation of Alcohols." *Journal of the American Chemical Society* 126 (21): 6554–55. https://doi.org/10.1021/ja031936l.

J. S. Bradley, Roy L. Pruett, Ernestine Hill, Gerald B. Ansell, Micheal E. Leonowicz, and Michelle A. Modrick. 1982. "Synthesis and Molecular Structure of Bis(Acetonitri1ecuprio)Carbidohexadecacarbonylhexauthenium, [(CH3CN)2Cu2Ru6C(CO)16], a Bimetallic Carbidocarbonyl Cluster Containing a Copper-Copper Bond." *Organometallics* 1 (5): 748–52.

Jeong, Hojin, Dongjae Shin, Beom-Sik Kim, Junemin Bae, Sangyong Shin, Chanyeong Choe, Jeong Woo Han, and Hyunjoo Lee. 2020. "Controlling the Oxidation State of Pt Single Atoms for Maximizing Catalytic Activity." *Angewandte Chemie* 132 (46): 20872–77. https://doi.org/10.1002/ange.202009776.

Jiang, Kang, Boyang Liu, Min Luo, Shoucong Ning, Ming Peng, Yang Zhao, Ying-Rui Lu, Ting-Shan Chan, Frank M F de Groot, and Yongwen Tan. 2019. "Single Platinum Atoms Embedded in Nanoporous Cobalt Selenide as Electrocatalyst for Accelerating Hydrogen Evolution Reaction." *Nature Communications* 10 (1): 1743. https://doi.org/10.1038/s41467-019-09765-y.

Jiao, Ling, and John R Regalbuto. 2008. “The Synthesis of Highly Dispersed Noble and Base Metals on Silica via Strong Electrostatic Adsorption: I. Amorphous Silica.” *Journal of Catalysis* 260 (2): 329–41. https://doi.org/https://doi.org/10.1016/j.jcat.2008.09.022.

Jin, Zhaoyu, Panpan Li, Yan Meng, Zhiwei Fang, Dan Xiao, and Guihua Yu. 2021. “Understanding the Inter-Site Distance Effect in Single-Atom Catalysts for Oxygen Electroreduction.” *Nature Catalysis* 4 (7): 615–22. https://doi.org/10.1038/s41929-021-00650-w.

Kaiser, Selina K, Zupeng Chen, Dario Faust Akl, Sharon Mitchell, and Javier Pérez-Ramírez. 2020. “Single-Atom Catalysts across the Periodic Table.” *Chemical Reviews*, October. https://doi.org/10.1021/acs.chemrev.0c00576.

Khivantsev, Konstantin, Alessandro Biancardi, Mahdi Fathizadeh, Fahad Almalki, Job L. Grant, Huynh Ngoc Tien, Abolfazl Shakouri, et al. 2018. “Catalytic N−H Bond Activation and Breaking by a Well-Defined CoII1O4 Site of a Heterogeneous Catalyst.” *ChemCatChem* 10 (4): 736–42. https://doi.org/10.1002/cctc.201701268.

Kim, Jiwhan, Hee-Eun Kim, and Hyunjoo Lee. 2018. “Single-Atom Catalysts of Precious Metals for Electrochemical Reactions.” *ChemSusChem* 11 (1): 104–13. https://doi.org/10.1002/cssc.201701306.

Kim, Jiwhan, Chi-Woo Roh, Suman Kalyan Sahoo, Sungeun Yang, Junemin Bae, Jeong Woo Han, and Hyunjoo Lee. 2018. “Highly Durable Platinum Single-Atom Alloy Catalyst for Electrochemical Reactions.” *Advanced Energy Materials* 8 (1):

1701476. https://doi.org/10.1002/aenm.201701476.

Kou, Zongkui, Wenjie Zang, Peikui Wang, Xin Li, and John Wang. 2020. “Single Atom Catalysts: A Surface Heterocompound Perspective.” *Nanoscale Horizons* 5 (5): 757–64. https://doi.org/10.1039/D0NH00088D.

Kruppe, Christopher M, Joel D Krooswyk, and Michael Trenary. 2017a. “Polarization-Dependent Infrared Spectroscopy of Adsorbed Carbon Monoxide To Probe the Surface of a Pd/Cu(111) Single-Atom Alloy.” *The Journal of Physical Chemistry C* 121 (17): 9361–69. https://doi.org/10.1021/acs.jpcc.7b01227.

———. 2017b. “Selective Hydrogenation of Acetylene to Ethylene in the Presence of a Carbonaceous Surface Layer on a Pd/Cu(111) Single-Atom Alloy.” *ACS Catalysis* 7 (12): 8042–49. https://doi.org/10.1021/acscatal.7b02862.

Kumar, M Santhosh, M Schwidder, W Grünert, and A Brückner. 2004. “On the Nature of Different Iron Sites and Their Catalytic Role in Fe-ZSM-5 DeNOx Catalysts: New Insights by a Combined EPR and UV/VIS Spectroscopic Approach.” *Journal of Catalysis* 227 (2): 384–97. https://doi.org/https://doi.org/10.1016/j.jcat.2004.08.003.

Lambert, Stéphanie, Nathalie Job, Lawrence D’Souza, Manuel Fernando Ribeiro Pereira, René Pirard, Benoît Heinrichs, José Luis Figueiredo, Jean-Paul Pirard, and John R Regalbuto. 2009. “Synthesis of Very Highly Dispersed Platinum Catalysts Supported on Carbon Xerogels by the Strong Electrostatic Adsorption Method.” *Journal of Catalysis* 261 (1): 23–33. https://doi.org/https://doi.org/10.1016/j.jcat.2008.10.014.

Li, Hao, Wenrui Chai, and Graeme Henkelman. 2019. “Selectivity for Ethanol Partial Oxidation: The Unique Chemistry of Single-Atom Alloy Catalysts on Au, Ag, and Cu(111).” *Journal of Materials Chemistry A* 7 (41): 23868–77. https://doi.org/10.1039/C9TA04572D.

Li, Zejun, Zeyu Wang, Shibo Xi, Xiaoxu Zhao, Tao Sun, Jing Li, Wei Yu, et al. 2021. “Tuning the Spin Density of Cobalt Single-Atom Catalysts for Efficient Oxygen Evolution.” *ACS Nano* 15 (4): 7105–13. https://doi.org/10.1021/acsnano.1c00251.

Liu, Jilei, Junjun Shan, Felicia R Lucci, Sufeng Cao, E Charles H Sykes, and Maria Flytzani-Stephanopoulos. 2017. “Palladium–Gold Single Atom Alloy Catalysts for Liquid Phase Selective Hydrogenation of 1-Hexyne.” *Catalysis Science & Technology* 7 (19): 4276–84. https://doi.org/10.1039/C7CY00794A.

Liu, Jilei, Matthew B Uhlman, Matthew M Montemore, Antonios Trimpalis, Georgios Giannakakis, Junjun Shan, Sufeng Cao, Ryan T Hannagan, E Charles H Sykes, and Maria Flytzani-Stephanopoulos. 2019. “Integrated Catalysis-Surface Science-Theory Approach to Understand Selectivity in the Hydrogenation of 1-Hexyne to 1-Hexene on PdAu Single-Atom Alloy Catalysts.” *ACS Catalysis* 9 (9): 8757–65. https://doi.org/10.1021/acscatal.9b00491.

Liu, Jing, Benjamin R Bunes, Ling Zang, and Chuanyi Wang. 2018. “Supported Single-Atom Catalysts: Synthesis, Characterization, Properties, and Applications.” *Environmental Chemistry Letters* 16 (2): 477–505. https://doi.org/10.1007/s10311-017-0679-2.

Liu, Lichen, and Avelino Corma. 2018. “Metal Catalysts for Heterogeneous Catalysis: From Single Atoms to Nanoclusters and Nanoparticles.” *Chemical Reviews* 118 (10): 4981–5079. https://doi.org/10.1021/acs.chemrev.7b00776.

Liu, Rui, Shejiang Liu, Hui Ding, Dan Zhao, Jianfeng Fu, Yuxin Zhang, Wangchen Huo, and Gang “Kevin” Li. 2021. “Unveiling the Role of Atomically Dispersed Active Sites over Amorphous Iron Oxide Supported Pt Catalysts for Complete Catalytic Ozonation of Toluene at Low Temperature.” *Industrial & Engineering Chemistry Research* 60 (10): 3881–92. https://doi.org/10.1021/acs.iecr.0c05549.

López Nieto, José M, and Benjamín Solsona. 2018. “5 - Gas Phase Heterogeneous Partial Oxidation Reactions.” In *Metal Oxides*, edited by Jacques C B T - Metal Oxides in Heterogeneous Catalysis Védrine, 211–86. Elsevier. https://doi.org/https://doi.org/10.1016/B978-0-12-811631-9.00005-3.

Lucci, Felicia R, Matthew T Darby, Michael F G Mattera, Christopher J Ivimey, Andrew J Therrien, Angelos Michaelides, Michail Stamatakis, and E Charles H Sykes. 2016. “Controlling Hydrogen Activation, Spillover, and Desorption with Pd–Au Single-Atom Alloys.” *The Journal of Physical Chemistry Letters* 7 (3): 480–85. https://doi.org/10.1021/acs.jpclett.5b02400.

Lucci, Felicia R, Jilei Liu, Matthew D Marcinkowski, Ming Yang, Lawrence F Allard, Maria Flytzani-Stephanopoulos, and E Charles H Sykes. 2015. “Selective Hydrogenation of 1,3-Butadiene on Platinum–Copper Alloys at the Single-Atom Limit.” *Nature Communications* 6 (1): 8550. https://doi.org/10.1038/ncomms9550.

Lucci, Felicia R, Matthew D Marcinkowski, Timothy J Lawton, and E Charles H Sykes. 2015. “H2 Activation and Spillover on Catalytically Relevant Pt–Cu Single Atom Alloys.” *The Journal of Physical Chemistry C* 119 (43): 24351–57. https://doi.org/10.1021/acs.jpcc.5b05562.

Luo, Li, Huan Liu, Guiying Li, and Changwei Hu. 2016. “Partial Oxidation of Ethylbenzene by H2O2 on VOx/HZSM-22 Catalyst.” *RSC Advances* 6 (60): 55463–71. https://doi.org/10.1039/C6RA05906F.

Malta, Grazia, Simon A Kondrat, Simon J Freakley, David J Morgan, Emma K Gibson, Peter P Wells, Matteo Aramini, et al. 2020. “In Situ K-Edge X-Ray Absorption Spectroscopy of the Ligand Environment of Single-Site Au/C Catalysts during Acetylene Hydrochlorination.” *Chemical Science* 11 (27): 7040–52. https://doi.org/10.1039/D0SC02152K.

Marcinkowski, Matthew D, Matthew T Darby, Jilei Liu, Joshua M Wimble, Felicia R Lucci, Sungsik Lee, Angelos Michaelides, Maria Flytzani-Stephanopoulos, Michail Stamatakis, and E Charles H Sykes. 2018. “Pt/Cu Single-Atom Alloys as Coke-Resistant Catalysts for Efficient C–H Activation.” *Nature Chemistry* 10 (3): 325–32. https://doi.org/10.1038/nchem.2915.

Martín, Julia. 2018. “An Overview on Ligands of Therapeutically Interest.” *Pharmacy & Pharmacology International Journal* 6 (3). https://doi.org/10.15406/ppij.2018.06.00177.

Maurer, Florian, Jelena Jelic, Junjun Wang, Andreas Gänzler, Paolo Dolcet, Christof

Wöll, Yuemin Wang, Felix Studt, Maria Casapu, and Jan-Dierk Grunwaldt. 2020. "Tracking the Formation, Fate and Consequence for Catalytic Activity of Pt Single Sites on CeO2." *Nature Catalysis* 3 (10): 824–33. https://doi.org/10.1038/s41929-020-00508-7.

Mehrabadi, B.A.T., R. White, A. Shakouri, J.R. Regalbuto, J.W. Weidner, and J.R. Monnier. 2019. "Ruthenium–Platinum Bimetallic Catalysts with Controlled Surface Compositions and Enhanced Performance for Methanol Oxidation." *Catalysis Today* 334. https://doi.org/10.1016/j.cattod.2018.11.042.

Mehrabadi, Bahareh Alsadat Tavakoli, Rembert White, Abolfazl Shakouri, John R Regalbuto, John W Weidner, and John R Monnier. 2018. "Ruthenium–Platinum Bimetallic Catalysts with Controlled Surface Compositions and Enhanced Performance for Methanol Oxidation." *Catalysis Today*. https://doi.org/https://doi.org/10.1016/j.cattod.2018.11.042.

Mehrabadi, Bahareh Alsadat Tavakoli, W Xiong, Rembert White, Abolfazl Shakouri, John R Regalbuto, and John W Weidner. 2019. "Rationalize Synthesis of Pt-Ru/Mwcnts Bimetallic Catalysts for Methanol Oxidation Reaction." In . Chicago, Illinois: North American Catalysis Society.

Mitchell, Sharon, and Javier Pérez-Ramírez. 2020. "Single Atom Catalysis: A Decade of Stunning Progress and the Promise for a Bright Future." *Nature Communications* 11 (1): 4302. https://doi.org/10.1038/s41467-020-18182-5.

Mlahi, Mosaad R, Elsayed M Afsah, Amr Negm, and Mohsen M Mostafa. 2015.

"Synthesis of 8-Hydroxyquinolium Chloroacetate and Synthesis of Complexes Derived from 8-Hydroxyquinoline, and Characterization, Density Functional Theory and Biological Studies." *Applied Organometallic Chemistry* 29 (4): 200–208. https://doi.org/https://doi.org/10.1002/aoc.3265.

Nicholls, J. N., and M. D. Vargas. 1983. "Carbido-Carbonyl Ruthenium Cluster Complexes." *Inorg. Syn.* 26: 281–84.

Nigam, Sandeep, and Chiranjib Majumder. 2018. "Single Atom Alloy Catalyst for SO3 Decomposition: Enhancement of Platinum Catalyst's Performance by Ag Atom Embedding." *Nanoscale* 10 (44): 20599–610. https://doi.org/10.1039/C8NR05179H.

Owen, Cameron J, and Stephen J Jenkins. 2021. "Comparative Study of Single-Atom Gold and Iridium on CeO2{111}." *The Journal of Chemical Physics* 154 (16): 164703. https://doi.org/10.1063/5.0048953.

Oyama, S Ted. 1996a. "Factors Affecting Selectivity in Catalytic Partial Oxidation and Combustion Reactions." In *Heterogeneous Hydrocarbon Oxidation*, 638:1–2. ACS Symposium Series. American Chemical Society. https://doi.org/doi:10.1021/bk-1996-0638.ch001.

———. 1996b. "Factors Affecting Selectivity in Catalytic Partial Oxidation and Combustion Reactions." In *Heterogeneous Hydrocarbon Oxidation*, 638:1–2. ACS Symposium Series. American Chemical Society. https://doi.org/doi:10.1021/bk-1996-0638.ch001.

Pei, Guang Xian, Xiao Yan Liu, Aiqin Wang, Lin Li, Yanqiang Huang, Tao Zhang,

Jonathan W Lee, Ben W L Jang, and Chung-Yuan Mou. 2014. “Promotional Effect of Pd Single Atoms on Au Nanoparticles Supported on Silica for the Selective Hydrogenation of Acetylene in Excess Ethylene.” *New Journal of Chemistry* 38 (5): 2043–51. https://doi.org/10.1039/C3NJ01136D.

Peterson, Eric J, Andrew T DeLaRiva, Sen Lin, Ryan S Johnson, Hua Guo, Jeffrey T Miller, Ja Hun Kwak, et al. 2014. “Low-Temperature Carbon Monoxide Oxidation Catalysed by Regenerable Atomically Dispersed Palladium on Alumina.” *Nature Communications* 5 (1): 4885. https://doi.org/10.1038/ncomms5885.

Prachayasittikul, Virapong, Veda Prachayasittikul, Supaluk Prachayasittikul, and Somsak Ruchirawat. 2013. “8-Hydroxyquinolines: A Review of Their Metal Chelating Properties and Medicinal Applications.” *Drug Design, Development and Therapy*, October, 1157. https://doi.org/10.2147/DDDT.S49763.

Qi, Ji, Jordan Finzel, Hossein Robatjazi, Mingjie Xu, Adam S Hoffman, Simon R Bare, Xiaoqing Pan, and Phillip Christopher. 2020. “Selective Methanol Carbonylation to Acetic Acid on Heterogeneous Atomically Dispersed ReO4/SiO2 Catalysts.” *Journal of the American Chemical Society* 142 (33): 14178–89. https://doi.org/10.1021/jacs.0c05026.

Qi, Kun, Manish Chhowalla, and Damien Voiry. 2020. “Single Atom Is Not Alone: Metal–Support Interactions in Single-Atom Catalysis.” *Materials Today* 40: 173–92. https://doi.org/https://doi.org/10.1016/j.mattod.2020.07.002.

Qiao, B, A Wang, X Yang, L F Allard, Z Jiang, Y Cui, J Liu, J Li, and T Zhang. 2011.

"Single-Atom Catalysis of CO Oxidation Using Pt1/FeOx." *Nat. Chem.* 3: 634.

Rafelt, John S., and James H. Clark. 2000. "Recent Advances in the Partial Oxidation of Organic Molecules Using Heterogeneous Catalysis." *Catalysis Today*. https://doi.org/10.1016/S0920-5861(99)00308-9.

Raji, Vadakkekara, Mousumi Chakraborty, and Parimal A. Parikh. 2012. "Catalytic Performance of Silica-Supported Silver Nanoparticles for Liquid-Phase Oxidation of Ethylbenzene." *Industrial and Engineering Chemistry Research*. https://doi.org/10.1021/ie2027603.

Ravindran, Varadarajan, Mario R Stevens, Badri N Badriyha, and Massoud Pirbazari. 1999. "Modeling the Sorption of Toxic Metals on Chelant-Impregnated Adsorbent." *AIChE Journal* 45 (5): 1135–46. https://doi.org/https://doi.org/10.1002/aic.690450520.

Regalbuto, John, ed. 2016. *Catalyst Preparation*. CRC Press. https://doi.org/10.1201/9781420006506.

Resasco, Joaquin, and Phillip Christopher. 2020. "Atomically Dispersed Pt-Group Catalysts: Reactivity, Uniformity, Structural Evolution, and Paths to Increased Functionality." *The Journal of Physical Chemistry Letters* 11 (23): 10114–23. https://doi.org/10.1021/acs.jpclett.0c02904.

Rodriguez, Abraham A, Christopher T Williams, and John R Monnier. 2014. "Selective Liquid-Phase Oxidation of Glycerol over Au–Pd/C Bimetallic Catalysts Prepared by Electroless Deposition." *Applied Catalysis A: General* 475: 161–68.

https://doi.org/https://doi.org/10.1016/j.apcata.2014.01.011.

Rohini, Kamaldeep Paul, and Vijay Luxami. 2020. “8-Hydroxyquinoline Fluorophore for Sensing of Metal Ions and Anions.” *The Chemical Record* n/a (n/a). https://doi.org/https://doi.org/10.1002/tcr.202000082.

Sa, Young Jin, Dong-Jun Seo, Jinwoo Woo, Jung Tae Lim, Jae Yeong Cheon, Seung Yong Yang, Jae Myeong Lee, et al. 2016. “A General Approach to Preferential Formation of Active Fe–Nx Sites in Fe–N/C Electrocatalysts for Efficient Oxygen Reduction Reaction.” *Journal of the American Chemical Society* 138 (45): 15046–56. https://doi.org/10.1021/jacs.6b09470.

Samantaray, Manoja K, Valerio D’Elia, Eva Pump, Laura Falivene, Moussab Harb, Samy Ould Chikh, Luigi Cavallo, and Jean-Marie Basset. 2020. “The Comparison between Single Atom Catalysis and Surface Organometallic Catalysis.” *Chemical Reviews* 120 (2): 734–813. https://doi.org/10.1021/acs.chemrev.9b00238.

Santhanam, N, T A Conforti, W Spieker, and J R Regalbuto. 1994. “Nature of Metal Catalyst Precursors Adsorbed onto Oxide Supports.” *Catalysis Today* 21 (1): 141–56. https://doi.org/https://doi.org/10.1016/0920-5861(94)80040-5.

Sartori, Giovanni, and Raimondo Maggi. 2006. “Use of Solid Catalysts in Friedel−Crafts Acylation Reactions.” *Chemical Reviews* 106 (3): 1077–1104. https://doi.org/10.1021/cr040695c.

Sengodan, Sivaprakash, Rong Lan, John Humphreys, Dongwei Du, Wei Xu, Huanting Wang, and Shanwen Tao. 2018. “Advances in Reforming and Partial Oxidation of

Hydrocarbons for Hydrogen Production and Fuel Cell Applications." *Renewable and Sustainable Energy Reviews* 82: 761–80. https://doi.org/https://doi.org/10.1016/j.rser.2017.09.071.

Serp, Philippe. 2021. "Cooperativity in Supported Metal Single Atom Catalysis." *Nanoscale* 13 (12): 5985–6004. https://doi.org/10.1039/D1NR00465D.

Shan, Junjun, Jilei Liu, Mengwei Li, Sylvia Lustig, Sungsik Lee, and Maria Flytzani-Stephanopoulos. 2018. "NiCu Single Atom Alloys Catalyze the CH Bond Activation in the Selective Non- Oxidative Ethanol Dehydrogenation Reaction." *Applied Catalysis B: Environmental* 226: 534–43. https://doi.org/https://doi.org/10.1016/j.apcatb.2017.12.059.

Sheikhmohammadi, Amir, Seyed Mohsen Mohseni, Rouhollah khodadadi, Mahdieh Sardar, Mehrnoosh Abtahi, Sakineh Mahdavi, Hassan Keramati, et al. 2017. "Application of Graphene Oxide Modified with 8-Hydroxyquinoline for the Adsorption of Cr (VI) from Wastewater: Optimization, Kinetic, Thermodynamic and Equilibrium Studies." *Journal of Molecular Liquids* 233: 75–88. https://doi.org/https://doi.org/10.1016/j.molliq.2017.02.101.

Shen, Lihua, Daixin Ye, Hongbin Zhao, and Jiujun Zhang. 2021. "Perspectives for Single-Atom Nanozymes: Advanced Synthesis, Functional Mechanisms, and Biomedical Applications." *Analytical Chemistry* 93 (3): 1221–31. https://doi.org/10.1021/acs.analchem.0c04084.

Shi, Yantao, Chunyu Zhao, Haisheng Wei, Jiahao Guo, Suxia Liang, Aiqin Wang, Tao

Zhang, Jingyue Liu, and Tingli Ma. 2014. “Single-Atom Catalysis in Mesoporous Photovoltaics: The Principle of Utility Maximization.” *Advanced Materials* 26 (48): 8147–53. https://doi.org/10.1002/adma.201402978.

Sietsma, Jelle R A, A Jos van Dillen, Petra E de Jongh, and Krijn P de Jong. 2006. “Application of Ordered Mesoporous Materials as Model Supports to Study Catalyst Preparation by Impregnation and Drying.” In *Scientific Bases for the Preparation of Heterogeneous Catalysts*, edited by E M Gaigneaux, M Devillers, D E De Vos, S Hermans, P A Jacobs, J A Martens, and P B T - Studies in Surface Science and Catalysis Ruiz, 162:95–102. Elsevier. https://doi.org/https://doi.org/10.1016/S0167-2991(06)80895-5.

Simonovis, Juan Pablo, Adrian Hunt, Sanjaya D Senanayake, and Iradwikanari Waluyo. 2019. “Subtle and Reversible Interactions of Ambient Pressure H2 with Pt/Cu(111) Single-Atom Alloy Surfaces.” *Surface Science* 679: 207–13. https://doi.org/https://doi.org/10.1016/j.susc.2018.09.003.

Singh, Baljeet, Vikas Sharma, Rahul P Gaikwad, Paolo Fornasiero, Radek Zbořil, and Manoj B Gawande. 2021. “Single-Atom Catalysts: A Sustainable Pathway for the Advanced Catalytic Applications.” *Small* 17 (16): 2006473. https://doi.org/https://doi.org/10.1002/smll.202006473.

Spezzati, Giulia, Yaqiong Su, Jan P Hofmann, Angelica D Benavidez, Andrew T DeLaRiva, Jay McCabe, Abhaya K Datye, and Emiel J M Hensen. 2017. “Atomically Dispersed Pd–O Species on CeO2(111) as Highly Active Sites for Low-Temperature CO Oxidation.” *ACS Catalysis* 7 (10): 6887–91.

https://doi.org/10.1021/acscatal.7b02001.

Spieker, W A, J Liu, X Hao, J T Miller, A J Kropf, and J R Regalbuto. 2003. “An EXAFS Study of the Coordination Chemistry of Hydrogen Hexachloroplatinate (IV): 2. Speciation of Complexes Adsorbed onto Alumina.” *Applied Catalysis A: General* 243 (1): 53–66. https://doi.org/https://doi.org/10.1016/S0926-860X(02)00537-9.

Su, Ya-Qiong, Ivo A W Filot, Jin-Xun Liu, and Emiel J M Hensen. 2018. “Stable Pd-Doped Ceria Structures for CH4 Activation and CO Oxidation.” *ACS Catalysis* 8 (1): 75–80. https://doi.org/10.1021/acscatal.7b03295.

Sun, Mingzi, Tong Wu, and Bolong Huang. 2020. “Designing the Future Atomic Electrocatalyst for Efficient Energy Systems.” *Engineering Reports* 2 (12): e12327. https://doi.org/https://doi.org/10.1002/eng2.12327.

Sun, Shijia, Guodong Sun, Chunlei Pei, Zhi-Jian Zhao, and Jinlong Gong. 2021. “Origin of Performances of Pt/Cu Single-Atom Alloy Catalysts for Propane Dehydrogenation.” *The Journal of Physical Chemistry C*, July. https://doi.org/10.1021/acs.jpcc.1c04295.

Sun, Shuhui, Gaixia Zhang, Nicolas Gauquelin, Ning Chen, Jigang Zhou, Songlan Yang, Weifeng Chen, et al. 2013. “Single-Atom Catalysis Using Pt/Graphene Achieved through Atomic Layer Deposition.” *Scientific Reports* 3 (1): 1775. https://doi.org/10.1038/srep01775.

Sun, Xi, Simon R Dawson, Tanja E Parmentier, Grazia Malta, Thomas E Davies, Qian

He, Li Lu, et al. 2020. “Facile Synthesis of Precious-Metal Single-Site Catalysts Using Organic Solvents.” *Nature Chemistry* 12 (6): 560–67. https://doi.org/10.1038/s41557-020-0446-z.

Takahashi, Masaki, Hiromu Koizumi, Wang-Jae Chun, Makoto Kori, Takane Imaoka, and Kimihisa Yamamoto. 2017. “Finely Controlled Multimetallic Nanocluster Catalysts for Solvent-Free Aerobic Oxidation of Hydrocarbons.” *Science Advances* 3 (7).

Tang, Yan, Chithra Asokan, Mingjie Xu, George W Graham, Xiaoqing Pan, Phillip Christopher, Jun Li, and Philippe Sautet. 2019. “Rh Single Atoms on TiO2 Dynamically Respond to Reaction Conditions by Adapting Their Site.” *Nature Communications* 10 (1): 4488. https://doi.org/10.1038/s41467-019-12461-6.

Thang, Ho Viet, Gianfranco Pacchioni, Leo DeRita, and Phillip Christopher. 2018. “Nature of Stable Single Atom Pt Catalysts Dispersed on Anatase TiO2.” *Journal of Catalysis* 367: 104–14. https://doi.org/https://doi.org/10.1016/j.jcat.2018.08.025.

Therrien, Andrew J, Alyssa J R Hensley, Matthew D Marcinkowski, Renqin Zhang, Felicia R Lucci, Benjamin Coughlin, Alex C Schilling, Jean-Sabin McEwen, and E Charles H Sykes. 2018. “An Atomic-Scale View of Single-Site Pt Catalysis for Low-Temperature CO Oxidation.” *Nature Catalysis* 1 (3): 192–98. https://doi.org/10.1038/s41929-018-0028-2.

Thirumalai, Hari, and John R Kitchin. 2018. “Investigating the Reactivity of Single Atom Alloys Using Density Functional Theory.” *Topics in Catalysis* 61 (5): 462–74.

https://doi.org/10.1007/s11244-018-0899-0.

Tieu, Peter, Xingxu Yan, Mingjie Xu, Phillip Christopher, and Xiaoqing Pan. 2021. "Directly Probing the Local Coordination, Charge State, and Stability of Single Atom Catalysts by Advanced Electron Microscopy: A Review." *Small* 17 (16): 2006482. https://doi.org/https://doi.org/10.1002/smll.202006482.

Uysal, Ahmet, William Rock, Baofu Qiao, Wei Bu, and Binhua Lin. 2017. "Two-Step Adsorption of PtCl62– Complexes at a Charged Langmuir Monolayer: Role of Hydration and Ion Correlations." *The Journal of Physical Chemistry C* 121 (45): 25377–83. https://doi.org/10.1021/acs.jpcc.7b09350.

Valange, Sabine, and Jacques Védrine. 2018. "General and Prospective Views on Oxidation Reactions in Heterogeneous Catalysis." *Catalysts*. https://doi.org/10.3390/catal8100483.

Vu, Bao Khanh, Myoung Bok Song, Sul-A Park, Youngil Lee, In Young Ahn, Young-Woong Suh, Dong Jin Suh, et al. 2011. "Electronic Density Enrichment of Pt Catalysts by Coke in the Propane Dehydrogenation." *Korean Journal of Chemical Engineering* 28 (2): 383–87. https://doi.org/10.1007/s11814-010-0363-8.

Wang, Jun, Qing Kuang, Xiaofang Su, Xiaowen Lu, Leipeng Leng, Mingyang Zhang, Chunmu Guo, et al. 2021. "Isolated Palladium Atoms Dispersed on Silicoaluminophosphate-31 (SAPO-31) for the Semihydrogenation of Alkynes." *ACS Applied Nano Materials* 4 (1): 861–68. https://doi.org/10.1021/acsanm.0c03216.

Wang, Wei, Ran Ran, and Zongping Shao. 2011. “Combustion-Synthesized Ru–Al2O3 Composites as Anode Catalyst Layer of a Solid Oxide Fuel Cell Operating on Methane.” *International Journal of Hydrogen Energy* 36 (1): 755–64. https://doi.org/https://doi.org/10.1016/j.ijhydene.2010.09.048.

Wang, Zhi-Tao, Robert A Hoyt, Mostafa El-Soda, Robert J Madix, Efthimios Kaxiras, and E Charles H Sykes. 2018. “Dry Dehydrogenation of Ethanol on Pt–Cu Single Atom Alloys.” *Topics in Catalysis* 61 (5): 328–35. https://doi.org/10.1007/s11244-017-0856-3.

Warr, Rebecca J., Arjan N. Westra, Katherine J. Bell, Jy Chartres, Ross Ellis, Christine Tong, Timothy G. Simmance, et al. 2009. “Selective Extraction and Transport of the [PtCl6]2− Anion through Outer-Sphere Coordination Chemistry.” *Chemistry – A European Journal* 15 (19): 4836–50. https://doi.org/https://doi.org/10.1002/chem.200802377.

Webb, Joanna R, Tamara Bolaño, and T Brent Gunnoe. 2010. “Catalytic Oxy-Functionalization of Methane and Other Hydrocarbons: Fundamental Advancements and New Strategies.” *ChemSusChem* 4 (1): 37–49. https://doi.org/10.1002/cssc.201000319.

Wei, Hehe, Kai Huang, Da Wang, Ruoyu Zhang, Binghui Ge, Jingyuan Ma, Bo Wen, et al. 2017. “Iced Photochemical Reduction to Synthesize Atomically Dispersed Metals by Suppressing Nanocrystal Growth.” *Nature Communications* 8 (1): 1490. https://doi.org/10.1038/s41467-017-01521-4.

Weon, Seunghyun, Dahong Huang, Kali Rigby, Chiheng Chu, Xuanhao Wu, and Jae-Hong Kim. 2021. “Environmental Materials beyond and below the Nanoscale: Single-Atom Catalysts.” *ACS ES&T Engineering* 1 (2): 157–72. https://doi.org/10.1021/acsestengg.0c00136.

Wong, A., Q. Liu, S. Griffin, A. Nicholls, and J. R. Regalbuto. 2017a. “Synthesis of Ultrasmall, Homogeneously Alloyed, Bimetallic Nanoparticles on Silica Supports.” *Science* 358 (6369): 1427–30. https://doi.org/10.1126/science.aao6538.

Wong, A, Q Liu, S Griffin, A Nicholls, and J R Regalbuto. 2017b. “Synthesis of Ultrasmall, Homogeneously Alloyed, Bimetallic Nanoparticles on Silica Supports.” *Science*, November. http://science.sciencemag.org/content/early/2017/11/20/science.aao6538.abstract.

Wu, Hangzhi, Tianxiang Zhao, and Xingbang Hu. 2018. “Friedel-Crafts Reaction of N,N-Dimethylaniline with Alkenes Catalyzed by Cyclic Diaminocarbene-Gold(I) Complex.” *Scientific Reports* 8 (1): 11449. https://doi.org/10.1038/s41598-018-29854-0.

Wu, Jie, Jia-Hui Li, and Yang-Xin Yu. 2021. “Single Nb or W Atom-Embedded BP Monolayers as Highly Selective and Stable Electrocatalysts for Nitrogen Fixation with Low-Onset Potentials.” *ACS Applied Materials & Interfaces* 13 (8): 10026–36. https://doi.org/10.1021/acsami.0c21429.

Xavier, K. O., J. Chacko, and K. K.Mohammed Yusuff. 2004. “Zeolite-Encapsulated Co(II), Ni(II) and Cu(II) Complexes as Catalysts for Partial Oxidation of Benzyl

Alcohol and Ethylbenzene." *Applied Catalysis A: General*. https://doi.org/10.1016/j.apcata.2003.09.027.

Xing, Feilong, Jaewan Jeon, Takashi Toyao, Ken-ichi Shimizu, and Shinya Furukawa. 2019. "A Cu–Pd Single-Atom Alloy Catalyst for Highly Efficient NO Reduction." *Chemical Science* 10 (36): 8292–98. https://doi.org/10.1039/C9SC03172C.

xiong, wen, Bahareh Mehrabadi, Stavros G Karakalos, Rembert White, Abolfazl Shakouri, Peter Kasak, Syed Javaid Zaidi, et al. 2020. "Enhanced Performance of Oxygen-Functionalized, Multi-Walled Carbon Nanotubes as Support for Pt and Pt-Ru Bimetallic Catalysts for Methanol Electrooxidation." *ACS Applied Energy Materials*, May. https://doi.org/10.1021/acsaem.0c00477.

Xu, Jun, Robert D Armstrong, Greg Shaw, Nicholas F Dummer, Simon J Freakley, Stuart H Taylor, and Graham J Hutchings. 2016. "Continuous Selective Oxidation of Methane to Methanol over Cu- and Fe-Modified ZSM-5 Catalysts in a Flow Reactor." *Catalysis Today* 270: 93–100. https://doi.org/https://doi.org/10.1016/j.cattod.2015.09.011.

Xu, Qionghao, Binbin Feng, Chunlin Ye, Yanghe Fu, De-Li Chen, Fumin Zhang, Jiangwei Zhang, and Weidong Zhu. 2021. "Atomically Dispersed Vanadium Sites Anchored on N-Doped Porous Carbon for the Efficient Oxidative Coupling of Amines to Imines." *ACS Applied Materials & Interfaces* 13 (13): 15168–77. https://doi.org/10.1021/acsami.0c22453.

Yang, Kunran, and Bo Yang. 2017. "Surface Restructuring of Cu-Based Single-Atom

Alloy Catalysts under Reaction Conditions: The Essential Role of Adsorbates." *Physical Chemistry Chemical Physics* 19 (27): 18010–17. https://doi.org/10.1039/C7CP02152F.

Yao, Yonggang, Zhennan Huang, Pengfei Xie, Lianping Wu, Lu Ma, Tangyuan Li, Zhenqian Pang, et al. 2019. "High Temperature Shockwave Stabilized Single Atoms." *Nature Nanotechnology* 14 (9): 851–57. https://doi.org/10.1038/s41565-019-0518-7.

Zborowski, Krzysztof K, Miquel Solá, Jordi Poater, and Leonard M Proniewicz. 2013. "Aromatic Properties of 8-Hydroxyquinoline and Its Metal Complexes." *Central European Journal of Chemistry* 11 (5): 655–63. https://doi.org/10.2478/s11532-013-0215-6.

Zhang, Huabin, Pengfei An, Wei Zhou, Bu Yuan Guan, Peng Zhang, Juncai Dong, and Xiong Wen (David) Lou. 2018. "Dynamic Traction of Lattice-Confined Platinum Atoms into Mesoporous Carbon Matrix for Hydrogen Evolution Reaction." *Science Advances* 4 (1): eaao6657. https://doi.org/10.1126/sciadv.aao6657.

Zhang, Huiyu, Xianming Zheng, Tongzhou Xu, and Pengyi Zhang. 2021. "Atomically Dispersed Y or La on Birnessite-Type MnO2 for the Catalytic Decomposition of Low-Concentration Toluene at Room Temperature." *ACS Applied Materials & Interfaces* 13 (15): 17532–42. https://doi.org/10.1021/acsami.1c01433.

Zhang, Jincheng, Hongbin Yang, and Bin Liu. 2021. "Coordination Engineering of Single-Atom Catalysts for the Oxygen Reduction Reaction: A Review." *Advanced*

Energy Materials 11 (3): 2002473. https://doi.org/https://doi.org/10.1002/aenm.202002473.

Zhang, Jing, Chithra Asokan, Gregory Zakem, Phillip Christopher, and J Will Medlin. 2021. "Enhancing Sintering Resistance of Atomically Dispersed Catalysts in Reducing Environments with Organic Monolayers." *Green Energy & Environment*. https://doi.org/https://doi.org/10.1016/j.gee.2021.01.022.

Zhao, Zhiying, Mingzhi Wang, Peijie Ma, Yanping Zheng, Jiayu Chen, Huiqi Li, Xibo Zhang, Kun Zheng, Qin Kuang, and Zhao-Xiong Xie. 2021. "Atomically Dispersed Pt/CeO2 Catalyst with Superior CO Selectivity in Reverse Water Gas Shift Reaction." *Applied Catalysis B: Environmental* 291: 120101. https://doi.org/https://doi.org/10.1016/j.apcatb.2021.120101.

Zhong, Wanfu, Rongjian Sa, Liuyi Li, Yajun He, Lingyun Li, Jinhong Bi, Zanyong Zhuang, Yan Yu, and Zhigang Zou. 2019. "A Covalent Organic Framework Bearing Single Ni Sites as a Synergistic Photocatalyst for Selective Photoreduction of CO2 to CO." *Journal of the American Chemical Society* 141 (18): 7615–21. https://doi.org/10.1021/jacs.9b02997.

Zhou, Linan, John Mark P Martirez, Jordan Finzel, Chao Zhang, Dayne F Swearer, Shu Tian, Hossein Robatjazi, et al. 2020. "Light-Driven Methane Dry Reforming with Single Atomic Site Antenna-Reactor Plasmonic Photocatalysts." *Nature Energy* 5 (1): 61–70. https://doi.org/10.1038/s41560-019-0517-9.

APPENDIX A

SUPLEMENTARY INFORMATION

Materials and Methods

Materials

Hexachloroplatinic(IV) acid hexahydrate and TiO_2-P25 were purchased from Sigma Aldrich. Norit ROX 0.8 was obtained from CABOT Corporation. The VXC-72 was purchased from the FuelcellStore. Ammonium hexachlororuthenate(IV) and Hexachloroiridic(IV) acid hydrate ≥99.9% (Ir basis) were supplied by STREM Chemical Inc. MS. The silica OX-50 support substrate was obtained from EVONIK company. Platinum(IV) nitrate solution (15% Pt) (w/w) and Tetraammineplatinum(II) nitrate were purchased from AlfaAesar materials company. Diamond Nanopowder (synthesized, 98+%, 3-10 nm) was obtained from Nanostructured & Amorphous Materials, Inc.

Methods

The synthesis procedure demonstrated in **Figure S8** is same as incipient wetness impregnation except the drying step replaced by chelate fixation. The detailed procedure starts with dissolution of predetermined amount of the catalyst precursor in water. Then, the support substrate is thoroughly mixed with a volume of the aqueous precursor solution equal to the titrated pore volume of the support substrate. The chelating agent is dissolved in a solvent with a larger dipole moment than water (i.e., acetone, DMF…), and added to

the aqueous precursor/support slurry in a 4:1 molar ratio of solvent to water. The 8-HQ concentration in the solvent is adjusted such that the 8-HQ:metal ion molar ratio is 2:1. After that, the resulting slurry is transferred to a tube furnace for reduction under 10% hydrogen balance nitrogen flow. For example, to deposit 7.7% Pt onto one gram of VXC-72, 0.1753 g H_2PtCl_6 (equivalent to 0.0834 g Pt) dissolved using 3.5 ml of DI water (titrated pore volume of the VXC-72). Then 1 g of VXC-72 was mixed with the solution and mixed thoroughly by a vortex mixer for two minutes at 3000rpm. The next step was dissolution of 0.1247 g of 8-HQ in 58 ml acetone (4:1 molar ratio of acetone to water), added to the mixture and thoroughly mixed for two minutes. The resulting suspension was loaded into a crucible boat and placed in the reduction furnace. A flow of 10% hydrogen balance nitrogen was set at 400 sccm in a 1inch diameter quartz tube. The suspension was dried at 50˚C for 30 minutes and then ramped up to 170˚C with a rate of 2˚C/minute. The catalyst soaked at 170˚C for one hour and cooled to the room temperature. The chelating agent can be removed either with high temperature treatment or by washing with acetone following by drying the catalyst.

X-ray photoelectron spectroscopy (XPS) were measured with a Kratos AXIS Ultra DLD XPS system with a monochromatic Al Ka source operated at 15 keV and 150W. Analysis was performed at a pressure below 1x10-9 mbar and the X-ray incident of 45°. High resolution core level spectra were measured with a pass energy of 40 eV and analysis of the data was carried out using XPSPEAK41 software. In the case of nonconductive support, the XPS experiments were performed while using a charge neutralization electron gun directed on the catalyst. The XPS instrument was equipped with an in-situ catalyst treatment cell. The in-situ treatments were done under flow of 5% H_2/Ar for 1 hour at

various temperature. An Inficon Transpector 2 Mass Spectrometer was utilized to study in situ CO temperature programmed as a function of time during a temperature ramp of 3°C/s.

All electron microscopy images were taken using a JEOL JEM-2100F Aberration Corrected Scanning Transmission Electron Microscope equipped with Fischione high angle annular darkfield detector (HAADF) with a camera length such that the detector spanned 50-163 mrad. The scanning acquisition was synchronized to 60 Hz AC electrical power to minimize 60Hz noise in the images and a pixel dwell time of 15.8μs was chosen. In some cases, when the support substrate is conductive and there is enough difference in atomic number between the elements in the system, it may be possible to characterize the SACs using Z-contrast imaging.

Nuclear magnetic resonance spectroscopy (NMR) was recorded using a Bruker Avance III-HD 500 MHz. The solution of K_2PtCl_6 was used as the reference to calibrate the NMR spectra. The solutions at different stage of synthesis procedure were subjected to the NMR measurements.

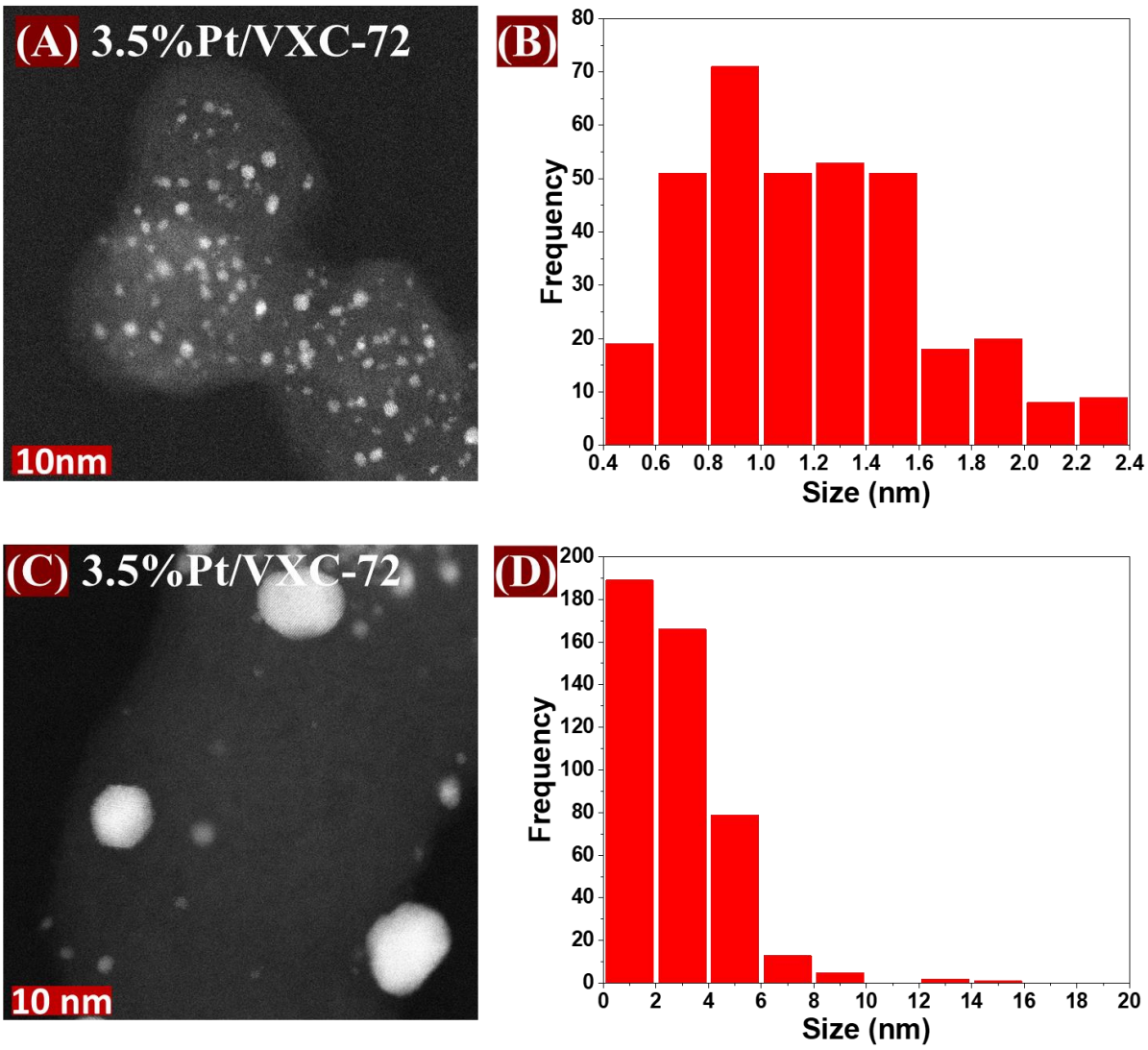

Figure A1. Excess water effect in the system during activation, (A) AC-STEM image of 3.5%Pt/VXC-72 prepared by SEA and well dried at room temperature before activation, (B) corresponding particle size distribution, (C) 3.5%Pt/VXC-72 prepared by SEA; activation started in the form of moist mud with excess water, and (D) corresponding particle size distribution of (C).

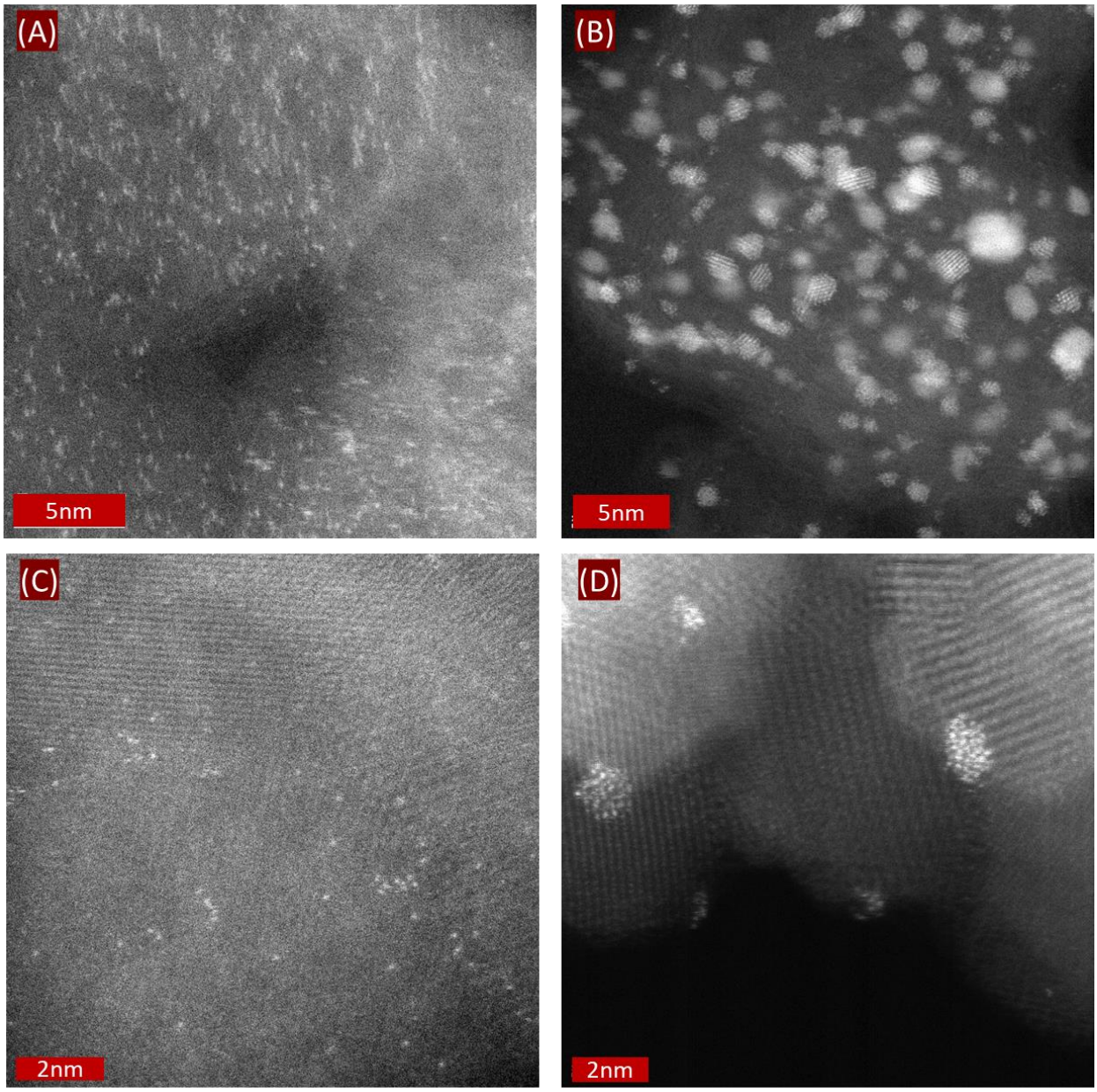

Figure A2. *AC-STEM images of (A) 3.5% Pt/VXC-72 CheFi, (B) 3.5%Pt/VXC-72 SEA, (C) 1.9% Pt/TiO_2 CheFi, and (D) 1.9% Pt/TiO_2 SEA catalysts.*

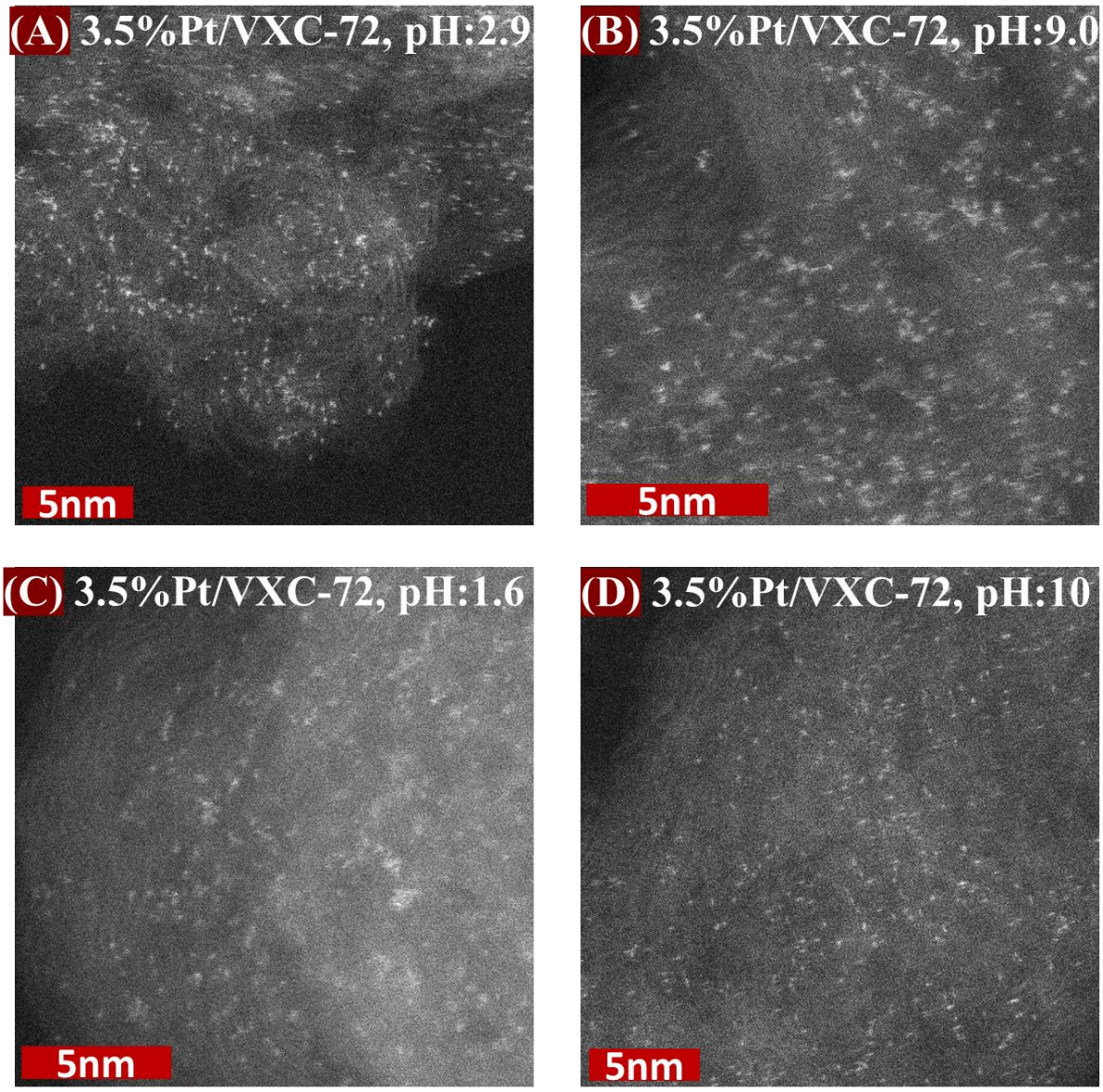

Figure A3. *STEM images of (A) SEA/CheFi catalyst (H_2PtCl_6), and (B) CheFi catalyst with anionic precursor (H_2PtCl_6), and (C) CheFi with high ionic strength of anionic precursor (H_2PtCl_6), and (D) CheFi catalyst with cationic precursor ($Pt(NH_3)_4NO_3$).*

Type or paste caption here. Create a page break and paste in the Figure above the caption.

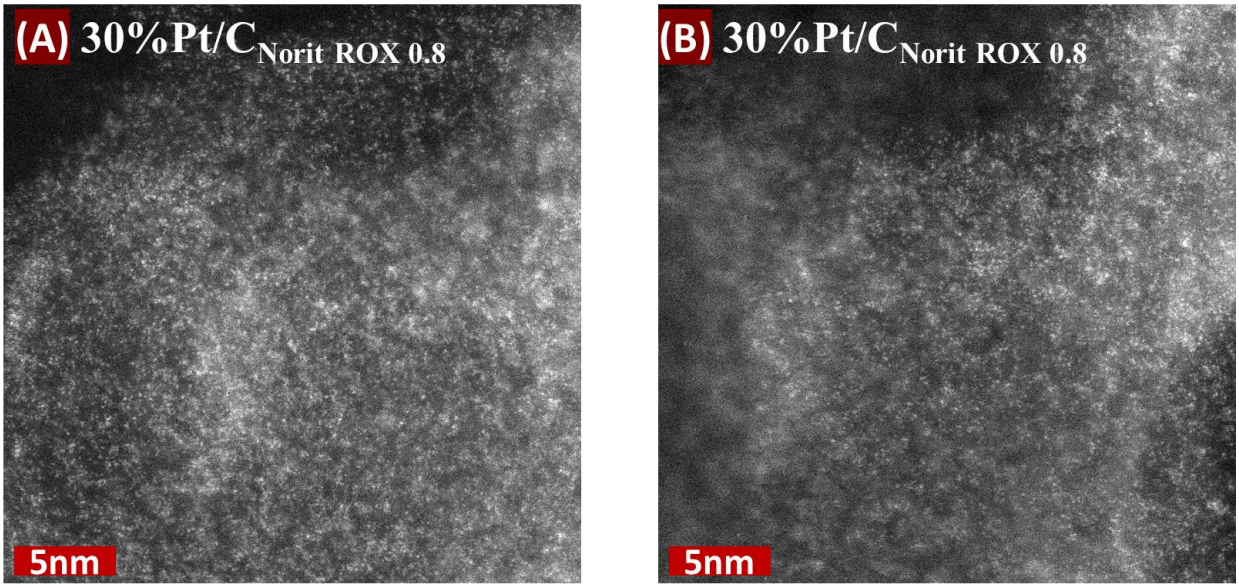

Figure A4. *Same frame AC-STEM images explaining contrast signal overlap in different focal planes, (A) 30%Pt/C CheFi catalyst with the focus on the left-hand side, and (B) 30%Pt/C CheFi catalyst with the focus on the right hand-side.*

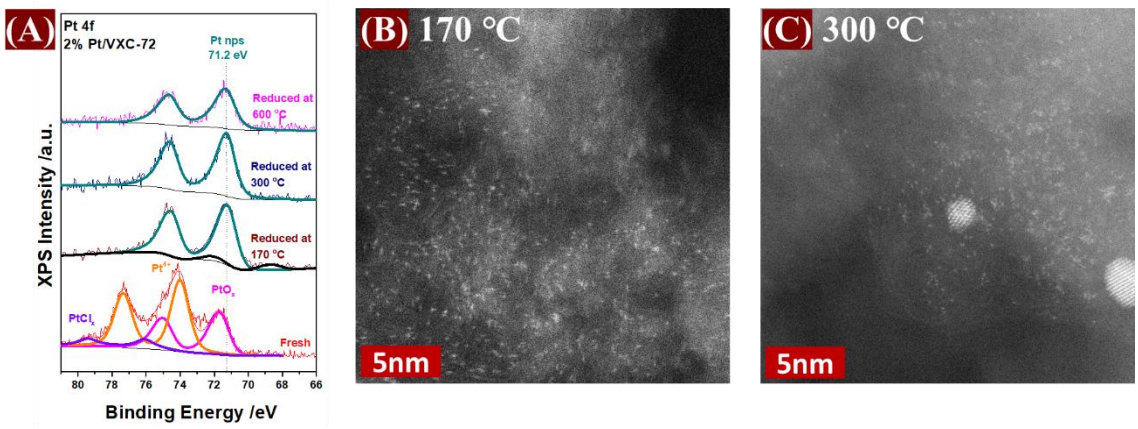

Figure A5. *In situ XPS and AC-STEM images, (A) XPS spectra of fresh, reduced at 170˚C, 300˚C, and 600˚C 2%Pt/VXC-72 nanoparticles, (B) STEM image of 2%Pt/VXC-72 prepared by CheFi in situ reduced at 170˚C (C) STEM image of 2%Pt/VXC-72 prepared by CheFi in situ reduced at 300˚C.*

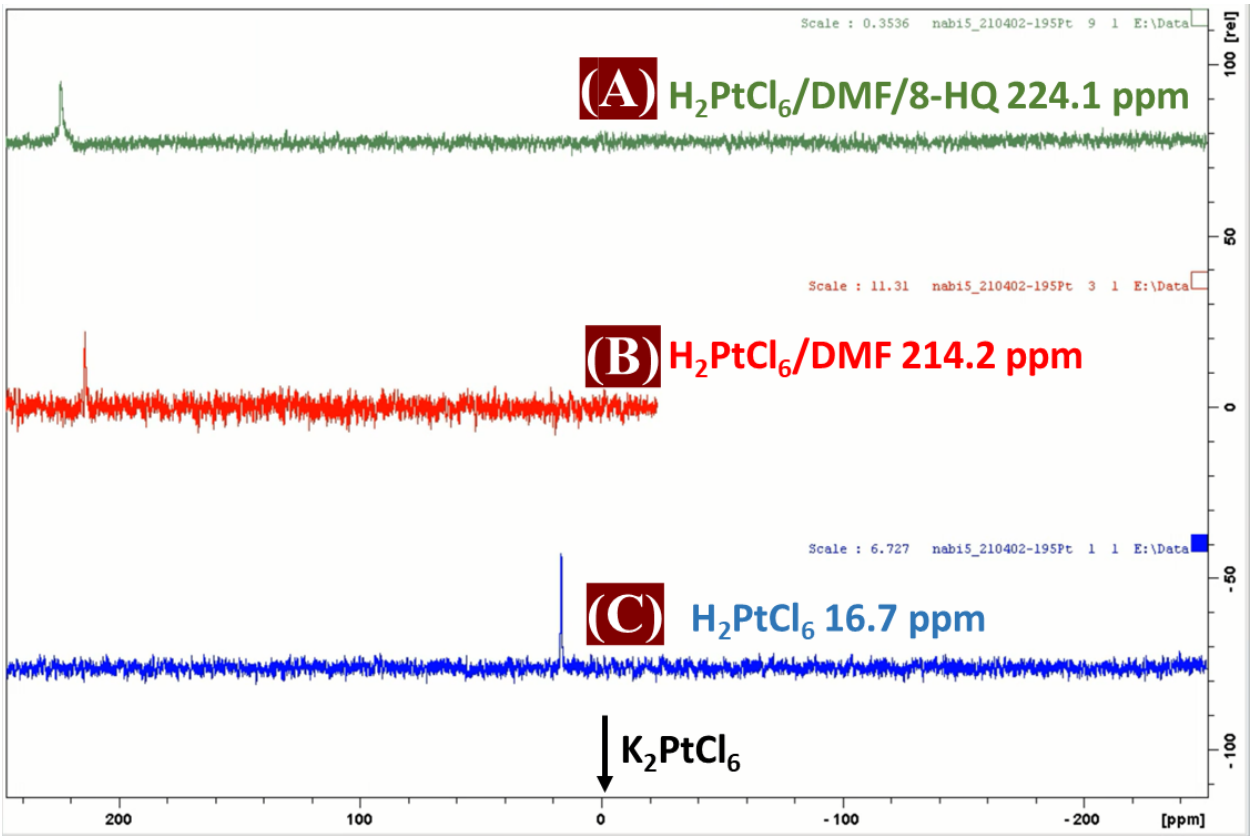

Figure A6. *NMR study of chelating Pt complex, the K_2PtCl_6 used as reference, (A) 8-HQ/DMF/aqueous chloroplatinic acid Pt peak at 224.1 ppm (B) DMF/aqueous chloroplatinic acid Pt peak at 214.2 ppm, and (C) aqueous chloroplatinic acid Pt peak observed at 16.7 ppm, addition of DMF solvent shifted the Pt peak to 214.2, 8-HQ/DMF addition Pt peak*

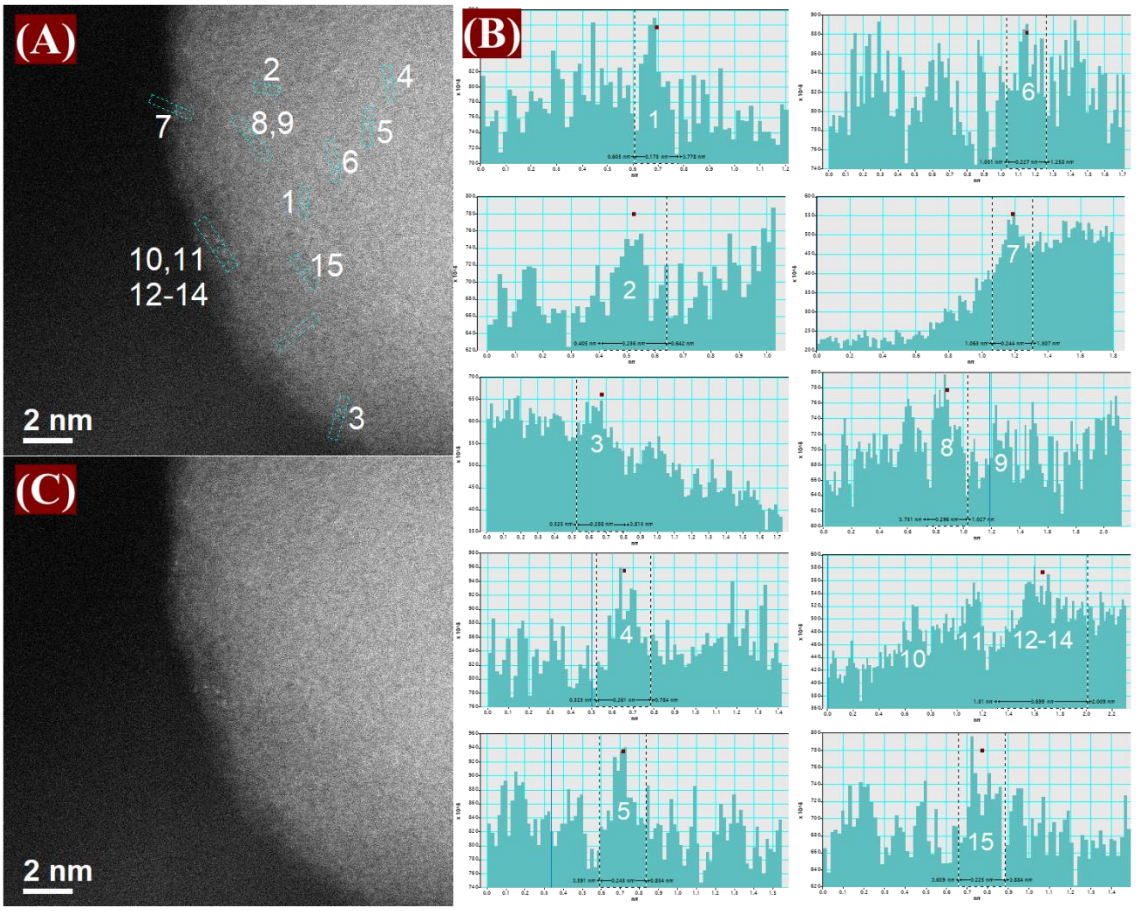

Figure A7. *Image processing contrast scan, (A) selected Pt single atoms on 0.78% Pt/SiO_2 catalyst, (B) corresponding contrast histograms of the selected Pt single atoms, (C) original AC-STEM image of 0.78% Pt/SiO_2 catalyst.*

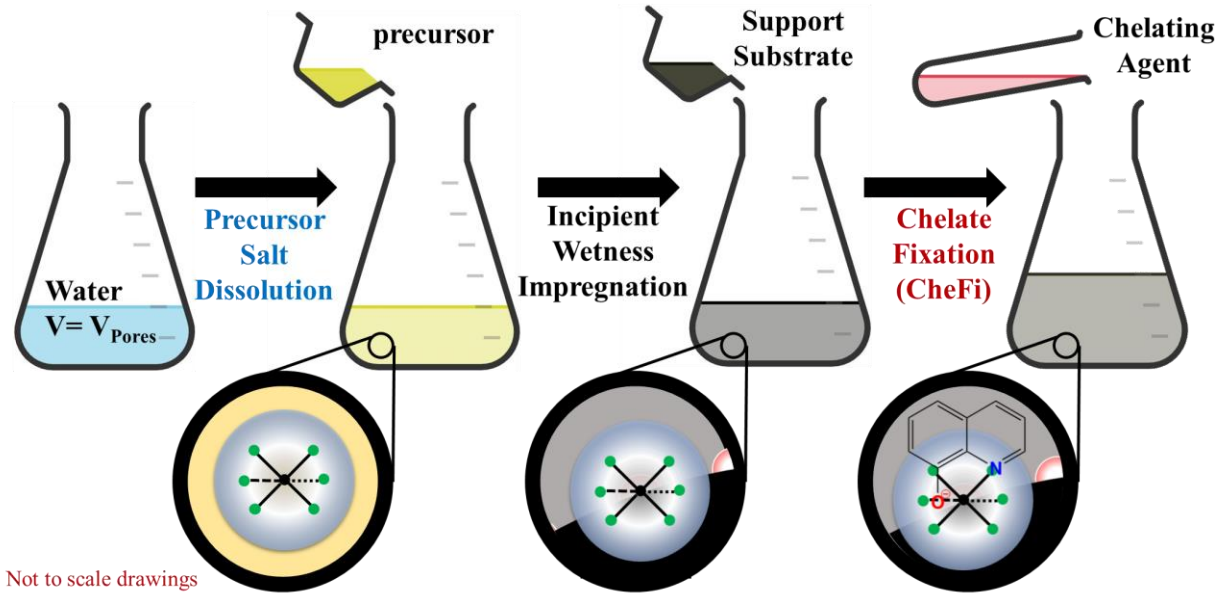

Figure A8. *Schematic of the synthesis procedure, from left to right, dissolution of catalyst precursor in water with a volume equal to the titration pore volume of the support, support substrate addition, and chelate fixation.*